

AD-A092 094

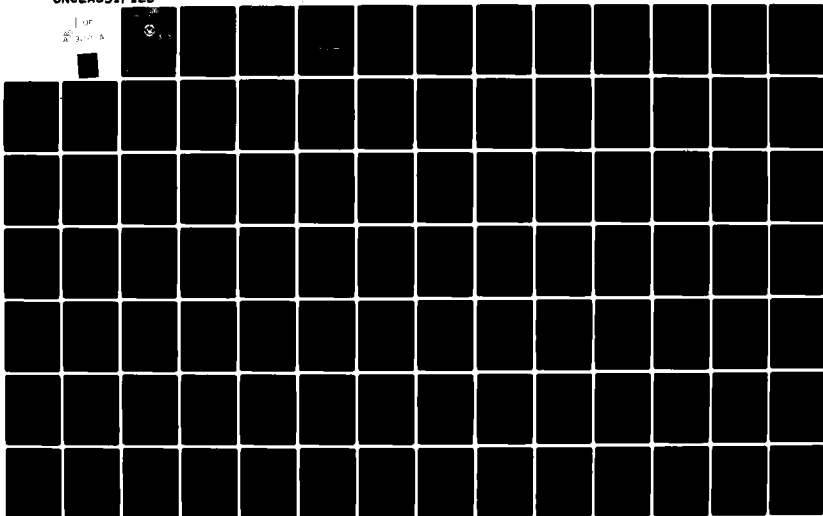
NAVAL POSTGRADUATE SCHOOL MONTEREY CA
ANALYSIS OF COMBUSTION AND HEAT TRANSFER IN A POROUS GRAPHITE M-ETC(U)
JUN 80 C S VATIKIOTIS

F/G 11/4

UNCLASSIFIED

NL

UP
A 3-17-8



LEVEL *II*

②
B.S.

NAVAL POSTGRADUATE SCHOOL
Monterey, California

AD-77092094



DTIC
ELECTE
S DEC 02 1980 **D**
E

THESIS

**ANALYSIS OF COMBUSTION AND HEAT TRANSFER
IN A POROUS GRAPHITE MEDIUM**

by

Costa Sozon Vatikiotis

June 1980

Thesis Advisor:

D. Salinas

Approved for public release; distribution unlimited.

BDC FILE COPY

80 12 01 248

UNCLASSIFIED

SECURITY CLASSIFICATION OF THIS PAGE (When Data Entered)

REPORT DOCUMENTATION PAGE		READ INSTRUCTIONS BEFORE COMPLETING FORM
1. REPORT NUMBER	2. GOVT ACCESSION NO.	3. RECIPIENT'S CATALOG NUMBER
	AD-A092094	094
4. TITLE (and Subtitle)		5. TYPE OF REPORT & PERIOD COVERED
Analysis of Combustion and Heat Transfer in a Porous Graphite Medium		Engineer's Thesis; June 1980
7. AUTHOR(s)		6. PERFORMING ORG. REPORT NUMBER
Costa Sozon/Vatikiotis		
8. PERFORMING ORGANIZATION NAME AND ADDRESS		9. CONTRACT OR GRANT NUMBER(s)
Naval Postgraduate School Monterey, California 93940		(13) 157
11. CONTROLLING OFFICE NAME AND ADDRESS		10. PROGRAM ELEMENT, PROJECT, TASK AREA & WORK UNIT NUMBERS
Naval Postgraduate School Monterey, California 93940		
14. MONITORING AGENCY NAME & ADDRESS (if different from Controlling Office)		12. REPORT DATE
(1) Master's thesis		June 1980
		13. NUMBER OF PAGES
		157
		15. SECURITY CLASS. (of this report)
		Unclassified
		16a. DECLASSIFICATION/DOWNGRADING SCHEDULE
16. DISTRIBUTION STATEMENT (of this Report)		
Approved for public release; distribution unlimited.		
17. DISTRIBUTION STATEMENT (of the abstract entered in Block 20, if different from Report)		
18. SUPPLEMENTARY NOTES		
19. KEY WORDS (Continue on reverse side if necessary and identify by block number)		
Combustion, Heat Transfer, Carbon, Graphite, Fiber, Porous Media, Conduction, Convection, Radiation, Diffusion, Exothermic Reaction, Nonvolatile, Finite Element Method, Galerkin Formulation		
20. ABSTRACT (Continue on reverse side if necessary and identify by block number)		
<p>The problem of a porous graphite fiber plate subject to combustion is formulated. The transient one-dimensional model leads to two heat transfer equations on the graphite and air, and a mass transfer equation on the oxygen. In addition to a combustion heat generation term, the heat transfer model includes the mechanisms of conduction, radiation between fibers, and convection due to induced air flow through the mat. The mass transfer model</p>		

DD FORM 1473
1 JAN 73
(Page 1)EDITION OF 1 NOV 68 IS OBSOLETE
S/N 0102-014-6001UNCLASSIFIED 352450
SECURITY CLASSIFICATION OF THIS PAGE (When Data Entered)

UNCLASSIFIED

SECURITY CLASSIFICATION OF THIS PAGE/When Data Entered

#20 - ABSTRACT - CONTINUED

includes diffusion and convection mechanisms, as well as a combustion consumption term. The temperature dependency of the system parameters is taken into account. The resulting nonlinear, coupled partial differential equations are solved by a Galerkin formulation of the finite element method. A number of computer analysis results are presented. The results show the effects of initial conditions, plate thickness, fiber diameter and air flow rate on ignition and extinction.

Accession For	
NTIS GRA&I	<input checked="checked" type="checkbox"/>
DDC TAB	<input type="checkbox"/>
Unannounced	<input type="checkbox"/>
Justification	
By _____	
Distribution/	
Availability Codes	
Dist.	Avail and/or special
A	

DD Form 1473
Jan 73
S/N 0102-014-6601

2

UNCLASSIFIED

SECURITY CLASSIFICATION OF THIS PAGE/When Data Entered

Approved for public release; distribution unlimited.

Analysis of Combustion and Heat Transfer
in a Porous Graphite Medium

by

Costa Sozon Vatikiotis
Lieutenant, United States Navy
B.S., Florida State University, 1971

Submitted in partial fulfillment of the
requirements for the degrees of

MASTER OF SCIENCE IN MECHANICAL ENGINEERING

and

MECHANICAL ENGINEER

from the

NAVAL POSTGRADUATE SCHOOL

June 1980

Author

Costa Sozon Vatikiotis

Approved by:

David Salinas

Thesis Advisor

Matthew Kelleher

Second Reader

D.J. Warts
Chairman, Department of Mechanical Engineering

William M. Jolley

Dean of Science and Engineering

ABSTRACT

The problem of a porous graphite fiber plate subject to combustion is formulated. The transient one-dimensional model leads to two heat transfer equations on the graphite and air, and a mass transfer equation on the oxygen. In addition to a combustion heat generation term, the heat transfer model includes the mechanisms of conduction, radiation between fibers, and convection due to induced air flow through the mat. The mass transfer model includes diffusion and convection mechanisms, as well as a combustion consumption term. The temperature dependency of the system parameters is taken into account. The resulting nonlinear, coupled partial differential equations are solved by a Galerkin formulation of the finite element method. A number of computer analysis results are presented. The results show the effects of initial conditions, plate thickness, fiber diameter and air flow rate on ignition and extinction.

TABLE OF CONTENTS

I.	INTRODUCTION -----	12
II.	THEORY AND BACKGROUND -----	15
	A. INTERACTION OF HEAT TRANSFER AND COMBUSTION -	15
	B. HEAT TRANSFER EQUATIONS FOR POROUS MEDIA ----	18
III.	FORMULATION OF FIELD EQUATIONS -----	20
	A. INTERNAL FLOW MODEL -----	20
	B. ENERGY EQUATIONS -----	28
	1. Fiber Heat Transfer Equation -----	30
	a. Thermal Conduction -----	31
	b. Radiation Heat Transfer in Fibers ---	32
	c. Convection Heat Transfer -----	34
	d. Heat Generation Rate -----	36
	e. Change in Internal Energy -----	38
	2. Internal Flow Heat Transfer Equation ----	39
	a. Thermal Conduction -----	40
	b. Energy Transport by Flow -----	40
	c. Convection Heat Transfer -----	41
	d. Change in Internal Energy -----	41
	3. Oxygen Transport Equation -----	43
	a. Molecular Diffusion -----	44
	b. Convective Transport -----	46
	c. Consumption Rate -----	46
IV.	BOUNDARY CONDITIONS -----	48

V.	FINITE ELEMENT METHOD -----	51
A.	GALERKIN FORMULATION -----	51
B.	IMPLEMENTATION OF BOUNDARY CONDITIONS -----	60
	1. Fiber Heat Transfer Equation -----	60
	2. Internal Flow Heat Transfer Equation -----	61
	3. Oxygen Transport Equation -----	62
VI.	RESULTS AND CONCLUSION -----	65
A.	NUMERICAL CONSIDERATIONS -----	65
B.	RESULTS AND OBSERVATIONS -----	67
	1. Effects of Exterior Velocity -----	69
	2. Effects of Fiber Diameter -----	70
	3. Effects of Plate Thickness -----	71
C.	DISCUSSION -----	72
D.	CONCLUDING REMARKS -----	74
APPENDIX A:	NONDIMENSIONALIZATION OF FIELD EQUATIONS --	76
APPENDIX B:	POLYNOMIAL APPROXIMATIONS OF THERMAL PROPERTIES -----	81
APPENDIX C:	TRANSFORMATION OF THE REACTION RATE TERM --	84
APPENDIX D:	JUSTIFICATION OF THE DANKWERTS' BOUNDARY CONDITIONS -----	87
APPENDIX E:	DERIVATION OF THE FEM OPERATORS -----	92
TABLES AND FIGURES	-----	99
COMPUTER PROGRAM "CARBO" AND SAMPLE INPUT FILE	-----	116
LIST OF REFERENCES	-----	154
INITIAL DISTRIBUTION LIST	-----	156

LIST OF SYMBOLS

A^{-1}	- characteristic time of reaction
A	- stiffness matrix
\tilde{B}	- molecular diffusivity
B	- Gram matrix
c	- specific heat at constant pressure
D	- ply thickness
d	- filament diameter
E	- activation energy
e	- element number
F	- excitation vector
f	- stoichiometric ratio
G	- global basis function
g	- local basis function
Gr	- Grashof number
G_o	- pseudo mass velocity
h	- convection heat transfer coefficient
\hat{h}	- specific enthalpy
ΔH	- enthalpy of formation
J	- Colburn j-factor
k	- thermal conductivity
L	- plate thickness
L^*	- reference length (= unity)
l_e	- element length

M	-	molecular weight
m	-	specific permeability
\dot{m}	-	mass flow rate
n	-	number of nodal points
P	-	pressure
p	-	porosity
Pr	-	Prandtl number
q_g	-	heat generation
q_l	-	heat loss
R	-	Universal Gas constant
R_A	-	gas constant for air
r	-	reaction rate
r_i	-	residual function
Re	-	Reynolds number
s	-	spacing between fibers
T	-	temperature
\hat{T}	-	absolute temperature
t	-	time
U_∞	-	flow over exterior surface
u_p	-	pore velocity
V	-	molecular volume
w	-	mean free path
x	-	one-dimensional coordinate
y	-	ratio of a fibers' surface area to its volume
z	-	ratio of fiber surface area per unit volume

Greek symbols

Γ	-	nondimensional air temperature
Δ	-	difference
δ	-	average pore diameter
δ_{ij}	-	kronecker delta
ϵ	-	emissivity
ξ	-	local coordinates
η	-	nondimensional length
θ	-	nondimensional fiber temperature
Λ	-	spacial operator
λ	-	coefficient defined in Appendix A
μ	-	dynamic viscosity of air
ν	-	coefficient defined in Appendix A
ρ	-	density
σ	-	Stefan-Boltzmann constant
τ	-	tortuosity
Φ	-	nondimensional oxygen concentration
ϕ	-	oxygen concentration
Ψ	-	approximate solution values
Ψ_0	-	shape parameter for h_i
ω	-	coefficient defined in Appendix A; dummy variable

subscripts

a	-	air
B	-	diffusion
b	-	bulk property

c - convection
e - effective
f - fluid
g - fiber
i - internal
K - Kelvin
L - at $x = L$
O₂ - oxygen
p - pore
r - radiation
s - solid
∞ - ambient condition

ACKNOWLEDGMENTS

The author wishes to express his sincere appreciation to Professor David Salinas for his invaluable guidance, assistance and friendship as instructor and thesis advisor. In addition, the author wishes to thank Mr. John Fontenot and Mr. Joseph Mansfield for their interest, comments and thoughtful advice.

The author is obligated to Professor Richard Franke, Professor Matthew Kelleher, Professor David Netzer and Mr. Roger Hilleary for their assistance during the early stages of this work.

Finally, the author would like to thank his wife, Darlene, for her understanding and encouragement.

I. INTRODUCTION

The combustion of a composite laminate plate consisting of graphite fibers in an epoxy matrix is discussed. The combustion process for a graphite laminate takes place in two stages, epoxy combustion followed by combustion of the graphite. At the end of the first stage the epoxy has burned away exposing a porous graphite mat. Spacing between the fibers is maintained by the residue of the combustion products. This present work is concerned with the last stage of the combustion process, specifically, the thermal response of the remaining graphite fiber mat.

The selection of the second stage for the analysis was made as a result of observations during composite plate "burn" experiments at the Naval Weapons Center, China Lake [1]. The objective of the experiments was to assess damage of composite aircraft structures subjected to open deck fires on aircraft carriers. For the experiments, an epoxy-graphite laminate was mounted into the wall of a wind tunnel parallel to the flow. One side of the composite plate was exposed to the wind tunnel flow and the opposite side was open to the environment. This arrangement was to simulate a composite wing section or fuselage subjected to typical wind conditions present on a carrier flight deck. It was observed that after being subjected to a fire which resulted in the

epoxy burning away, the graphite fibers would continue to smolder or burn. In other instances, the fibers would cool depending on the flow velocity and plate thickness. To understand this behavior better, a mathematical model was formulated to predict the conditions for which the exothermic process is self-sustaining.

The air flow over one surface produces a pressure differential across the plate which induces a convective air flow through the porous medium governed by Darcy's Law. As a result, there is an enhancement of internal convection heat transfer, as well as a source of oxygen for combustion. The heat transfer mechanisms included in the model are (1) conduction, (2) convection, and (3) radiation. In addition, non-volatile combustion is included in the energy balance as a heat generation term of Arrhenius type. The oxygen concentration is accounted for by a molecule-mass balance which includes (1) molecular diffusion, and (2) mass transfer by convection. Consumption of oxygen due to combustion is accounted for by a term similar to the heat generation term.

The formulation of a one-dimensional model is presented. All properties are treated as temperature dependent in the transient analysis. To account for heat transfer mechanisms between the air and porous graphite medium, the air and graphite temperatures are treated as independent variables. The energy balance on the graphite and on the air, and the

molecule-mass balance on oxygen result in a system of three nonlinear, coupled partial differential equations.

Integration of the field equations is accomplished by a Galerkin formulation of the finite element method. Due to the inherent stiffness of the field equations in the time domain, a modified implicit-Gear integration scheme developed by Franke [2] is used for a more efficient solution.

II. THEORY AND BACKGROUND

A. INTERACTION OF HEAT TRANSFER AND COMBUSTION

In this work, the combustion model proposed by Semenov was adopted. It is described in the texts of Frank-Kamenetskii [3] and Vulis [4]. A brief discussion of those features of the model which relate to the present investigation will be given. Fundamental to the model is the relation of reaction rate to temperature, and the interaction of the heat generation and the heat transfer from the system. In general, the reaction rate, r , may be shown by the Arrhenius law as,

$$r = A(T, \phi) \exp(-E/\hat{R}\hat{T})$$

where A^{-1} is the characteristic time of the chemical reaction, E is the activation energy, R is the universal gas constant, \hat{T} is absolute temperature and ϕ is the concentration of oxygen. The concentration appears as ϕ^n in $A(\hat{T}, \phi)$ for an n th order reaction. The heat generated by the exothermic process is obtained by multiplying the reaction rate, r , by the enthalpy of formation of the combustion products.

In Figure 1, the heat generation, q_g , is plotted as a function of temperature. The curve is referred to as the S-curve for apparent reasons. The S-curves are distinguished

by two regions. Lower temperatures and reaction rates characterize region I, while region II is characterized by higher temperatures and reaction rates. In region I, for low reaction rates, there is an abundant supply of oxygen. The reaction is controlled by the temperature and the region is known as the kinetic regime. Here, the reaction rate increases exponentially with increasing temperature. In region II, the reaction is limited by oxygen concentration and is known as the diffusion regime. The reaction's weak dependence on temperature in region II is shown by the characteristic flattening of the S-curve in Figure 1. For higher concentrations of oxygen, the diffusion region is associated with higher reaction rates. The interaction of heat generation, q_g , and heat loss, q_l , will now be described.

In addition to the S-curve, Figure 1 shows two heat loss lines, q_{l1} and q_{l2} . They represent the heat transfer by convection for air temperatures, T_1 and T_2 , respectively. The intersection of the heat generation curve and the heat loss curve, $q_g = q_l$, defines the stable quasi-stationary point, A. As the air flow temperature increases from T_1 to T_2 , the quasi-stationary temperature increases continuously from T_A to T_I . For temperature T_I , q_{l2} is tangent to q_g and an infinitesimal increase in the air flow temperature results in a jump of the reaction temperature from T_I to T_B . At point I, which is defined as the "critical ignition condition", the reaction moves from the kinetic to the diffusion regime.

Temperature T_i is referred to as the ignition temperature. Frank-Kamenetskii states the ignition temperature of graphite is approximately 1100 to 1300 degrees Celsius. In order to keep the reaction model simple, the present investigation was limited to the kinetic regime. Although the description of the heat transfer process just presented is for convection only, the underlying ideas are valid for the conduction and radiation heat transfer mechanisms as well. The slope of the heat loss lines, q_ℓ , is equal to the product of the internal heat transfer coefficient and the surface area of fiber per unit volume. The slopes would not appear constant, and slight curvature in the heat loss lines, q_ℓ , is apparent when radiation effects are included. As shown in Figure 1, an increase in the heat transfer rate resulting, for example, by an increase in the internal flow rate would result in a lower graphite temperature for a given air temperature.

One reason for limiting the model to the kinetic regime was due to the jump in temperature and reaction rate at ignition. Though the discontinuity may be accounted for, the results show that for the region of temperatures approaching the diffusion regime, the heat generation will dominate the process. The system temperatures then rise rapidly. Other factors that limit the model to the lower temperatures are (1) the chemical reaction fixing the heat of combustion (complex at higher temperatures) and (2) the rapid consumption of fibers after ignition.

B. HEAT TRANSFER EQUATIONS FOR POROUS MEDIA

In their investigation of oil recovery from underground reservoirs, Green and Perry [5] developed heat transfer equations for the solid and fluid phases in a porous medium. Their model included the three basic mechanisms: (1) physical movement of the fluid which carries its own heat capacity, (2) conduction of heat through the solid and fluid phases, and (3) convective heat transfer between the solid and fluid phases. Radiation heat transfer was assumed to be negligible, and combustion was not a consideration. The differential equations for the fluid and solid phases

$$\text{Fluid: } \rho_f c_f p \frac{\partial T_f}{\partial t} = -u \rho_f c_f p \frac{\partial T_f}{\partial x} + k_f p \frac{\partial^2 T_f}{\partial x^2} - hz(T_f - T_s) \quad (\text{II.1})$$

$$\text{Solid: } \rho_s c_s (1-p) \frac{\partial T_s}{\partial t} = k_s (1-p) \frac{\partial^2 T_s}{\partial x^2} + hz(T_f - T_s) \quad (\text{II.2})$$

were solved numerically by the finite difference method. In equations II.1 and II.2, c is the specific heat at constant pressure, u is the fluid velocity through the medium, h is the coefficient of heat transfer, and k is a pseudothermal conductivity. The model did not include change of properties with temperature. Their numerical results showed good agreement with their experimental results. Two useful conclusions derived from their analysis were: (1) both conduction and convection heat transfer mechanisms are important for internal Reynolds numbers less than one, and (2) for values of the

dimensionless parameter, $\xi = (hz/k_f)^{1/2} (k_f/\rho_f c_f u)$ greater than .342, the fluid temperature is approximately the solid temperature. Riaz [6] proposed the following equation resulting from the equal fluid-solid temperature assumption,

$$\rho_s c_s \frac{\partial T}{\partial t} + \rho_f c_f u \frac{\partial T}{\partial x} = k_s \frac{\partial^2 T}{\partial x^2} \quad (\text{II.3})$$

where the coefficients are defined as those in equations II.1 and II.2. For the present model, the more general approach (i.e., Green and Perry) will be taken in the formulation of the energy equations.

III. FORMULATION OF THE FIELD EQUATIONS

A. INTERNAL FLOW MODEL

Referring to Figure 2, the porous mat may be represented by a flat plate. One side is exposed to still air, and the other to an air flow of velocity, U_{∞} . The environment on both sides is at ambient temperature, T_{∞} .

The first step in developing the model was to derive an expression for the flow through the porous plate. Effects of the combustion process on the physical properties were neglected. Specifically, these were (1) variations in the porosity due to fiber consumption, and (2) effects on the viscosity and density of air from the introduction of combustion by-products into the flow. Preliminary calculations showed that the porosity and density of the material did not change appreciably until temperatures reached approximately 2000 degrees Fahrenheit. Further, since eighty percent of air by volume is essentially inert, it was reasonable that its properties would not be significantly altered during the combustion process. Assuming a heterogeneous material of constant porosity, a Reynold's number for the interior flow is defined as

$$Re_i = \rho_a u_p d / \mu \quad (III.1)$$

where ρ_a is the mass density of air, u_p is the pore velocity, d is the diameter of the fiber, and μ is the dynamic viscosity. Extensive experimental work shows that Darcy's law for flow through a porous medium is valid for a limited range of Reynolds numbers. Muskat [7] proposed that Darcy's flow is valid for $Re_i < 1$. Scheidegger [8] points out that a number of investigators give a much higher upper limit. Preliminary calculations of Re_i for the model showed typical magnitudes on the order of 1. Neglecting the gravity term, Darcy's law for flow in porous media is,

$$u_p = - \frac{m}{\mu} \frac{dP}{dx} \quad (III.2)$$

assuming a constant pressure gradient, equation III.2 becomes,

$$u_p = - \frac{m}{\mu} \frac{\Delta P}{L} \quad (III.3)$$

where ΔP is the pressure differential across the plate thickness, m is the specific permeability of the medium, and μ is the dynamic viscosity. In equations III.1 and III.3, ρ_a and μ were treated as temperature dependent.

Specific permeability is a measure of a porous medium's ability to allow fluid to flow through. It is dependent only on geometry and the physical nature of the medium. It has dimensions of length squared. Specific permeability is often

called the hydraulic conductivity due to the similarity of Darcy's law to that of Fourier's law for heat conduction. The permeability for a particular medium is normally measured by experimentation. However, there are several empirical models that may be used to obtain values for permeability that are in agreement with experimental results. For the idealized geometry of the porous medium shown in Figure 2, the permeability was obtained by a serial type model, equation III.4, proposed by Scheidegger [8],

$$m = \frac{1}{96} p (\delta/\tau)^2 \quad (\text{III.4})$$

where the porosity, p , is defined for a porous material comprised of fibers with cylindrical shape as,

$$p = 1 - \frac{\pi}{4} (d/D)^2 \quad (\text{III.5})$$

and D is the thickness of a ply. Porosity has units of volume of void per unit volume of medium. The average pore diameter, δ was defined as,

$$\delta = (s + D)/2$$

for the geometry in Figure 2. The tortuosity, τ , is a measure of length of travel for a fluid particle per unit thickness of the medium. Referring to the geometry of Figure 2, the

tortuosity depends on the ratio, d/D . The lower limit occurs when d/D equals zero and for the upper limit, d/D equals 1. Carman [9] presents a table of tortuosities for given geometries and particle shapes. For the model, Carman's suggested value of $\tau = 1.4$ was used.

To obtain the pressure differential, ΔP , across the porous plate, Bernoulli's equation was used. The following observations showed this to be a valid assumption. Schlichting [10] points out that for the ratio of u_p/U_∞ in the range of .0001 to .01, the effects of "blowing" or "suction" on the potential flow over the porous plate may be neglected. A typical value of u_p/U_∞ for the model at which $U_\infty = 25$ kt. was .0028. For steady flow over a flat plate, the flow field outside the boundary layer may be described by Bernoulli's equation. This is a direct result of the Navier-Stokes equation. In addition, the pressure gradient across the boundary layer may be taken equal to zero. Therefore, Bernoulli's equation (eq. III.6) may be used to obtain the pressure differential across the plate,

$$\int \frac{P}{\rho_a} dx + \frac{U^2}{2} = \text{constant.} \quad (\text{III.6})$$

The parameters in equation III.6 are defined as follows:

P , pressure; ρ_a , the density of air; U , velocity of the air over the flat plate. For the model, the density of air was approximated by the Ideal Gas law as

$$\rho_a = P/R_a \hat{T}_a \quad (\text{III.7})$$

where R_a is the gas constant for air, \hat{T}_a is the absolute temperature of air, and P is the pressure. Substituting this into equation III.6, gives

$$\int \left(\frac{R_a \hat{T}_a}{P} \right) dP + \frac{U^2}{2} = \text{constant}$$

and upon integrating, the expression becomes

$$R_a \hat{T}_a \ln P + \frac{U^2}{2} = \text{constant}$$

or,

$$R_a \hat{T}_{a1} \ln P_1 + \frac{U_1^2}{2} = R_a \hat{T}_{a2} \ln P_2 + \frac{U_2^2}{2}$$

Letting

$$P_1 = P_\infty, \quad U_1 = 0, \quad \hat{T}_{a1} = \hat{T}_{a2} = \hat{T}_\infty, \quad P_2 = P_L, \quad U_2 = U_\infty$$

and substituting these in above, yields

$$R_a \hat{T}_\infty \ln P_\infty = R_a \hat{T}_\infty \ln P_L + \frac{U_\infty^2}{2}$$

Rearranging the previous expression gives,

$$R_a \hat{T}_\infty \ln (P_\infty / P_L) = \frac{U_\infty^2}{2}$$

Taking the exponential of both sides and solving for P_L results in

$$P_L = P_\infty \exp (-U_\infty^2 / 2 R_a \hat{T}_\infty)$$

From the above expression and noting that $\Delta P = P_L - P_\infty$, ΔP may be expressed as

$$\Delta P = P_\infty [\exp (-U_\infty^2 / 2 R_a \hat{T}_\infty) - 1]$$

Darcy's law in approximate form (eq. III.3) for the model is

$$u_p = - \frac{m}{\mu} \frac{\Delta P}{L}$$

and substituting for ΔP , it follows that,

$$u_{p\infty} = \left\{ \frac{m}{\mu} \frac{P_\infty}{L} [1 - \exp (-U_\infty^2 / 2 R_a \hat{T}_\infty)] \right\} \quad (\text{III.8})$$

where

$$m = \frac{1}{96} P \left(\frac{\delta}{\tau} \right)^2$$

The pore velocity, $u_{p\infty}$ of equation III.8 is for an isothermal medium at ambient temperature, T_∞ . Since the model is to investigate the transient problem, a general expression to obtain pore velocity at different temperatures had to be developed.

Consideration of the continuity equation for one-dimensional steady flow,

$$d(\rho_a u_p)/dx = 0 \quad (\text{III.9})$$

becomes

$$u_p (d\rho_a/dx) + \rho_a (du_p/dx) = 0$$

or

$$u_p (d\rho_a/dx) = - \rho_a (du_p/dx)$$

Multiplying through both sides by dx , the expression becomes,

$$u_p d\rho_a = - \rho_a du_p$$

Separating variables and integrating both sides, gives

$$\int_{\rho_{\infty}}^{\rho_a} \frac{d\omega}{\omega} = - \int_{u_{p\infty}}^{u_p} \frac{d\omega}{\omega}$$

and the integral becomes

$$\ln(\rho_a/\rho_{\infty}) = \ln(u_{p\infty}/u_p)$$

Taking the exponential of both sides, gives

$$\rho_a/\rho_{\infty} = u_{p\infty}/u_p$$

Rearranging, the pore velocity is expressed as

$$u_p = \rho_{\infty} u_{p\infty} / \rho_a \quad (\text{III.10})$$

Referring to the Ideal Gas law for the density of air, and substituting this into equation III.10 gives

$$u_p = (\rho_{\infty} u_{p\infty} R \hat{T}_a) / P \quad (\text{III.11})$$

The pore velocity is now a function of air temperature and pressure. However, in preliminary calculations, the pressure difference, ΔP was small and for the range of parameters of interest, it did not exceed five percent of the magnitude of ambient pressure. Therefore, as a simplification, it was assumed that P equals the ambient pressure in equation III.11,

and the expression becomes

$$u_p = (\rho_\infty u_{p\infty} R_a \hat{T}_a) / P_\infty$$

Noting that $\rho_\infty = P_\infty / R_a T_\infty$, the pore velocity may be expressed as

$$u_p = u_{p\infty} \hat{T}_a / \hat{T}_\infty \quad (\text{III.12})$$

where $u_{p\infty}$ is obtained from equation III.8. \hat{T}_a and \hat{T}_∞ are the absolute temperatures of the air at a point in the interior of the medium and of the environment, respectively.

B. ENERGY EQUATIONS

Here we consider the development of the energy equations. However, before continuing, discussion must be made as to the approach taken for energy balances in porous media. In previous work by Denbigh and Turner [11], and by Colladay and Stepka [12], it was suggested that the temperature of the porous solid and of the fluid be considered equal. This greatly simplifies the formulation of the problem. However, under certain conditions, as shown by Green and Perry [5], the assumption of equal temperatures may not be valid. With recent developments in numerical techniques permitting the solution of non-linear systems, the development of the present model for heat transfer in a porous medium was not restricted

to the assumption of equal temperatures. Therefore, the temperatures of the air and of the porous solid are treated as independent variables in the present formulation.

The model is based on two assumptions. First, due to the small thickness of the graphite fibers, the temperature across each individual fiber was assumed to be constant. Second, for a similar size consideration, the temperature of the air in each individual pore was assumed constant. However, the temperature from fiber to fiber and from pore to pore was not restricted, and was allowed to vary according to the heat transfer mechanisms described next.

To perform energy balances on both the porous solid and on the air, a differential volume of porous material was segregated into respective volumes of constituents, that is, graphite fibers and air (Figure 3). An energy balance may be done on each volume separately. The convention used for the balance is:

$$\begin{array}{ccccccc} \text{Heat into} & & \text{Heat} & & \text{Heat out} & & \text{Increase in} \\ dV & + & \text{Generation} & = & \text{of } dV & + & \text{Internal} \\ & & & & & & \text{Energy} \end{array}$$

where

$$dV = dx \, dy \, dz$$

1. Fiber Heat Transfer Equation

Considering the differential volume, $(1-p)dV$ of graphite fibers, and "smearing" the fibers to form a macroscopically homogeneous material, the heat transfer mechanisms are shown for the x-direction in Figure 4. The heat transfer mechanisms are: q_{cond} , heat conduction through the medium; q_{conv} , convection from the fibers to the air; q_{rad} , radiation transfer from fiber to fiber; $\Delta H r(T_g, \phi)$ heat generation rate per unit volume. ΔH is the enthalpy of formation, and $r(T_g, \phi)$ is the fiber mass consumption rate. This term will be discussed in detail later.

Representing the terms in Figure 4 by Taylor series expansions and combining them with respect to the convention previously stated, the energy balance is

$$q_{\text{cond}} + q_{\text{rad}} + \Delta H r(T_g, \phi) (1-p) dx dy dz = q_{\text{cond}} + \frac{\partial q_{\text{cond}}}{\partial x} dx + q_{\text{rad}} + \frac{\partial q_{\text{rad}}}{\partial x} dx + q_{\text{conv}} + \frac{\partial E}{\partial t} (1-p) dx dy dz$$

Subtracting terms, q_{cond} and q_{rad} from each side and rearranging, the expression becomes (neglecting the higher order terms)

$$\begin{aligned} - \frac{\partial q_{\text{cond}}}{\partial x} dx - \frac{\partial q_{\text{rad}}}{\partial x} dx - q_{\text{conv}} + \Delta H r(T_g, \phi) (1-p) dx dy dz \\ = \frac{\partial E}{\partial t} (1-p) dx dy dz \end{aligned} \quad (\text{III.13})$$

The heat transfer terms in equation III.13 will now be considered.

a. Thermal Conduction

Fourier's law for conduction may be written for the incremental volume as

$$q_{\text{cond}} = -k_g \frac{\partial T_g}{\partial x} dydz \quad (\text{III.14})$$

where k_g is the effective conductivity of the porous solid, and T_g is the temperature of the fibers. There are a variety of models for the effective conductivities of porous media. They depend largely on the geometry and on the nature of the constituents. For the cylindrical shape of the fibers, the empirical relation proposed by Rohsenow [13] was used

$$k_g = k_a \{ 1 - \beta \left[1 + \frac{\gamma}{(1-\gamma)^{1/2}} \ln \left(\frac{1 - (1-\gamma^2)^{1/2}}{\gamma} \right) \right] \} \quad (\text{III.15})$$

for $\gamma^2 < 1$. The parameters of equation III.15 are defined as follows: $\beta = d/D$ (refer to Figure 2), γ is

$$\gamma = \frac{1}{\beta} \left[\frac{\Lambda}{(1-\Lambda)} \right]$$

where $\Lambda = k_a/k'_g$, k_a is the conductivity of the air; and k'_g is the actual conductivity of the graphite in bulk form. Since k_a depends on temperature, k_g was also treated as temperature dependent.

b. Radiation Heat Transfer in Fibers

Radiation heat transfer in the model was represented by an analog to Fourier's law of conduction as

$$q_{\text{rad}} = -k_r \frac{\partial T}{\partial x} dy dz \quad (\text{III.16})$$

where k_r is an equivalent conductivity of the fibers due to radiation. Simple assumptions and approximations may be made to show this. Assuming air to be transparent to radiation, and treating a ply of graphite fibers as an infinite wall, the net heat flux between plies may be written as

$$q_{\text{rad}}'' = \frac{\sigma \epsilon}{(2-\epsilon)} (\hat{T}_{gx}^4 - \hat{T}_{gx+dx}^4) \quad (\text{III.17})$$

where \hat{T}_{gx} and \hat{T}_{gx+dx} are the respective absolute ply temperatures, ϵ is the emissivity of the graphite, and σ is the Stefan-Boltzman constant. Treating T_{gx} as the variable temperature, q_{rad}'' may be expanded in a Taylor series about \hat{T}_{gx+dx} . Neglecting the higher order terms, the series expansion may be written as

$$q_{\text{rad}}'' = \frac{\sigma \epsilon}{2-\epsilon} (\hat{T}_{gx+dx}^4 - \hat{T}_{gx+dx}^4) + \frac{4\sigma \epsilon}{2-\epsilon} \hat{T}_{gx+dx}^3 (\hat{T}_{gx} - \hat{T}_{gx+dx})$$

Simplifying, the above equation becomes,

$$q_{\text{rad}}'' = \frac{4\sigma \epsilon}{2-\epsilon} \hat{T}_{gx+dx}^3 (\hat{T}_{gx} - \hat{T}_{gx+dx}) \quad (\text{III.18})$$

Taking Fourier's law for heat transfer,

$$q''_{\text{rad}} = -k_r \frac{dT_g}{dx}$$

and approximating $\frac{dT_g}{dx}$ with

$$\frac{dT_g}{dx} = \frac{\Delta \hat{T}_g}{\Delta x} = \frac{\hat{T}_{gx+dx} - \hat{T}_{gx}}{\Delta x}$$

q''_{rad} becomes

$$q''_{\text{rad}} = -k_r \frac{(\hat{T}_{gx+dx} - \hat{T}_{gx})}{\Delta x} \quad (\text{III.19})$$

Multiplying the right side of equation III.18 by $\Delta x/\Delta x$, equation III.18 and equation III.19 may be equated

$$q''_{\text{rad}} = -k_r \frac{(\hat{T}_{gx+dx} - \hat{T}_{gx})}{\Delta x} = -\frac{4\sigma\epsilon\Delta x}{2-\epsilon} \hat{T}_{gx+dx}^3 \frac{(\hat{T}_{gx+dx} - \hat{T}_{gx})}{\Delta x}$$

Cancelling terms, k_r becomes

$$k_r = \frac{4\sigma\epsilon\Delta x}{2-\epsilon} \hat{T}_{gx+dx}^3 \quad (\text{III.20})$$

where Δx is now equal to δ , the average pore diameter.

From the close spacing of the fiber layers, the temperature difference will be small as compared to the magnitude of the temperature. Noting this the average absolute temperature of

the fibers, \hat{T}_g may be substituted for \hat{T}_{gx+dx} . The equivalent radiation conductivity expression becomes

$$k_r = \frac{4\sigma\epsilon\delta}{2-\epsilon} \hat{T}_g^3 \quad (\text{III.21})$$

and the radiation heat transfer from fiber to fiber may be represented by,

$$q_{\text{rad}} = -k_r \frac{\partial T_g}{\partial x} = -\frac{4\sigma\epsilon\delta}{2-\epsilon} \hat{T}_g^3 \frac{\partial T_g}{\partial x} dy dz \quad (\text{III.22})$$

If the temperature gradient in the fibers is not large, then equation III.22 will be a good approximation of the radiation heat transfer between the fibers.

c. Convection Heat Transfer

The convection heat transfer term in Figure 4 was treated in a similar manner to that of the one-dimensional fin equation. q_{conv} was introduced as

$$q_{\text{conv}} = h_i (T_g - T_a) dA \quad (\text{III.23})$$

where T_g is the temperature of the graphite, T_a is the temperature of the air, dA is the surface area of graphite in the differential volume, and h_i is the internal convection heat transfer coefficient. An empirical expression in the form of a Colburn j -factor was developed by Yoshida, Ramaswami, Hougen [14]. This was used to determine h_i ,

$$J = \frac{h_i}{c_b G_o} \left[\frac{c_a \mu}{k_a} \right]^{2/3} = .91 \text{ Re}^{-.51} \psi_o \quad (\text{III.24})$$

for $\text{Re} < 50$. c_b is the effective specific heat of the porous medium and is defined as,

$$c_b = p c_a + (1-p) c_g$$

where c_a is the specific heat of air at constant pressure; c_g is the specific heat of graphite; and p is the porosity as defined by equation III.5. G_o is a pseudo mass velocity defined as $G_o = \rho_a u_p p$. Also in equation III.24, μ is the viscosity of air, and k_a is the conductivity of air. The Reynolds number appearing in equation III.24 is defined as

$$\text{Re} = G_o / z \mu \psi_o$$

and is not the same as Re_i defined previously for Darcy's law. z is the surface area of graphite fibers per unit volume, and is determined from geometrical considerations which will be described shortly. The parameter, ψ_o , is a dimensionless shape factor which depends on the geometry of the fibers. For a cylindrical fiber shape, ψ_o is equal to .91. From the assumption of constant porosity, z remains constant. However, the air properties are temperature dependent; therefore, h_i is allowed to vary with temperature.

d. Heat Generation Rate

The reaction rate, $r(T_g, \phi)$, whether based upon the Collision Theory or on the Theory of Absolute Reaction Rates, results in an expression of Arrhenius type,

$$r = A(\hat{T}, \phi) \exp(-E/R\hat{T})$$

where E is the activation energy, R is the universal gas constant, and \hat{T} is absolute temperature. Although E is well defined for the combustion of graphite, $A(\hat{T}, \phi)$ is a function of temperature and concentration and depends upon chemical kinetic theory. Development of a general model for the chemical kinetics is beyond the scope of this work. A less elegant, but useful approach of using a relation obtained experimentally was taken. A relation derived from the work of Parker and Hottel [15] was used to predict the combustion rate of graphite fibers,

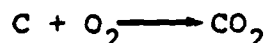
$$r = 4.014 \times 10^7 R_A \hat{T}_g^{1/2} Y \phi \exp\left(\frac{-39,883}{\hat{T}_g}\right) \frac{\text{lbm}}{\text{ft}^3\text{-hr}} \quad (\text{III.25})$$

The development of equation III.25 from the original work may be found in the appendix. This expression assumes a simple first-order reaction for the combustion of graphite in air. However, Frank-Kamenetskii [3] has further refined Parker and Hottel's expression to yield for the present model,

$$r = 4.014 \times 10^7 R_A T_g^{1/2} y \phi^n \exp\left(\frac{-39,883}{T_g}\right) \frac{\text{lbm}}{\text{ft}^3\text{-hr}} \quad (\text{III.26})$$

The combustion is now characterized as an nth order reaction, where n is in the range of 1/3 to 2/3. This form of the reaction rate expression better approximates Parker and Hottel's experimental data. For the analysis, n was chosen to be 1/2. However, it should be pointed out that the behavior of the reaction varies significantly within the range of n proposed by Frank-Kamenetskii.

In limiting the model to the kinetic regime of combustion, it was assumed that the dominant chemical reaction is



This is an idealized treatment of the reaction that actually takes place. Kanury [16] states that, the actual reaction is more complex, yielding various concentrations of carbon dioxide and carbon monoxide, depending on the temperature. Noting the abundant oxygen supply present in the kinetic regime, it is reasonable that the leaner oxide is the prevalent by-product of combustion. The fuel-oxygen ratio, f, for this mechanism is 12/32. Carbon monoxide may be formed when there is little free-oxygen present, such as, during combustion in the diffusion regime. The stoichiometric

fuel-oxygen ratio, $f = 12/16$, for this mechanism is naturally greater. To obtain the heat generation rate, the reaction rate, r , was multiplied by the enthalpy of formation, ΔH , of carbon dioxide. ΔH has units of Btu per lbm of graphite consumed.

e. Change in Internal Energy

The last term of the graphite energy equation, the rate of change of internal energy, $\frac{\partial E}{\partial t}$, results by setting $E = \rho_g c_g T_g$. Thus,

$$\frac{\partial E}{\partial t}(1-p)dxdydz = (1-p)\rho_g c_g \frac{\partial T_g}{\partial t} dxdydz \quad (\text{III.27})$$

where ρ_g is the density of graphite in bulk; c_g is the specific heat of graphite; and p is the porosity.

The heat transfer mechanisms for the graphite fibers, equations III.14, III.16, III.23, III.26, III.27 are substituted into equation III.13 which upon dividing through by $dV = dxdydz$ yields the heat transfer equation for the fibers,

$$\begin{aligned} (1-p) \frac{\partial}{\partial x} \left(k_g \frac{\partial T_g}{\partial x} \right) + (1-p) \frac{\partial}{\partial x} \left(k_r \frac{\partial T_g}{\partial x} \right) - h_i \frac{dA}{dV} (T_g - T_a) \\ + (1-p) \Delta H r(T_g, \phi) = (1-p) \rho_g c_g \frac{\partial T_g}{\partial t} \end{aligned}$$

The coefficient, $(1-p)$, accounts for the fact that not all of the volume of porous medium is comprised of graphite.

Dividing through by $(1-p)$, combining the first two terms, and defining dA/dV as z , the surface area of graphite per unit volume, the expression becomes

$$\begin{aligned} \frac{\partial}{\partial x}[(k_g + k_r) \frac{\partial T_g}{\partial x}] - \frac{h_i z}{(1-p)}(T_g - T_a) + \Delta H_r(T_g, \phi) \\ = \rho_g c_g \frac{\partial T_g}{\partial t} \end{aligned} \quad (\text{III.28})$$

The parameter, z , is obtained from geometry considerations. For a cylindrical fiber shape, the expression for z is,

$$z = \pi d / 2D^2 \quad (\text{III.29})$$

The one-half factor in equation III.29 accounts for the uncertainty of the actual amount of exposed fiber surface area, which resulted from the initial combustion of epoxy. The non-dimensionalization of equation III.28 is presented in Appendix A.

2. Internal Flow Heat Transfer Equation

The energy balance on the internal flow is obtained by a procedure similar to the energy balance on graphite. Figure 5 presents a "smeared" differential volume of air, $p dV$, which shows the heat transfer mechanisms. The heat transfer mechanisms are: q_{cond} , heat conduction through the air; q_{conv} , convection from the fibers to the air; $\dot{m}_a \hat{h}$,

energy transport due to the air flow, where \hat{h} is the enthalpy of the air.

Performing the energy balance (neglecting the higher order terms) yields,

$$q_{\text{cond}} + \dot{m}_a \hat{h} + q_{\text{conv}} = q_{\text{cond}} + \frac{\partial q_{\text{cond}}}{\partial x} dx + \dot{m}_a \hat{h} + \dot{m}_a \frac{\partial \hat{h}}{\partial x} dx + \frac{\partial E}{\partial t} p dx dy dz \quad (\text{III.30})$$

Cancelling terms and rearranging, the expression becomes,

$$- \frac{\partial q_{\text{cond}}}{\partial x} dx - \dot{m}_a \frac{\partial \hat{h}}{\partial x} dx + q_{\text{conv}} = \frac{\partial E}{\partial t} p dx dy dz \quad (\text{III.31})$$

a. Thermal Conduction

As before, q_{cond} was replaced by Fourier's law of heat conduction in the form,

$$q_{\text{cond}} = - k_a \frac{\partial T_a}{\partial x} dy dz \quad (\text{III.32})$$

where k_a is the conductivity of air.

b. Energy Transport by Flow

Using the perfect gas assumption for air, the enthalpy \hat{h} was expressed as,

$$d\hat{h} = c_a dT_a$$

where c_a is the specific heat of air at constant pressure. The specific heat is treated as constant since it does not vary appreciably over the range of temperatures associated with the problem under investigation. It follows that,

$$\frac{\partial \hat{h}}{\partial x} = c_a \frac{\partial T_a}{\partial x} \quad (\text{III.33})$$

Assuming the effects of the combustion by-products on air are negligible, continuity considerations give the mass flow as,

$$\dot{m}_a = \rho_a u_p dy dz \quad (\text{III.34})$$

where the density of air and the pore velocity are evaluated at ambient conditions.

c. Convection Heat Transfer

The convection heat transfer, q_{conv} given by equation III.23, with h_i obtained from equation III.24, becomes

$$q_{\text{conv}} = h_i (T_g - T_a) dA \quad (\text{III.35})$$

d. Change in Internal Energy

For a perfect gas, the internal energy is,

$$dE = \rho_a c_a dT_a$$

where c_a is the specific heat of air at constant pressure.

From this it follows that

$$\frac{\partial E}{\partial t} p \, dx dy dz = \rho_a c_a \frac{\partial T_a}{\partial x} p \, dx dy dz \quad (\text{III.36})$$

Substituting equations III.32-III.36 into equation III.31, the heat transfer equation for the internal flow becomes,

$$\begin{aligned} \frac{\partial}{\partial x} (k_a \frac{\partial T_a}{\partial x}) p \, dx dy dz - \dot{m}_a c_a \frac{\partial T_a}{\partial x} p \, dx dy dz \\ + h_i \, dA (T_g - T_a) = \rho_a c_a \frac{\partial T_a}{\partial t} p \, dx dy dz \end{aligned}$$

As in the energy equation for the fibers, the porosity, p , accounts for the fact that some of the volume of the porous medium is not air. Dividing the last equation through by $p \, dx dy dz$ and letting z denote $dA/dx dy dz$, yields

$$\begin{aligned} \frac{\partial}{\partial x} (k_a \frac{\partial T_a}{\partial x}) - \dot{m}_a c_p \frac{\partial T_a}{\partial x} + \frac{h_i z}{p} (T_g - T_a) \\ = \rho_a c_a \frac{\partial T_a}{\partial t} \end{aligned} \quad (\text{III.37})$$

Non-dimensionalization of equation III.37 may be found in Appendix A.

3. Oxygen Transport Equation

The final consideration in the formulation of the model is the mass transport of oxygen. The mass transport equation is obtained by a mass balance on a differential volume of porous medium. In accordance with convention, the mass balance is given by

$$\text{Oxygen into } \frac{dV}{dV} = \text{Oxygen out of } dV + \text{Oxygen Consumption} + \text{Oxygen Accumulation}$$

Figure 6 presents a differential volume, pdV , showing the relevant molecule-mass transport mechanisms. The mass transport mechanisms are: \dot{m}_B is the molecular diffusion; \dot{m}_C is the convective transport due to mass flow; $\frac{1}{f}r(T_g, \phi)$ is the consumption of oxygen due to combustion; r is the reaction rate, and f is the stoichiometric ratio of the reaction. Representing the terms in Figure 6 by Taylor series expansions, the molecule-mass balance becomes (neglecting higher order terms),

$$\begin{aligned} \dot{m}_B + \dot{m}_C &= \dot{m}_B + \frac{\partial \dot{m}_B}{\partial x} dx + \dot{m}_C + \frac{\partial \dot{m}_C}{\partial x} dx \\ &+ \frac{1}{f}r(T_g, \phi) p dx dy dz + \frac{\partial \phi}{\partial t} p dx dy dz \end{aligned} \quad (\text{III.38})$$

Upon cancelling terms and rearranging, equation III.38 becomes

$$- \frac{\partial \dot{m}_B}{\partial x} dx - \frac{\partial \dot{m}_C}{\partial x} dx - \frac{1}{F} r(T_g, \phi) p dx dy dz = \frac{\partial \phi}{\partial t} p dx dy dz \quad (\text{III.39})$$

where ϕ is the concentration of oxygen. The individual mass transfer terms in equation III.39 will now be developed.

a. Molecular Diffusion

Molecular diffusion \dot{m}_B , is given by Fick's law,

$$\dot{m}_B = - B \frac{\partial \phi}{\partial x} dy dz \quad (\text{III.40})$$

where B is the diffusivity of oxygen into the porous medium.

The diffusion of gases in porous media is limited by two factors. One is the collision of the gas molecules with other molecules, and the second is the collision of the gas molecules with the solid pore walls. This second phenomenon is discussed by Bennett and Myers [17] and is referred to as Knudsen diffusion. To establish which behavior dominates, the mean free path of the gas (in this case, oxygen), must be calculated. Using the expression given by Treybal [18],

$$w = (3.2\mu/P) (RT/2\pi g_c M)^{1/2}$$

where g_c is the gravitational constant, the value obtained for mean free path, w , is smaller than 0.1 δ . Thus, the collision of the oxygen molecules with those of air will restrict the diffusion process. On the contrary, if the pore

diameter is smaller than the mean free path, then the collision of the molecules with the solid walls will be the limiting factor. In the intermediate case, the mean free path and the pore diameter are of the same order of magnitude. In this case, Bennett and Myers [17] proposed the following expression be used to obtain a value of diffusivity,

$$\frac{1}{B_R} = \frac{1}{B_g} + \frac{1}{B_w} \quad (\text{III.41})$$

where B_R is the resulting diffusivity; B_g is the diffusivity based on molecule-molecule collisions; and B_w is the diffusivity based on molecule-pore wall collisions.

For the problem under investigation here, preliminary calculations of the mean free path of the oxygen showed that diffusion is primarily of the inter-molecular collision type. With respect to this, and knowing that molecular diffusion is highly temperature dependent, the diffusivity, B^* was obtained from an expression presented by Gilliland [19].

$$B^* = 435.7 \frac{\hat{T}_a^{3/2}}{P} (V_a^{1/3} + V_{O_2}^{1/3})^{-2} (M_a^{-1} + M_{O_2}^{-1})^{1/2} \text{ cm}^2/\text{s} \quad (\text{III.42})$$

where P is the absolute pressure; V_a and V_{O_2} are the molecular volumes of air and oxygen respectively; M_a and M_{O_2} are the molecular weights of air and oxygen, respectively, and B^* is the diffusivity. For this expression, \hat{T}_a is in degrees

Kelvin, and B^* has the units of cm^2/s . As a result of tortuosity and porosity affecting the process, Denbigh and Turner [11] proposed that the effective molecular diffusivity for a porous medium is given by

$$B_e = pB^*/\tau.$$

The porosity p accounts for the void in a differential cross-section.

b. Convective Transport

The convective term in equation III.39 is given by

$$\dot{m}_c = pu_p \phi dydz \quad (\text{III.43})$$

The pore velocity u_p is a temperature dependent variable, and is so treated.

c. Consumption Rate

The reaction rate term, $r(T_g, \phi)$ was discussed previously as equation III.26. The consumption rate of oxygen is determined by multiplying r by $1/f$.

Substituting equations III.40 and III.43 into equation III.39, the oxygen transport equation becomes,

$$\begin{aligned} \frac{\partial}{\partial x} \left(\frac{B^*}{\tau} \frac{\partial \phi}{\partial x} \right) p dx dy dz - \frac{\partial}{\partial x} (u_p \phi) p dx dy dz \\ - \left(\frac{1}{f} \right) r(T_g, \phi) p dx dy dz = \frac{\partial \phi}{\partial t} p dx dy dz \end{aligned}$$

Dividing both sides by $\rho dx dy dz$, and letting $B = B^*/\tau$, the expression becomes

$$\frac{\partial}{\partial x} \left(B \frac{\partial \phi}{\partial x} \right) - \frac{\partial}{\partial x} (u_p \phi) - \left(\frac{1}{f} \right) r(T_g, \phi) = \frac{\partial \phi}{\partial t} . \quad (\text{III.44})$$

Expanding the second term of equation III.44,

$$\frac{\partial}{\partial x} (u_p \phi) = u_p \frac{\partial \phi}{\partial x} + \frac{\partial u_p}{\partial x} \phi$$

and noting that u_p depends on T_a from equation III.12, the expression yields

$$\frac{\partial}{\partial x} (u_p \phi) = u_p \frac{\partial \phi}{\partial x} + \frac{\partial u_p}{\partial T_a} \frac{\partial T_a}{\partial x} \phi . \quad (\text{III.45})$$

$\partial u_p / \partial T_a$ is obtained from equation III.12.

Substituting equation III.45 into equation III.44, the oxygen transport equation becomes,

$$\frac{\partial}{\partial x} \left(B \frac{\partial \phi}{\partial x} \right) - u_p \frac{\partial \phi}{\partial x} - \frac{\partial u_p}{\partial T_a} \frac{\partial T_a}{\partial x} \phi - \left(\frac{1}{f} \right) r(t_g, \phi) = \frac{\partial \phi}{\partial t} \quad (\text{III.46})$$

In contrast with the heat transfer equations, mass balance does not depend on porosity. However, porosity does influence the oxygen concentration by appearing in the boundary conditions. Non-dimensionalization of equation III.46 is presented in Appendix A.

IV. BOUNDARY CONDITIONS

It was intended that boundary conditions be imposed which simulate the composite plate "burn" experiments of Fontenot [1]. However, for a one-dimensional model, the boundary conditions can only be approximated at best. The difficulty is associated with the existence of momentum and thermal boundary layers on the exterior surface of the porous plate. Complications also arise from the "blowing and suction" effects which are caused by the flow through the plate.

The following boundary conditions provide a reasonable model for the one-dimensional problem,

$$(k_g + k_r) \frac{\partial T_g}{\partial x} = h_1 (T_g - T_\infty) + \sigma \epsilon (\hat{T}_g^4 - \hat{T}_\infty^4) \quad \text{at } x = 0 \quad (\text{IV.1})$$

$$(k_g + k_r) \frac{\partial T_g}{\partial x} = -h_2 (T_g - T_\infty) - \sigma \epsilon (\hat{T}_g^4 - \hat{T}_\infty^4) \quad \text{at } x = L \quad (\text{IV.2})$$

$$T_a = T_\infty \quad \text{at } x = 0 \quad (\text{IV.3})$$

$$\frac{\partial T_a}{\partial x} = \frac{\partial T_g}{\partial x} \quad \text{at } x = L \quad (\text{IV.4})$$

$$B \frac{\partial \phi}{\partial x} = u_p (\phi - p\phi_\infty) \quad \text{at } x = 0 \quad (\text{IV.5})$$

$$\frac{\partial \phi}{\partial x} = 0 \quad \text{at } x = L \quad (\text{IV.6})$$

Boundary conditions IV.1 and IV.2 account for convection and radiation heat transfer from the porous solid. With an influx of air at $x = 0$, the heat transfer coefficient, h_1 , will depend on the magnitude of the flow entering the plate. Neglecting "blowing and suction" effects, several empirical expressions based on free convection were used to obtain a heat transfer coefficient at $x = 0$. These expressions yielded a range of values for h_1 from 1 to 3 Btu/hr.ft².F. As an approximation, h_1 was taken as the average value, 2.0 Btu/hr.ft².F. However, choosing h_1 as any value in the above range did not affect the results of the analysis.

The magnitude of the forced convection heat transfer coefficient at $x = L$, h_2 , varies in a direction parallel to that of the external flow, U_∞ . In addition, h_2 depends on the efflux of the gas at the surface. To simplify the analysis, h_2 was approximated by the relation for a smooth flat plate given by Holman [20] as

$$h_2 = .664 \frac{k_a}{L^*} Pr^{1/3} Re^{1/2} \quad (IV.7)$$

for laminar flow, where Pr is the Prandtl number and L^* is a reference length, arbitrarily taken as unity. For turbulent flow,

$$h_2 = \frac{k_a}{L^*} Pr^{1/3} (.037 Re^{.8} - 850) . \quad (IV.8)$$

Kays [21] provides an alternate scheme for treating boundary layers and "blowing and suction" effects.

Boundary condition IV.3 accounts for the air entering the porous plate at ambient temperature. The Dankwerts boundary condition proposed by Riaz [6] which accounts for conduction-convection interaction, is a more reasonable simulation.

The boundary condition at $x = L$ for the air heat transfer equation appears to be a reasonable one. It follows the behavior observed in the interior of the plate and does not fix the temperature of the air at the wall. The boundary condition, $\partial T_a / \partial x = 0$, used initially provided results similar to those obtained using equation IV.4.

Boundary conditions IV.5 and IV.6 are Dankwert conditions [22] for flow through porous media. A convincing discussion for the Dankwerts conditions is given by Bischoff [23]. A brief summary of the discussion is presented in Appendix D.

V. FINITE ELEMENT METHOD

A. GALERKIN FORMULATION

A Galerkin formulation of the Finite Element Method was used to obtain solutions of the field equations. A convenient form of the field equations was used in the formulation. These equations are presented in Appendix A.

graphite energy equation

$$\frac{\partial}{\partial \eta} (\lambda_1 \frac{\partial \theta}{\partial \eta}) - \lambda_2 (\theta - r) + \lambda_3 r (T_g, \phi) = \lambda_4 \frac{\partial \theta}{\partial t} \quad (V.1)$$

air energy equation

$$\frac{\partial}{\partial \eta} (v_1 \frac{\partial \Gamma}{\partial \eta}) - v_2 \frac{\partial \Gamma}{\partial \eta} + v_3 (\theta - r) = v_4 \frac{\partial \Gamma}{\partial t} \quad (V.2)$$

oxygen diffusion equation

$$\frac{\partial}{\partial \eta} (\omega_1 \frac{\partial \phi}{\partial \eta}) - \omega_2 \frac{\partial \phi}{\partial \eta} - \omega_3 \frac{\partial \Gamma}{\partial \eta} \phi - \omega_4 r (T_g, \phi) = \omega_5 \frac{\partial \phi}{\partial t} \quad (V.3)$$

where the coefficients are defined in Appendix A.

Field equations III.28, III.37 and III.46 subject to boundary conditions, IV.1 - IV.6, and initial conditions define the problem. The closed domain (0,L) was partitioned into (n-1) contiguous elements of variable length ℓ_i , $i = 1, \dots, (n-1)$. This defines an n nodal point model. The three

non-dimensional field variables θ , r , ϕ were approximated by

$$\theta(n,t) \approx \psi_1(n,t) = \sum G_i(n) \theta_i(t) \quad (V.4)$$

$$r(n,t) \approx \psi_2(n,t) = \sum G_i(n) r_i(t) \quad (V.5)$$

$$\phi(n,t) \approx \psi_3(n,t) = \sum G_i(n) \phi_i(t) \quad (V.6)$$

where G_i , for $i = 1, \dots, n$, is a set of specified basis functions with local support, and the sets $\{\theta_i, r_i, \phi_i; i = 1, \dots, n\}$ are the solution coefficients to be determined. The G_i were selected to satisfy the condition $G_i(n_j) = \delta_{ij}$, where the kronecker delta δ_{ij} is defined by $\delta_{ij} = 1$ for $i = j$, and $\delta_{ij} = 0$ for $i \neq j$. As a result, θ , r , and ϕ are the values ψ_1, ψ_2, ψ_3 at the nodal points (i.e., $\theta_i(t) = \psi_1(n_i, t)$).

Linear interpolation functions (Figure 7) were used as the basis functions. These are the lowest polynomial functions which provide the necessary function continuity.

As a measure of error, a residual function, r_i , is defined for each field equation by

$$r_i(n,t) = \Lambda_i(\psi) - \dot{\psi}_i \quad i = 1, 2, 3 \quad (V.7)$$

where Λ_i denotes the spatial operator of the i th equation. For convenience, the following convention for differentiation

is adopted,

$$\frac{\partial ()}{\partial \eta} = ()'$$

$$\frac{\partial^2 ()}{\partial \eta^2} = ()''$$

$$\frac{\partial ()}{\partial t} = ()\dot{ }$$

For field equations V.1, V.2, and V.3 the residuals are:

$$\begin{aligned} r_1 = & [\lambda_1(\theta, \underline{r}) \sum_{i=1}^n G_i' \theta_i]' - \lambda_2(\underline{r}) \sum_{i=1}^n G_i (\theta_i - r_i) \\ & + \lambda_3 r(\theta, \underline{\phi}) - \lambda_4 \sum_{i=1}^n G_i \dot{\theta}_i \end{aligned} \quad (V.8)$$

$$\begin{aligned} r_2 = & [v_1(\underline{r}) \sum_{i=1}^n G_i' r_i]' - v_2 \sum_{i=1}^n G_i' r_i + v_3(\underline{r}) \sum_{i=1}^n G_i (\theta_i - r_i) \\ & - v_4(\underline{r}) \sum_{i=1}^n G_i \dot{r}_i \end{aligned} \quad (V.9)$$

$$\begin{aligned} r_3 = & [\omega_1(\underline{r}) \sum_{i=1}^n G_i' \phi_i]' - \omega_2(\underline{r}) \sum_{i=1}^n G_i' \phi_i - \omega_3(\underline{r}) \sum_{i=1}^n G_i r_i G_i \phi_i \\ & - \omega_4 r(\theta, \underline{\phi}) - \omega_5 \sum_{i=1}^n G_i \dot{\phi}_i \end{aligned} \quad (V.10)$$

where the coefficients multiplying the response variables are themselves functions of the response variables, and thus the equations are nonlinear. In accordance with the Galerkin method, the final system of ordinary differential equations was obtained by setting each residual, r_j , orthogonal to each basis function, G_i , that is

$$\int_0^1 G_i r_j dn = 0 \quad \begin{matrix} i = 1, 2, \dots, n; \\ j = 1, 2, \dots, n \end{matrix} \quad (V.11)$$

The $3n$ ordinary differential equations given by equations V.11 retain the character of the original set of partial differential equations. Thus linear field equations transform to matrix operators and nonlinear, coupled field operators become nonlinear, coupled algebraic operators. Incorporation of the boundary conditions resulted in $3n$ nonlinear, coupled ordinary differential equations

$$\underline{\dot{A}}(t) \underline{\psi}(\theta, r, \phi) + \underline{F}(t) = \underline{B}(t) \underline{\dot{\psi}} \quad (V.12)$$

subject to initial conditions, where \underline{B} is a $3n \times 3n$ matrix, \underline{A} is the operator associated with the field operator Λ_i in expression V.7, and $\underline{F}(t)$ is an excitation vector.

Adopting the convention,

$$\langle G_i \rangle \{ \psi_i \} = \sum_{i=1}^n G_i \psi_i$$

and applying the operation of expression V.11 with an integration by parts on the second order derivatives gives,

$$\begin{aligned} \{G_i\} \lambda_1 \langle G_i \rangle' \{\theta\} \Big|_0^1 - \bar{\lambda}_1 \int_0^1 \{G_i\}' \langle G_j \rangle' d\eta\{\theta\} \\ - \bar{\lambda}_2 \int_0^1 \{G_i\} \langle G_j \rangle d\eta\{\theta\} + \bar{\lambda}_2 \int_0^1 \{G_i\} \langle G_j \rangle d\eta\{r\} \end{aligned} \quad (V.13)$$

$$+ \bar{\lambda}_3 \int_0^1 \{G_i\} d\eta r(\theta, \phi) = \bar{\lambda}_4 \int_0^1 \{G_i\} \langle G_j \rangle d\eta\{\dot{\theta}\}$$

$$\begin{aligned} \{G_i\} \bar{\nu}_1 \langle G_j \rangle' \{r\} \Big|_0^1 - \bar{\nu}_1 \int_0^1 \{G_i\}' \langle G_j \rangle' d\eta\{r\} \\ - \bar{\nu}_2 \int_0^1 \{G_i\} \langle G_j \rangle' d\eta\{r\} + \bar{\nu}_3 \int_0^1 \{G_i\} \langle G_j \rangle d\eta\{\theta\} \end{aligned} \quad (V.14)$$

$$- \bar{\nu}_3 \int_0^1 \{G_i\} \langle G_j \rangle d\eta\{r\} = \bar{\nu}_4 \int_0^1 \{G_i\} \langle G_j \rangle d\eta\{\dot{r}\}$$

$$\begin{aligned}
& \{G_i\} \omega_1 \langle G_j \rangle' \{\phi\} \Big|_0^1 - \bar{\omega}_1 \int_0^1 \{G_i\}' \langle G_j \rangle' d\eta \{\phi\} \\
& - \bar{\omega}_2 \int_0^1 \{G_i\} \langle G_j \rangle' d\eta \{\phi\} - \bar{\omega}_3 \int_0^1 \{G_i\} \langle G_j \rangle' \{r\} \langle G_j \rangle d\eta \{\phi\} \\
& - \bar{\omega}_4 \int_0^1 \{G_i\} d\eta r(\theta, \phi) = \bar{\omega}_5 \int_0^1 \{G_i\} \langle G_j \rangle d\eta \{\phi\} \quad (V.15)
\end{aligned}$$

The first term in each of the above expressions is a boundary term which permits the incorporation of natural boundary conditions which will be shown in Section V.B. Coefficients $\bar{\lambda}$, $\bar{\nu}$, $\bar{\omega}$ are variable-dependent properties, and were taken as the average value of the properties over an element. In the limit, as the elements get smaller (i.e., $n \rightarrow \infty$), the average values converge to the exact values.

Inspection of expression V.13, V.14, V.15 shows the five operators,

$$\int_0^1 \{G_i\}' \langle G_j \rangle' d\eta \quad (V.16)$$

$$\int_0^1 \{G_i\} \langle G_j \rangle' d\eta \quad (V.17)$$

$$\int_0^1 \{G_i\} \langle G_j \rangle dn \quad (V.18)$$

$$\int_0^1 \{G_i\} \langle G_j \rangle' \{\psi\} \langle G_j \rangle dn \quad (V.19)$$

$$\int_0^1 \{G_i\} dn \quad (V.20)$$

To formulate these operators, the global shape function, G_i , was defined on the local level by

$$G_i = g_1^{(i-1)} \oplus g_2^{(i)} \quad (V.21)$$

where g_1 and g_2 were defined by

$$g_1^{(e)} = \begin{cases} (1 - \frac{\xi}{l_e}) & \text{for } \xi \text{ in element } (e) \\ 0 & \text{for } \xi \text{ not in element } (e) \end{cases}$$

$$g_2^{(e)} = \begin{cases} \frac{\xi}{l_e} & \text{for } \xi \text{ in element } (e) \\ 0 & \text{for } \xi \text{ not in element } (e) \end{cases}$$

and l_e is the length of the eth element. The \oplus notation in expression V.21 means that G_i is the union of $g_1^{(i-1)}$ and $g_2^{(i)}$. The local (element) shape functions have the following properties,

$$(i) \quad \int_0^{l_e} g_i^{(j)} g_k^{(m)} = 0 \quad \text{if } j \neq m$$

$$(ii) \quad g_i^{(e)}(\eta_j) = \delta_{ij} = \begin{matrix} 1 & \text{if } i = j \\ 0 & \text{if } i \neq j \end{matrix}$$

Having defined the local shape functions, the elemental matrix operators contributing to the global matrix operators V.16 through V.20 are,

$$\int_0^1 \{G_i\}' \langle G_j \rangle' d\eta \Rightarrow \frac{1}{l_e} \begin{bmatrix} 1 & -1 \\ -1 & 1 \end{bmatrix} \quad (V.16')$$

$$\int_0^1 \{G_i\} \langle G_j \rangle d\eta \Rightarrow \frac{1}{2} \begin{bmatrix} -1 & 1 \\ -1 & 1 \end{bmatrix} \quad (V.17')$$

$$\int_0^1 \{G_i\} \langle G_j \rangle dn \quad \Rightarrow \quad \frac{\ell e}{6} \begin{bmatrix} 2 & 1 \\ 1 & 2 \end{bmatrix} \quad (V.18')$$

$$\int_0^1 \{G_i\} \langle G_j \rangle \{\psi\} \langle G_j \rangle dn \quad \Rightarrow \quad \frac{-1}{3} \begin{bmatrix} (\psi_{i-1} - \psi_i) \left(\frac{\psi_{i-1} - \psi_i}{2} \right) \\ \left(\frac{\psi_{i-1} - \psi_i}{2} \right) (\psi_{i-1} - \psi_i) \end{bmatrix} \quad (V.19')$$

$$\int_0^1 \{G_i\} dn \quad \Rightarrow \quad \frac{\ell e}{2} \begin{pmatrix} 1 \\ 1 \end{pmatrix} \quad (V.20')$$

The derivations of these operators are shown in Appendix E.

Since there is extensive coupling in the field equations and there are three degrees of freedom at each nodal point, the numbering scheme for the system matrices was important. To minimize the bandwidth of the matrices, the numbering scheme represented in Figure 8 was used.

Figure 9 represents the matrix $\underline{A}(t)$ of expression V.12 for any three successive nodal points. The distribution of the elemental matrices for the FEM operators is shown, as well as the possible locations for the coupling of the field equations over an element. In addition, Figure 9 shows the bandwidth that would be observed for any n-1 element solution. For this scheme, the bandwidth is nine. If coupling is not present, the bandwidth is seven. Figure 9 reflects the extensive coupling that is present in the model. All the

matrix elemental locations are filled except those which are shaded in.

B. IMPLEMENTATION OF BOUNDARY CONDITIONS

Having formulated the system matrices for the field equations, treatment of the boundary conditions will now be discussed. Each field equation is considered individually.

1. Fiber Heat Transfer Equation

The fiber heat transfer boundary conditions in non-dimensional form from Appendix A are

$$\eta = 0 \quad \lambda_1 \frac{\partial \theta}{\partial \eta} = h_1 L(\theta - 1) + \frac{\sigma \epsilon L}{T_\infty} (\hat{T}_g^4 - \hat{T}_\infty^4) \quad (V.22)$$

$$\eta = 1 \quad \lambda_1 \frac{\partial \theta}{\partial \eta} = -h_2 L(\theta - 1) - \frac{\sigma \epsilon L}{T_\infty} (\hat{T}_g^4 - \hat{T}_\infty^4) \quad (V.23)$$

Since the first term in expression V.13 is

$$\{G_i\} \lambda_1 \langle G_j \rangle' \{ \theta \} \bigg|_0^1$$

or in analogous form

$$\lambda_1 \frac{\partial \theta}{\partial \eta} \bigg|_0^1 \quad (V.24)$$

natural boundary conditions V.22 and V.23 may be directly substituted in equation V.24.

The response dependent parameters, h_1 , h_2 , \hat{T}_g , changing with time, are evaluated at the previous time step. Thus, the boundary conditions are incorporated in the system matrices as follows,

- (1) $-h_1 L$: added to the stiffness matrix $\underline{A}(t)$ at location $A_{1,1}$
- (2) $h_1 L - \frac{\sigma \epsilon L}{T_\infty} (\hat{T}_g^4 - \hat{T}_\infty^4)$: added to the excitation vector $\underline{F}(t)$ at location F_1
- (3) $-h_2 L$: added to the stiffness matrix $\underline{A}(t)$ at location $A_{3n-2,3n-2}$
- (4) $h_2 L - \frac{\sigma \epsilon L}{T_\infty} (\hat{T}_g^4 - \hat{T}_\infty^4)$: added to the excitation vector $\underline{F}(t)$ at location F_{3n-2}

2. Internal Flow Heat Transfer Equation

The non-dimensional boundary conditions presented in Appendix A for the air energy equation are

$$\eta = 0 \quad \Gamma = 1 \quad (V.25)$$

$$\eta = 1 \quad \frac{\partial \Gamma}{\partial \eta} = \frac{\partial \Theta}{\partial \eta} \quad (V.26)$$

The essential boundary condition at $\eta = 0$, $\Gamma(\eta = 0) = 1$ is imposed in the Galerkin equation as follows. The $A_{2,i}$ row of the $\underline{A}(t)$ matrix, the $B_{2,i}$ row and the $B_{1,2}$ column of the \underline{B} matrix, and the F_2 location of the excitation vector, $\underline{F}(t)$,

are all set equal to zero. The $B_{2,2}$ location of the B matrix is then set equal to one. The natural boundary condition at $\eta = 1$ for the air heat transfer equation was treated in the same manner as that of the fiber heat transfer equation. Foregoing the individual steps the boundary condition is implemented by

- (1) $-\frac{h_2 L v_1}{\lambda_1}$: added to the stiffness matrix $A(t)$ at location $A_{3n-1,3n-2}$
- (2) $\frac{h_2 L v_1}{\lambda_1} - \frac{\sigma \epsilon v_1}{T_\infty \lambda_1} (\hat{T}_g^4 - \hat{T}_\infty^4)$: added to the excitation vector $F(t)$ at location F_2 .

3. Oxygen Transport Equation

For the oxygen diffusion equation, the boundary conditions in non-dimensional form from Appendix A are:

$$\eta = 0 \quad \omega_1 \frac{\partial \phi}{\partial \eta} = \omega_2 (\phi - p) \quad (V.27)$$

$$\eta = 1 \quad \frac{\partial \phi}{\partial \eta} = 0 \quad (V.28)$$

Since these are both natural boundary conditions, they were substituted for the first term in expression V.15 at $\eta = 0$ and $\eta = 1$, respectively. Coefficients ω_1 and ω_2 are evaluated at the previous time step. The boundary conditions are implemented by adding

(1) $-\omega_2$: to the stiffness matrix $\underline{A}(t)$ at location $A_{3,3}$

and

(2) ω_{2p} : to the excitation vector $\underline{F}(t)$ at location F_3

This concludes the discussion for the implementation of the boundary conditions. A word of caution is in order. After each time step integration, the time-dependent coefficients of the boundary conditions (i.e., h_1 , h_2 , λ , ν , ω) are reevaluated. Before incorporating the updated coefficients into the stiffness matrix $\underline{A}(t)$, the previous values must be subtracted out. The results of not taking this into account will be obvious.

The implicit system of ordinary differential equations was integrated numerically by a modified implicit-Gear method developed by Franke [2]. The time-dependent coefficients of the FEM operators in expression V.13, V.14, and V.15 were updated at the previous time. The reaction rate term (III.26) was also evaluated at the previous time, and appears in the excitation vector $\underline{F}(t)$. In this way, the final system of ordinary differential equations was

$$\underline{A}(t)\underline{\psi} + \underline{F}(t) = \underline{B} \dot{\underline{\psi}}$$

where \underline{A} and \underline{B} are $(3n \times 3n)$ matrices of temperature dependent

coefficients. \underline{F} is a $(3n \times 1)$ vector arising partly from the reaction rate terms and partly from the boundary conditions. As noted, the elements of \underline{F} are dependent on both temperature and oxygen concentration.

VI. RESULTS AND CONCLUSION

A. NUMERICAL CONSIDERATIONS

The input parameters which were varied in the computer analysis include (1) plate thickness, L , (2) fiber diameter, d , and (3) air flow rate, U_{∞} . Other parameters which could be varied are the ply thickness, D , ambient temperature, T_{∞} , and fiber emissivity, ϵ . One set of initial conditions was used for the analysis. These are shown in Figures 10 and 11. For this initial effort, the actual initial conditions were not of prime consideration. The selection of initial conditions of Figures 10 and 11 will be discussed in Section VI.C. The finite element program calculates the remaining system parameters such as permeability, porosity, pressure differential, and the response variables as functions of time and position. Parameters which are functions of temperature, such as k_a , k_g , k_r , h_i , ρ_a , u_p , and μ are continuously updated during the transient analysis.

The preliminary solution effort showed the system of equations to be very stiff (refer to Shampine/Gordon [24] and Gear [25] for a discussion of "stiffness"). Changing the integration algorithm from a sixth-order Runge-Kutta (IMSL subroutine DVERK) to a modified implicit-Gear method for stiff systems, developed by Franke [2], resulted in a significant reduction in CPU time. The computational effort

was carried out on an IBM 360/70. Typical runs required 20-30 minutes CPU time for problems for which ignition occurred, and 6-25 minutes CPU time for extinction problems. Ignition problems were terminated when the temperature at any nodal point exceeded 2200 degrees Fahrenheit, or when the graphite at a nodal point was totally consumed. Extinction problems were carried out to steady state.

A twenty five nodal point model (75 o. d. e.) provided results which differed less than five percent from the results of a 32 nodal point model (96 o. d. e.) and was adopted for all computer runs. For the twenty five nodal point model, approximately 275K bytes of core was required. The computer program which includes the FEM formulation and the integration routine as well as a sample input file is presented at the end of the appendices.

The numerical solution produced satisfactory results with one exception which will now be discussed. For a particular range of temperature and oxygen concentration (approximately 1500 degrees Fahrenheit and $.001 \text{ lbm/ft}^3$, respectively), there is a significant increase in reaction rate. This accelerated reaction rate produced a negative/positive oscillation for the nodal values of oxygen concentration. The oscillation occurred in a region of the plate where the oxygen appeared to be totally consumed. As discussed by Frank-Kamenetskii [3], nth order reactions may yield zero values for the oxygen concentration and gradient within the

medium. The cause of the oscillation was as follows. Although the reaction rate is a function of temperature and oxygen concentration, numerically, it is treated as constant during an integration interval. As a result, the concentration in the region of high reaction rate becomes negative. The reaction rate was updated for the next time interval by setting negative concentrations to zero. During this time interval, for the region of zero concentration, there is no reaction. Without consumption, the oxygen concentration will increase and the cycle repeats itself. The oscillation was aggravated by large plate thickness and low permeability. The instability occurring for the high reaction rate may be corrected by (1) numerically integrating the rate term in the time domain, (2) iterating until convergence is obtained between consecutive values of concentration, or (3) decreasing the time step and the length of the elements. As a matter of expediency, measure (3) was used to minimize the instability. The fiber and air temperatures were essentially unaffected by the oscillations in the oxygen concentration.

B. RESULTS AND OBSERVATIONS

Table 1 presents the results of fourteen problems. In Table 1, the parameters which depend upon temperature (u_p , Re_i , and h_i) are evaluated at ambient conditions for comparison purposes only. These parameters, in fact, will vary during the course of the transient analysis. In all cases,

the initial condition on graphite temperature was 1050 degrees Fahrenheit.

Figures 10, 11, and 12 show the transient behavior of Case 1. For the initial conditions shown, ignition occurred in approximately eight seconds. The reaction rate and oxygen concentration responses for Case 1 are typical of the problems for which ignition resulted. Figure 13 shows that the air and fiber temperatures for Case 1 do not differ significantly. This behavior is typical for most problems. However, for plates with high porosity (greater than .8) and subjected to relatively high flow rates, significant differences in the air and fiber temperatures do occur (see Figure 14 for Case 9). In a previous effort by Vatikiotis and Salinas [26], linearly varying initial conditions were investigated. Although the reaction rate used in that investigation differed from the one used in the present investigation, the overall results remain valid. The main observation was that ignition is less likely to occur for thin plates with the ambient air entering the hotter plate surface. Since temperature controls the reaction in the kinetic regime, cooler air entering the hotter plate surface enhances the heat loss. This reduces the fiber temperature, thereby decreasing the reaction rate. In effect, the cooler air enters the plate where it is most needed.

In the present analysis, observations were made by vary-
ing one input parameter (i.e., L or d or U_{∞}) while keeping

all others fixed. The effects of each parameter on the behavior will be discussed individually.

1. Effects of Exterior Velocity

As shown in Figures 15, 16 and 17 (cases 4, 1 and 2, respectively) for an initial condition of 1050 degrees Fahrenheit, three distinct regions of combustion were observed (extinction-ignition-extinction). These became apparent as U_{∞} was increased from low velocities (10 knots) to higher velocities (120 knots). Vulis [4] discusses an experiment of a heated carbon rod with an air jet impinging upon it. For a certain range of flow velocities, ignition was observed. However, extinction did occur for velocities less than and greater than the velocity for which ignition occurred. The behavior of the carbon rod and that of the graphite mat is similar. This behavior may be explained by the Semenov model of Figure 1. For high U_{∞} , the internal heat transfer coefficient, h_i , will be large as a result of an increase in the pore velocity. Since the slopes of the heat loss lines, q_l , increase with increasing h_i for a constant T_a , the graphite temperature decreases from the critical ignition point I. This causes extinction for the higher exterior flow velocities, U_{∞} . In contrast, for low U_{∞} , the slope of q_l will be small and ignition is more likely to occur. However, the heat generation curve, q_g , changes position due to a decrease in oxygen concentration. This reduction in oxygen concentration is caused by the lower induced flow rate through the

plate. The overall shape of q_g is flattened such that the q_l line crosses q_g behind the new critical point I. Thus extinction is observed for this region of low U_∞ .

2. Effects of Fiber Diameter

Varying the fiber diameter with the remaining input parameters fixed, also yields three regions of combustion (extinction-ignition-extinction) for a fixed initial temperature. The results are shown in Figures 16, 18 and 19 (Cases 1, 9 and 10, respectively). The fiber diameter and ply thickness determine the permeability of the plate. Similar to U_∞ , permeability affects the pore velocity (i.e., low permeability \rightarrow low velocity). In turn, this affects the convective heat transfer and the amount of oxygen entering the plate. These three regions of combustion are explained by the Semenov model for the same reasons as those of varying U_∞ .

Porosity is a measure of void space and denotes the space available for oxygen. Porosity is associated with the internal geometry of the medium, as is permeability. However, they are basically different parameters. Permeability (hydraulic conductivity) is associated with convective air flow through the medium. Thus, an n -fold increase in the fiber diameter and ply thickness will not affect a change in porosity, but will affect an n^2 order change in the permeability. For an n greater than one, the result is a decrease in pore velocity without a change in porosity. Porosity

determines the maximum oxygen concentration per unit volume of fibrous mat. This indirectly affects the reaction rate. Thus, for a given u_p , the lower the porosity, the less oxygen there is for combustion. It appears that high porosity would enhance combustion by the presence of more oxygen. However, higher porosities also provide more fluid per unit volume resulting in greater heat transfer. This is observed in Case 9, Figure 18.

3. Effects of Plate Thickness, L

For the given initial temperature of 1050 degrees Fahrenheit, varying the plate thickness yielded two regions of combustion (extinction-ignition). Extinction was observed for thin plates (Case 2, Figure 17). As shown by Figures 20 and 21 (Cases 7 and 11, respectively), ignition was observed when plate thickness was increased. Plate thickness also affects the pore velocity. Decreasing L , increases the pressure gradient across the plate, thus increasing the pore velocity. The result is that extinction is more likely for thin plates because of the enhanced convection heat transfer resulting from the increase in pore velocity. Whereas pore velocity is inversely proportional to L , it is an exponential function of U_∞ . For the range of parameters in this investigation (i.e., $.1" < L < 3."$, and $10 \text{ knots} < U_\infty < 100 \text{ knots}$), an n -fold change in U_∞ will produce a greater change in u_p , then will an n -fold change in L . Compare Cases 1 and 2 to Cases 7 and 8.

A characteristic feature of ignition for thick plates was observed. As the thickness increased, the ignition region (the spatial location) moved closer to the entrance surface of the ambient air. Compare Figures 20 and 21.

C. DISCUSSION

At this point, discussion is made of ignition temperatures for porous graphite plates. The ignition temperature for Case 1 was 1050 degrees Fahrenheit. This temperature was obtained by varying the initial temperature until ignition occurred. In all subsequent cases, 1050 degrees Fahrenheit was adopted as the initial condition, and we observed whether extinction or ignition occurred. The ignition temperatures given here are the result of taking $n = \frac{1}{2}$ in the n th order reaction rate. Significantly different ignition temperatures will result for other n . For example, for $n = 1$ (1st order reaction), the ignition temperature for Case 1 was approximately 1600 degrees Fahrenheit. As Frank-Kamenetskii [3] has suggested values of n between $1/3$ and $2/3$, the average value of $1/2$ was adopted for this analysis. The ignition temperatures obtained using $n = \frac{1}{2}$ agree favorably with the experiments of Fontenot [1]. For fiber combustion, ignition temperatures for porous graphite plates are on the order of 1100 degrees Fahrenheit.

Consider the results of varying U_{∞} . Extinction occurred for Case 2 and Case 4; thus, the ignition temperature

for each case is greater than 1050 degrees Fahrenheit. Since ignition does occur at 1050 degrees Fahrenheit for intermediate values of U_{∞} (Case 1, Case 7), ignition temperature is not a monotonic function of U_{∞} . The precise determination of ignition temperature for a specific value of air velocity can be obtained by a large number of computer runs. A similar discussion can be made for the ignition temperatures dependence on fiber diameter. The general shape of these functions is represented by the shaded region on Figure 22. These suppositions may only be valid in the limited range of parameters associated with the present investigation.

It is interesting to observe that changing the initial condition of the oxygen concentration only affects the early part of the problem. The response of the concentration is fast compared to that of temperature. After approximately one second, the transient behavior is the same regardless of the initial condition on the oxygen concentration.

A brief description of the Semenov model was given in Section II.A. That discussion was for a lumped parameter model. The actual combustion process is more complex since there are spatial variations in temperature and in oxygen concentration. The results of this analysis show that both kinetic and diffusion regimes may exist simultaneously in a porous medium. Hence, it is not reasonable to restrict an

analysis of combustion in a porous medium to the kinetic regime.

D. CONCLUDING REMARKS

The model has provided considerable insight as to the behavior of fibrous composites subject to combustion. Improvements may be realized by extending the model to include:

- (1) The combustion of the epoxy matrix (i.e., start problem with first stage of combustion process).
- (2) The change in geometry of the porous medium due to combustion (affects p , m and z).
- (3) A more complex reaction (i.e., secondary combustion of gaseous by-products, such as carbon monoxide).
- (4) The effect of gaseous by-products on fluid properties.
- (5) Generalization to two and three dimensional models (results in anisotropic properties).

The results show that certain properties, such as plate thickness, permeability and porosity, have significant effects on combustion. Therefore, one could select these design parameters to improve the flame resistance of composite materials. This would be beneficial to the survivability of a composite structure. A comprehensive set of analyses could be undertaken to couple the combustion problem to the strength problem. In this way, one could achieve a design which maximizes strength and minimizes combustion.

Another use of the present model would be in the study of energy systems utilizing particulate fuels (i.e., coal, biomass). In this case, the design parameters could be selected to maximize the performance of the system.

APPENDIX A

NONDIMENSIONALIZATION OF FIELD EQUATIONS

The field equations and boundary conditions are:

$$\frac{\partial}{\partial x}[(k_g + k_r) \frac{\partial T_g}{\partial x}] - \frac{h_i z}{(1-p)}(T_g - T_a) + \Delta H r(T_g, \phi) = \rho_g c_g \frac{\partial T_g}{\partial t} \quad (\text{III.28})$$

$$\frac{\partial}{\partial x}(k_a \frac{\partial T_a}{\partial x}) - \dot{m} c_a \frac{\partial T_a}{\partial x} + \frac{h_i z}{p}(T_g - T_a) = \rho_a c_a \frac{\partial T_a}{\partial t} \quad (\text{III.37})$$

$$\frac{\partial}{\partial x}(B \frac{\partial \phi}{\partial x}) - u_p \frac{\partial \phi}{\partial x} - \frac{\partial u_p}{\partial T_a} (\frac{\partial T_a}{\partial x}) \phi - (\frac{1}{f}) r(T_g, \phi) = \frac{\partial \phi}{\partial t} \quad (\text{III.46})$$

at $x = 0$

$$(k_g + k_r) \frac{\partial T_g}{\partial x} = h_1 (T_g - T_\infty) + \sigma \epsilon (\hat{T}_g^4 - \hat{T}_\infty^4) \quad (\text{IV.1})$$

$$T_a = T_\infty \quad (\text{IV.3})$$

$$B \frac{\partial \phi}{\partial x} = u_p (\phi - p \phi_\infty) \quad (\text{IV.5})$$

at $x = L$

$$(k_g + k_r) \frac{\partial T_g}{\partial x} = -h_2 (T_g - T_\infty) - \sigma \epsilon (\hat{T}_g^4 - \hat{T}_\infty^4) \quad (\text{IV.2})$$

$$\frac{\partial T_a}{\partial x} = \frac{\partial T_g}{\partial x} \quad (\text{IV.4})$$

$$\frac{\partial \phi}{\partial x} = 0$$

(IV.6)

The nondimensional variables are defined as:

$$\theta = T_g/T_\infty \quad \text{nondimensional fiber temperature}$$

$$\Gamma = T_a/T_\infty \quad \text{nondimensional air temperature}$$

$$\phi = \phi/\phi_\infty \quad \text{nondimensional oxygen concentration}$$

$$\eta = x/L \quad \text{nondimensional distance}$$

The time variable, t , will not be nondimensionalized.

Using the temperature of the fiber, T_g , to demonstrate the technique of transformation, we have,

$$T_g = T_\infty \theta$$

It follows that,

$$\frac{\partial T_g}{\partial x} = T_\infty \frac{\partial \theta}{\partial x}$$

$$\frac{\partial^2 T_g}{\partial x^2} = T_\infty \frac{\partial^2 \theta}{\partial x^2}$$

Using the chain rule to transform x to η , gives

$$\frac{\partial T_g}{\partial x} = T_\infty \frac{\partial \theta}{\partial \eta} \frac{\partial \eta}{\partial x}$$

Since $\eta = x/L$, the partial derivatives become

$$\frac{\partial T_g}{\partial x} = \frac{T_\infty}{L} \frac{\partial \theta}{\partial \eta}$$

and

$$\frac{\partial^2 T_g}{\partial x^2} = \frac{T_\infty}{L^2} \frac{\partial^2 \theta}{\partial \eta^2}$$

Therefore,

$$\frac{\partial^2 T_g}{\partial x^2} = \frac{T_\infty}{L^2} \frac{\partial^2 \theta}{\partial \eta^2}$$

Similar transformations for T_a and ϕ yield,

$$\frac{\partial T_a}{\partial x} = \frac{T_\infty}{L} \frac{\partial \Gamma}{\partial \eta}$$

$$\frac{\partial \phi}{\partial x} = \frac{\phi_\infty}{L} \frac{\partial \phi}{\partial \eta}$$

$$\frac{\partial^2 T_a}{\partial x^2} = \frac{T_\infty}{L^2} \frac{\partial^2 \Gamma}{\partial \eta^2}$$

$$\frac{\partial^2 \phi}{\partial x^2} = \frac{\phi_\infty}{L^2} \frac{\partial^2 \phi}{\partial \eta^2}$$

Substituting these relations into the field equations and removing the constants from the differential operators gives,

$$\frac{T_\infty}{L^2} \frac{\partial}{\partial \eta} [(k_g + k_r) \frac{\partial \theta}{\partial \eta}] - \frac{h_1 z}{(1-p)} (\theta - \Gamma) + \Delta H r (T_g, \phi) = \rho_g c_g \frac{\partial \theta}{\partial t}$$

$$\frac{T_\infty}{L^2} \frac{\partial}{\partial \eta} (k_a \frac{\partial \Gamma}{\partial \eta}) - \frac{\dot{m} c_a T_\infty}{L} \frac{\partial \Gamma}{\partial \eta} + \frac{h_1 z}{p} (\theta - \Gamma) = \rho_a c_a \frac{\partial \Gamma}{\partial t}$$

$$\frac{\phi_{\infty}}{L^2} \frac{\partial}{\partial \eta} (B \frac{\partial \phi}{\partial \eta}) - \frac{u_p T_{\infty}}{L} \frac{\partial \phi}{\partial \eta} - \frac{\phi_{\infty} T_{\infty}}{L} (\frac{\partial u_p}{\partial T_a}) \frac{\partial \Gamma}{\partial \eta} \phi - (\frac{1}{f}) r(T_g, \phi) = \phi_{\infty} \frac{\partial \phi}{\partial t}$$

Upon rearrangement, the equations become,

$$\frac{\partial}{\partial \eta} [(k_g + k_r) \frac{\partial \Theta}{\partial \eta}] - \frac{h_i z L^2}{(1-p)} (\Theta - \Gamma) + \frac{\Delta H L^2}{T_{\infty}} r(T_g, \phi) = \rho_g c_g L^2 \frac{\partial \Theta}{\partial t}$$

$$\frac{\partial}{\partial \eta} (k_a \frac{\partial \Gamma}{\partial \eta}) - \dot{m} c_a L \frac{\partial \Gamma}{\partial \eta} + \frac{h_i z L^2}{p} (\Theta - \Gamma) = \rho_a c_a L^2 \frac{\partial \Gamma}{\partial t}$$

$$\frac{\partial}{\partial \eta} (B \frac{\partial \phi}{\partial \eta}) - u_p L \frac{\partial \phi}{\partial \eta} - T_{\infty} L (\frac{\partial u_p}{\partial T_a}) \frac{\partial \Gamma}{\partial \eta} \phi - (\frac{1}{f}) \frac{L^2}{\phi_{\infty}} r(T_g, \phi) = L^2 \frac{\partial \phi}{\partial t}$$

Letting,

$$\lambda_1 = (k_g + k_r) \quad \lambda_2 = \frac{h_i z L^2}{(1-p)} \quad \lambda_3 = \frac{\Delta H L^2}{T_{\infty}} \quad \lambda_4 = \rho_g c_g L^2$$

$$v_1 = k_a \quad v_2 = \dot{m} c_a L \quad v_3 = \frac{h_i z L^2}{p} \quad v_4 = \rho_a c_a L^2$$

$$\omega_1 = B \quad \omega_2 = u_p L \quad \omega_3 = T_{\infty} L \frac{\partial u_p}{\partial T_a} \quad \omega_4 = \frac{1}{f} \frac{L^2}{\phi_{\infty}}$$

$$\omega_5 = L^2$$

the field equations may be written as,

$$\frac{\partial}{\partial \eta} (\lambda_1 \frac{\partial \Theta}{\partial \eta}) - \lambda_2 (\Theta - \Gamma) + \lambda_3 r(T_g, \phi) = \lambda_4 \frac{\partial \Theta}{\partial t} \quad (A.1)$$

$$\frac{\partial}{\partial \eta} (v_1 \frac{\partial \Gamma}{\partial \eta}) - v_2 \frac{\partial \Gamma}{\partial \eta} + v_3 (\Theta - \Gamma) = v_4 \frac{\partial \Gamma}{\partial t} \quad (A.2)$$

$$\frac{\partial}{\partial \eta} (\omega_1 \frac{\partial \phi}{\partial \eta}) - \omega_2 \frac{\partial \phi}{\partial \eta} - \omega_3 \frac{\partial \Gamma}{\partial \eta} \phi - \omega_4 r(T_g, \phi) = \omega_5 \frac{\partial \phi}{\partial t} \quad (A.3)$$

Noting that the coefficients λ , ν , ω are response dependent variables, equations A.1, A.2, and A.3 are considered in their final form in Section III.

Substituting the nondimensional variables into the boundary conditions gives,

$$\lambda_1 \frac{\partial \theta}{\partial \eta} = h_1 L(\theta - 1) + \frac{\sigma \epsilon L}{T_\infty} (\hat{T}_g^4 - \hat{T}_\infty^4) \quad x = 0$$

$$\Gamma = 1 \quad x = 0$$

$$\omega_1 \frac{\partial \phi}{\partial \eta} = \omega_2 (\phi - p) \quad x = 0$$

and

$$\lambda_1 \frac{\partial \theta}{\partial \eta} = -h_2 L(\theta - 1) - \frac{\sigma \epsilon L}{T_\infty} (\hat{T}_g^4 - \hat{T}_\infty^4) \quad x = L$$

$$\frac{\partial \Gamma}{\partial \eta} = \frac{\partial \theta}{\partial \eta} \quad x = L$$

$$\frac{\partial \phi}{\partial \eta} = 0 \quad x = L$$

The dimensional form of the absolute temperature will be retained for convenience.

APPENDIX B

POLYNOMIAL APPROXIMATIONS OF THERMAL PROPERTIES

Relations giving the viscosity and thermal conductivities of air for varying temperature were required. A simple way to obtain values for these properties is to fit empirical data with 2nd order Lagrange polynomials.

The general form of the 2nd order Lagrange polynomials for thermal conductivity and viscosity are

$$k_a = \frac{(T_a - T_{a2})(T_a - T_{a3})}{(T_{a1} - T_{a2})(T_{a1} - T_{a3})} k_{a1} + \frac{(T_a - T_{a3})(T_a - T_{a1})}{(T_{a2} - T_{a3})(T_{a2} - T_{a1})} k_{a2} + \frac{(T_a - T_{a1})(T_a - T_{a2})}{(T_{a3} - T_{a1})(T_{a3} - T_{a2})} k_{a3} \quad (B.1)$$

$$\mu = \frac{(T_a - T_{a2})(T_a - T_{a3})}{(T_{a1} - T_{a2})(T_{a1} - T_{a3})} \mu_1 + \frac{(T_a - T_{a3})(T_a - T_{a1})}{(T_{a2} - T_{a3})(T_{a2} - T_{a1})} \mu_2 + \frac{(T_a - T_{a1})(T_a - T_{a2})}{(T_{a3} - T_{a1})(T_{a3} - T_{a2})} \mu_3 \quad (B.2)$$

Choosing three points from a range of temperatures that would be representative of those observed during the analysis, the corresponding values of the properties are:

(subscript)	Temp (F)	k_a $\left(\frac{\text{Btu}}{\text{lbm-hr-ft}}\right)$	μ $\left(\frac{\text{lbm}}{\text{ft-hr}}\right)$
1	0	.0131	.0394
2	700	.0284	.0765
3	1500	.0423	.107

Substituting these values into expressions B.1 and B.2 gives,

$$\begin{aligned}
 k_a &= \frac{(T_a - 700)(T_a - 1500)}{(0 - 700)(0 - 1500)} (.0131) + \frac{(T_a - 1500)(T_a - 0)}{(700 - 1500)(700 - 0)} (.0284) \\
 &\quad + \frac{(T_a - 0)(T_a - 700)}{(1500 - 0)(1500 - 700)} (.0423) \\
 \mu &= \frac{(T_a - 700)(T_a - 1500)}{(0 - 700)(0 - 1500)} (.0394) + \frac{(T_a - 1500)(T_a - 0)}{(1500 - 0)(1500 - 700)} (.0765) \\
 &\quad + \frac{(T_a - 0)(T_a - 700)}{(1500 - 0)(1500 - 700)} (.107)
 \end{aligned}$$

These expressions reduce to,

$$\begin{aligned}
 k_a &= -3.232 \times 10^{-9} T_a^2 + 2.412 \times 10^{-5} T_a + .0131 \quad \frac{\text{Btu}}{\text{lbm-hr-ft}} \\
 \mu &= -1.041 \times 10^{-8} T_a^2 + 6.029 \times 10^{-5} T_a + .0394 \quad \frac{\text{lbm}}{\text{ft-hr}}
 \end{aligned}$$

Both expressions give property values which are within five percent of the data for temperatures to 2000 degrees Fahrenheit.

APPENDIX C

TRANSFORMATION OF THE REACTION RATE TERM

The expression for the oxidation rate of graphite fibers taken from Parker and Hottel [15] is

$$r_g = \frac{9.55 \times 10^6}{\hat{T}_{gk}^{1/2}} P_{O_2} \exp\left(\frac{-44000}{R \hat{T}_{gk}}\right) \quad \frac{\text{gm}}{\text{cm}^2\text{-sec}} \quad (\text{C.1})$$

where R is the universal gas constant (1.958 cal/gmole-K) and P_{O_2} is the partial pressure of oxygen (atm.). The partial pressure may be represented in terms of the temperature, \hat{T} , and oxygen concentration, ϕ , by the Ideal Gas law in the form given by Kanury [16]

$$P_{O_2} = \left(\frac{M_a}{M_{O_2}}\right) R_A \hat{T} \phi \quad (\text{C.2})$$

where $M_a/M_{O_2} = .9$ is the ratio of the molecular weights of air and oxygen; R_A ($= 53.34 \text{ ft.-lbf/lbm R}$) is the gas constant for air. Substituting M_a/M_{O_2} into equation C.2 and converting P_{O_2} to atmospheric units the expression becomes

$$P_{O_2} = 4.25 \times 10^{-4} R_A \hat{T} \phi \quad \text{atm.}$$

Converting r_g to $\text{lbm/ft}^2\text{-hr}$ from $\text{gm/cm}^2\text{-sec}$, equation C.1 becomes

$$r_g = \frac{7.04 \times 10^{10}}{T_{gk}^{1/2}} P_{02} \exp\left(\frac{-44000}{R T_{gk}}\right) \frac{\text{lbm}}{\text{ft}^2\text{-hr}}$$

Substituting in for P_{02} and converting the absolute temperatures from Kelvin to Rankine, the rate expression becomes,

$$r_g = 4.014 \times 10^7 \frac{R_A \hat{T} \phi}{\hat{T}_g^{1/2}} \exp\left(\frac{-39883}{\hat{T}_g}\right) \frac{\text{lbm}}{\text{ft}^2\text{-hr}}$$

The absolute temperature at the fiber surfaces is \hat{T}_g . Thus, \hat{T} in the numerator becomes \hat{T}_g , and the expression becomes

$$r_g = 4.014 \times 10^7 R_A T_g^{1/2} \phi \exp\left(\frac{-39883}{T_g}\right)$$

To transform the reaction rate to $\text{lbm/ft}^3\text{-hr}$, y , the ratio of a fibers surface area to its volume is placed in the numerator of r_g . The expression for y is,

$$y = \frac{1}{2} \frac{\pi d}{\frac{\pi d^2}{4}} = \frac{2}{d} \quad (\text{C.3})$$

where d is the fiber diameter, and the $\frac{1}{2}$ factor accounts for the uncertainty of the actual amount of fiber surface after the epoxy has burned away. The reaction rate of the graphite

fibers per unit volume is expressed as

$$r = 4.014 \times 10^7 y R_A \hat{T}_g^{1/2} \phi \exp\left(\frac{-39883}{\hat{T}_g}\right) \frac{\text{lbm}}{\text{ft}^3\text{-hr}}$$

To obtain the heat liberated per lbm of fiber, r is multiplied by ΔH , the enthalpy of formation of carbon dioxide per unit mass of graphite consumed. This value is approximately 14,085 BTU per pound-mass of fiber and was obtained from Kanury [16]

$$\text{Heat generation rate} = \Delta H r(T_g, \phi)$$

To obtain the oxygen consumption rate, r is multiplied by the inverse of the fuel-air stoichiometric ratio,

$$\text{Oxygen consumption rate} = \left(\frac{1}{F}\right) r(T_g, \phi).$$

APPENDIX D

JUSTIFICATION OF THE DANKWERTS' BOUNDARY CONDITIONS

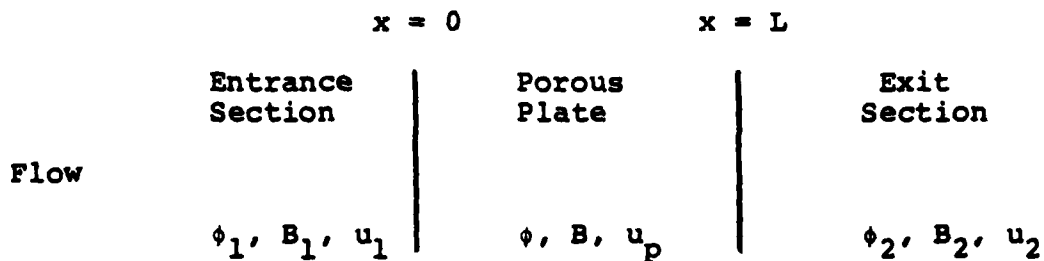
The Dankwerts' boundary conditions for the oxygen diffusion equation are:

$$\frac{d\phi}{dx} = \frac{u_p}{B}(\phi - p\phi_\infty) \quad x = 0$$

$$\frac{d\phi}{dx} = 0 \quad x = L$$

Bischoff [23] presents a discussion of these equations. A brief summary is provided for completeness.

Figure 10 shows the one-dimensional oxygen transport region considered in this analysis.



The concentration of oxygen, ϕ , for each region is distinguished by subscripts; B and u are the diffusivity and the velocity, respectively, for each region. The oxygen diffusion equations for each section are as follows,

$$\frac{B_1}{u_1} \frac{d^2 \phi_1}{dx^2} - \frac{d\phi}{dx} = 0 \quad x \leq 0 \quad (D.1)$$

$$\frac{B}{u_p} \frac{d^2 \phi}{dx^2} - \frac{d\phi}{dx} - r(T, \phi) = 0 \quad 0 \leq x \leq L \quad (D.2)$$

$$\frac{B_2}{u_2} \frac{d^2 \phi}{dx^2} - \frac{d\phi_2}{dx} = 0 \quad x \geq L \quad (D.3)$$

with the general boundary conditions,

$$\phi_1(-\infty) = \phi_\infty \quad (D.4)$$

$$p\phi_1(0^-) = \phi(0^+) \quad (D.5)$$

$$p\phi_1(0^-) - p \frac{B_1}{u_1} \frac{d\phi_1(0^-)}{dx} = \phi(0^+) - \frac{B}{u_p} \frac{d\phi(0^+)}{dx} \quad (D.6)$$

$$p\phi(L^-) = \phi_2(L^+) \quad (D.7)$$

$$p\phi(L^-) - p \frac{B}{u_p} \frac{d\phi(L^-)}{dx} = \phi_2(L^+) - \frac{B_2}{u_2} \frac{d\phi_2(L^+)}{dx} \quad (D.8)$$

$$\phi_2(+\infty) = \text{finite} \quad (D.9)$$

For convenience, the parameters u_i , B_i will be treated as constant. In addition, the porosity, p , has been included to account for the discontinuity that exist for the concentration. The discontinuity is caused by the oxygen from a totally gaseous environment to one that is partly occupied by solid.

An analytical closed-form solution for this set of equations is not possible because of the nonlinearity of equation D.2. However, the solutions of equations D.1 and D.3 are,

$$\phi_1 = A_1 + A_2 \exp(u_1 x / B_1) \quad (D.10)$$

$$\phi_2 = A_3 + A_4 \exp(u_2 x / B_2) \quad (D.11)$$

Applying boundary conditions D.4 and D.9, the following results are obtained,

$$A_1 = \phi_\infty$$

$$A_4 = 0$$

The solutions D.10 and D.11 become

$$\phi_1 = \phi_\infty + A_2 \exp(u_1 x / B_1) \quad (D.12)$$

$$\phi_2 = A_3 \quad (D.13)$$

It would be necessary to have the solution for the non-linear equation D.2 to solve for A_2 and A_3 . However, the constants need not be known to continue with the analysis.

From equation D.12,

$$\phi_1(0^-) = \phi_\infty + A_2$$

and,

$$\frac{d\phi_1(0^-)}{dx} = \frac{u_1}{B_1} A_2$$

Substituting these into equation D.9 gives

$$p\phi_\infty + pA_2 - p \frac{B_1}{u_1} \left(\frac{u_1}{B_1} A_2 \right) = \phi(0^+) - \frac{B}{u_p} \frac{d\phi(0^+)}{dx}$$

Cancelling terms yields,

$$p\phi_\infty = \phi(0^+) - \frac{B}{u_p} \frac{d\phi(0^+)}{dx}$$

Rearranging, the Dankwerts' boundary condition at $x = 0$ is

$$\frac{d\phi}{dx} = \frac{u_p}{B} (\phi - p\phi_\infty) \quad x = 0$$

From equation D.13, and noting that A_3 is a constant, we have

$$\frac{d\phi_2}{dx} = 0$$

and

$$\frac{d\phi_2(L^+)}{dx} = 0$$

Substituting these expressions and equation D.7 into equation D.8,

$$p\phi(L^-) - p \frac{B}{u_p} \frac{d\phi(L^-)}{dx} = p\phi(L^-) - \frac{B_2}{u_2}(0)$$

Upon cancelling terms, the second Dankwerts' boundary condition becomes,

$$\frac{d\phi}{dx} = 0 \qquad x = L$$

An important underlying consideration for using the Dankwerts' boundary conditions is that it simplifies the analysis since equation D.2 may be solved independently without having to consider entrance and exit regions.

APPENDIX E

DERIVATION OF THE FEM OPERATORS

In the section on the finite element formulation, the following five differential operators were identified,

$$\int_0^1 \{G_i'\} \langle G_j' \rangle dn \quad (E.1)$$

$$\int_0^1 \{G_i\} \langle G_j' \rangle dn \quad (E.2)$$

$$\int_0^1 \{G_i\} \langle G_j \rangle dn \quad (E.3)$$

$$\int_0^1 \{G_i\} \langle G_j' \rangle \{\psi\} \langle G_j \rangle dn \quad (E.4)$$

$$\int_0^1 \{G_i\} dn \quad (E.5)$$

where the G_i are the global basis functions. These operators are constructed on the element level by introducing the corresponding element basis functions, g_i . The global and element basis functions are related by,

$$G_i = g_1^{(i-1)} \oplus g_2^{(i)}$$

where g_1 and g_2 are defined by

$$g_1^{(e)} = \begin{cases} (1 - \frac{\xi}{l_e}) & \text{for } \xi \text{ in element } (e) \\ 0 & \text{for } \xi \text{ not in element } (e) \end{cases}$$

$$g_2^{(e)} = \begin{cases} \frac{\xi}{l_e} & \text{for } \xi \text{ in element } (e) \\ 0 & \text{for } \xi \text{ not in element } (e) \end{cases}$$

and l_e is the length of the (e)th element.

The derivation of the local elemental matrices according to the Galerkin method for the global operations E.1 through E.5 proceeds as follows:

For operator E.1,

$$\begin{array}{ccc} \text{global} & & \text{local} \\ \int_0^1 \{G_1'\} \langle G_j' \rangle d\eta & \Rightarrow & U \left[\int_0^{l_e} \begin{pmatrix} g_1' \\ g_2' \end{pmatrix} \langle g_1' \ g_2' \rangle d\xi \right] \end{array}$$

Noting that,

$$g_1' = -\frac{1}{l_e}$$

$$g_2' = \frac{1}{l_e}$$

the elemental matrix becomes

$$\int_0^{l_e} \begin{bmatrix} \left(\frac{1}{l_e}\right)^2 & -\left(\frac{1}{l_e}\right)^2 \\ -\left(\frac{1}{l_e}\right)^2 & \left(\frac{1}{l_e}\right)^2 \end{bmatrix} d\xi \Rightarrow \frac{1}{l_e} \begin{bmatrix} 1 & -1 \\ -1 & 1 \end{bmatrix}$$

For operator E.2,

global

local

$$\int_0^1 \{G_i\} \langle G_j' \rangle d\eta \Rightarrow U \left[\int_0^{l_e} \begin{Bmatrix} g_1 \\ g_2 \end{Bmatrix} \langle g_1' \ g_2' \rangle d\xi \right]$$

Substituting in the local shape functions gives,

$$\int_0^{l_e} \begin{Bmatrix} \left(1 - \frac{\xi}{l_e}\right) \\ \left(\frac{\xi}{l_e}\right) \end{Bmatrix} \left\langle \left(-\frac{1}{l_e}\right) \left(\frac{1}{l_e}\right) \right\rangle d\xi$$

Carrying out the operations gives

$$\int_0^{l_e} \begin{bmatrix} (-\frac{1}{l_e} + \frac{\xi}{l_e}) & (\frac{1}{l_e} - \frac{\xi}{l_e}) \\ -(\frac{\xi^2}{2l_e^2}) & (\frac{\xi^2}{2l_e^2}) \end{bmatrix} d\xi \Rightarrow \frac{1}{2} \begin{bmatrix} -1 & 1 \\ -1 & 1 \end{bmatrix}$$

For operator E.3,

$$\begin{array}{cc} \text{global} & \text{local} \\ \int_0^1 \{G_1\} \langle G_j \rangle d\eta & \Rightarrow U \left[\int_0^{l_e} \begin{pmatrix} g_1 \\ g_2 \end{pmatrix} \langle g_1 \ g_2 \rangle d\xi \right] \end{array}$$

Substituting in for the local shape functions

$$\int_0^{l_e} \begin{pmatrix} (1 - \frac{\xi}{l_e}) \\ (\frac{\xi}{l_e}) \end{pmatrix} \langle (1 - \frac{\xi}{l_e}) (\frac{\xi}{l_e}) \rangle d\xi$$

the elemental matrix becomes

$$\int_0^{l_e} \begin{bmatrix} (1 - 2\frac{\xi}{l_e} + \frac{\xi^2}{l_e^2}) & (\frac{\xi}{l_e} - \frac{\xi^2}{l_e^2}) \\ (\frac{\xi}{l_e} - \frac{\xi^2}{l_e^2}) & (1 - 2\frac{\xi}{l_e} + \frac{\xi^2}{l_e^2}) \end{bmatrix} d\xi \Rightarrow \frac{l_e}{3} \begin{bmatrix} 1 & \frac{1}{2} \\ \frac{1}{2} & 1 \end{bmatrix}$$

AD-A092 094

NAVAL POSTGRADUATE SCHOOL MONTEREY CA
ANALYSIS OF COMBUSTION AND HEAT TRANSFER IN A POROUS GRAPHITE M--ETC(U
JUN 80 C S VATIKIOTIS

F/G 11/4

UNCLASSIFIED

NL

2
2000000

END
DATE
FILMED
M-2
DTIC

For operator E.4,

$$\begin{array}{ccc} \text{global} & & \text{local} \\ \int_0^1 \{G_i\} \langle G_j' \rangle \{\Psi\} \langle G_j \rangle d\eta & \Rightarrow & U \left\{ \int_0^{l_e} \begin{array}{cc} g_1 & \\ & g_2 \end{array} \langle g_1' g_2' \rangle \left\{ \begin{array}{c} \Psi \\ \Psi \end{array} \right\} \langle g_1 g_2 \rangle d\xi \right\} \end{array}$$

Multiplying out the matrices, the expression becomes,

$$\int_0^{l_e} \begin{bmatrix} (g_1 g_1 g_1' \Psi_{i-1} + g_1 g_1 g_2' \Psi_i) & (g_1 g_1 g_2 \Psi_{i-1} + g_1 g_2 g_2' \Psi_i) \\ (g_1 g_1' g_2 \Psi_{i-1} + g_1 g_2 g_2 \Psi_i) & (g_1' g_2 g_2 \Psi_{i-1} + g_2 g_2 g_2' \Psi_i) \end{bmatrix} d\xi$$

Integrating each term separately,

$$\int_0^{l_e} g_1 g_1 g_1' d\xi = \int_0^{l_e} \left(-\frac{1}{l_e} + \frac{2\xi}{l_e^2} - \frac{\xi^2}{l_e^3} \right) d\xi = -\frac{1}{3}$$

$$\int_0^{l_e} g_1 g_1 g_2' d\xi = \int_0^{l_e} \left(\frac{1}{l_e} - \frac{2\xi}{l_e^2} + \frac{\xi^2}{l_e^3} \right) d\xi = \frac{1}{3}$$

$$\int_0^{l_e} g_1 g_1' g_2 d\xi = \int_0^{l_e} \left(-\frac{\xi}{l_e^2} + \frac{\xi^2}{l_e^3} \right) d\xi = -\frac{1}{6}$$

$$\int_0^{l_e} g_1 g_2 g_2' d\xi = \int_0^{l_e} \frac{\xi}{l_e} - \frac{\xi^2}{l_e} d\xi = \frac{1}{6}$$

$$\int_0^{l_e} g_1 g_1' g_2 d\xi = -\frac{1}{6}$$

$$\int_0^{l_e} g_1 g_2 g_2' d\xi = \frac{1}{6}$$

$$\int_0^{l_e} g_1' g_2 g_2 d\xi = \int_0^{l_e} -\frac{\xi^2}{l_e} d\xi = -\frac{1}{3}$$

$$\int_0^{l_e} g_1 g_2 g_2' d\xi = \int_0^{l_e} \frac{\xi}{l_e} d\xi = \frac{1}{3}$$

Substituting the values into the expression

$$\begin{bmatrix} (-\frac{1}{3} \psi_{i-1} + \frac{1}{3} \psi_i) & (-\frac{1}{6} \psi_{i-1} + \frac{1}{6} \psi_i) \\ (-\frac{1}{6} \psi_{i-1} + \frac{1}{6} \psi_i) & (-\frac{1}{3} \psi_{i-1} + \frac{1}{3} \psi_i) \end{bmatrix}$$

factoring out a $-1/3$, the local matrix for the global operator becomes

$$\int_0^1 \{G_i\} \langle G_j \rangle \{ \Psi \} \langle G_j \rangle d\eta \quad \Rightarrow \quad -\frac{1}{3} \begin{bmatrix} (\Psi_{i-1} - \Psi_i) & (\frac{\Psi_{i-1} - \Psi_i}{2}) \\ (\frac{\Psi_{i-1} - \Psi_i}{2}) & (\Psi_{i-1} - \Psi_i) \end{bmatrix}$$

For operator E.5,

global

local

$$\int_0^1 \{G_i\} d\eta \quad \Rightarrow \quad U \left[\int_0^{l_e} \begin{Bmatrix} g_1 \\ g_2 \end{Bmatrix} d\xi \right]$$

Substituting in the local shape function, and integrating, the expression becomes

$$\int_0^{l_e} \begin{Bmatrix} (1 - \frac{\xi}{l_e}) \\ \frac{\xi}{l_e} \end{Bmatrix} d\xi \quad \Rightarrow \quad \frac{l_e}{2} \begin{Bmatrix} 1 \\ 1 \end{Bmatrix}$$

This last operator is used for the excitation vector as described in the FEM formulation.

TABLES AND FIGURES

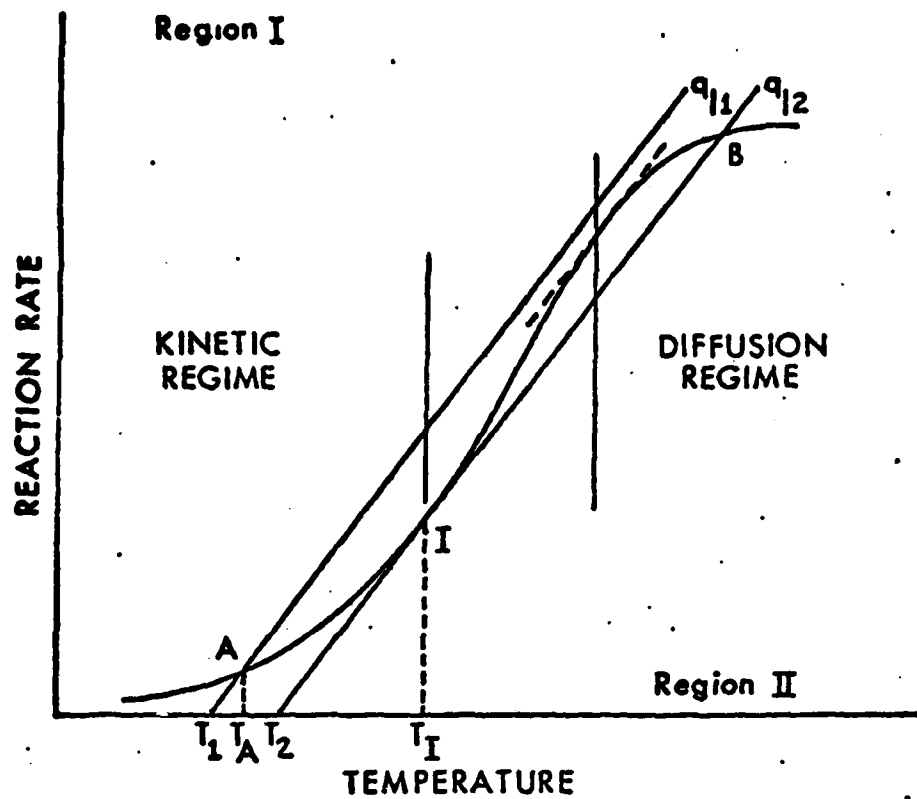


FIGURE 1 Semenov model of combustion.

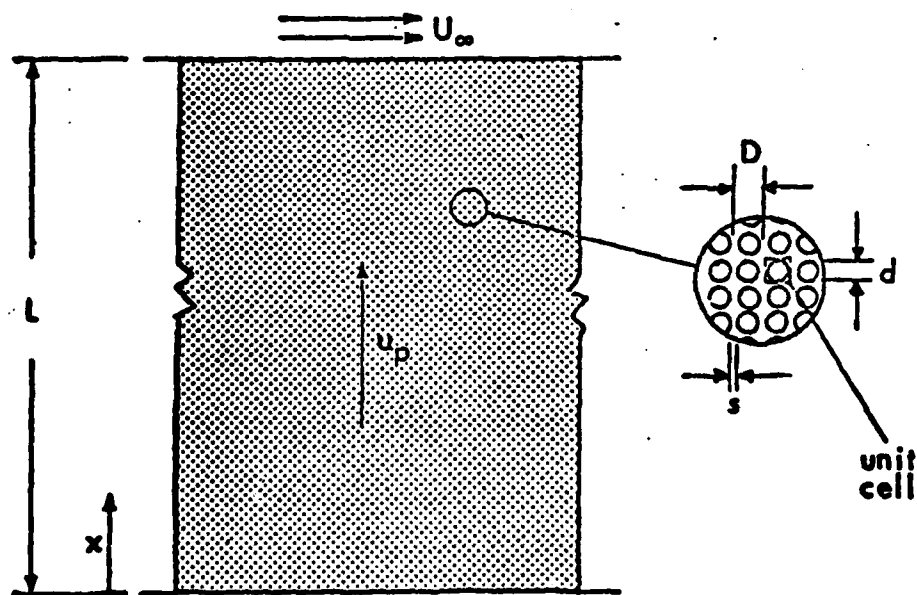


FIGURE 2 Idealized geometry of a fibrous graphite plate.

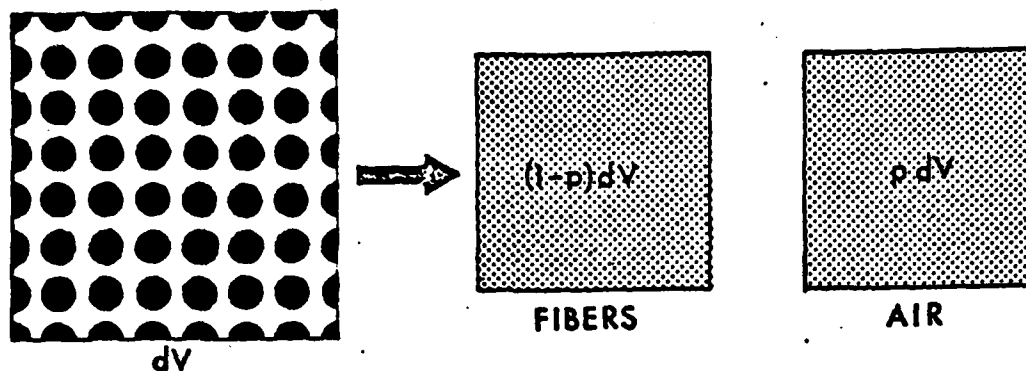


FIGURE 3 Separating a differential volume of porous medium into respective volumes of fiber and air.

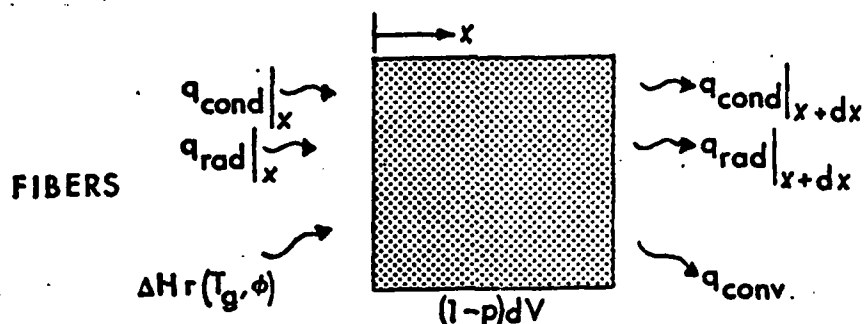


FIGURE 4 Energy balance on the fibers.

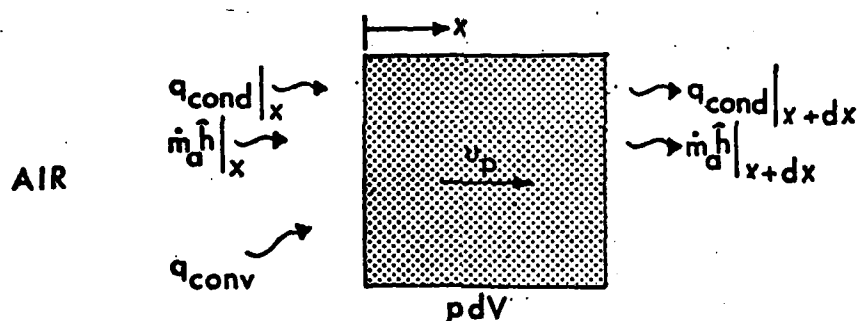


FIGURE 5 Energy balance on the internal flow.

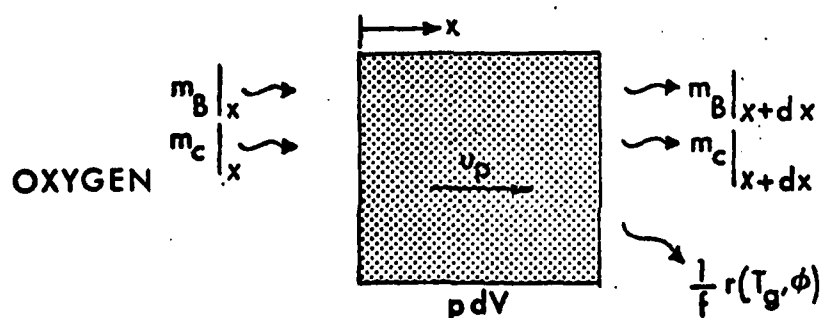


FIGURE 6 Molecule-mass balance on the oxygen.

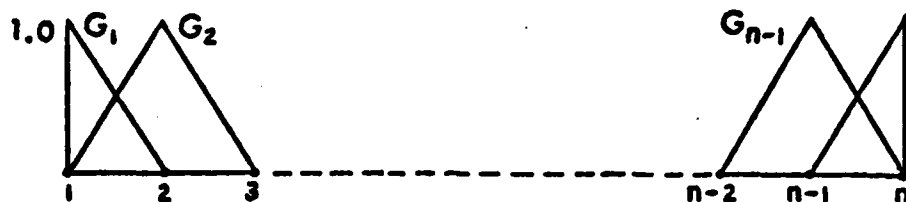


FIGURE 7 Linear shape functions for the Galerkin formulation of FEM.

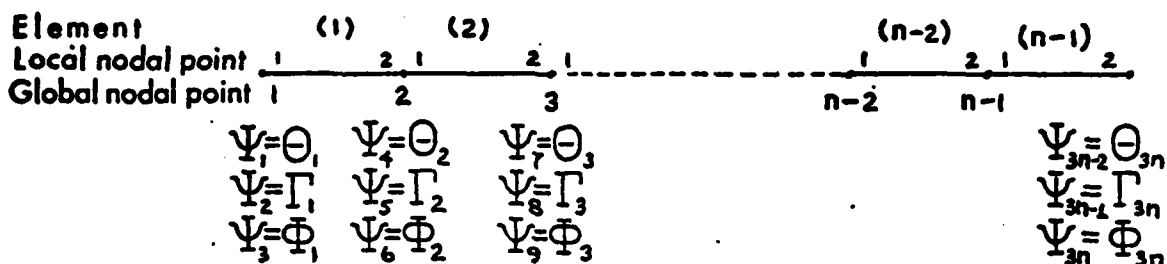


FIGURE 8 Numbering scheme used in system matrices.

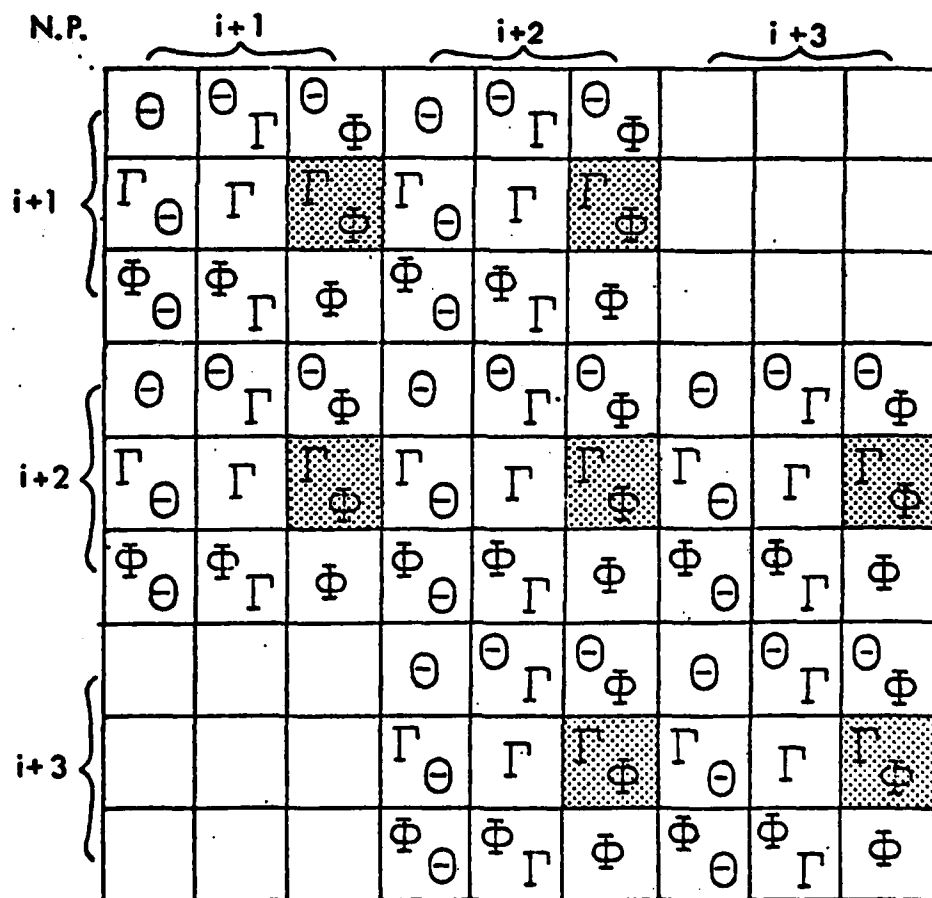


FIGURE 9 Shows coupling in system of p. d. e.

TABLE 1

SUMMARY OF RESULTS*

Case	U_∞ kt.	d in.	L in.	u_p ft./s.	ΔP psi.	Re_j	m $ft^2 \times 10^3$	P	h_j $btu/ft^2 \cdot hr \cdot ft$	z ft^2/ft	Remarks
1	50.	.004	.25	.3745	.0597	.4487	.1652	.497	19.19	3016.	ignition @ 8.3s
2	90.	.004	.25	1.208	.1925	1.447	.1652	.497	34.06	3016.	extinction
3	120.	.004	.25	2.140	.3405	2.56	.1652	.497	45.04	3016.	extinction
4	20.	.004	.25	.060	.0096	.0719	.1652	.497	7.82	3016.	extinction
5	70.	.004	.25	.7235	.1168	.8778	.1652	.497	26.70	3016.	ignition @ 6.7s
6	10.	.004	.25	.015	.0024	.0180	.1652	.497	3.97	3016.	extinction
7	90.	.004	.5	.6039	.1925	.7236	.1652	.497	24.25	3016.	ignition @ 4.9s
8	90.	.004	1.0	.3019	.1925	.3618	.1652	.497	17.27	3016.	ignition @ 6.0s
9	50.	.002	.25	.6657	.0597	2.80	.5163	.8743	23.85	1508.	extinction
10	50.	.0048	.25	.2813	.0597	.156	.0689	.276	13.62	3619.	extinction
11	90.	.004	1.5	.2013	.1925	.2412	.1652	.497	14.16	3016.	ignition @ 6.6s
12	90.	.004	2.0	.151	.1925	.1809	.1652	.497	12.29	3016.	ignition @ 8.0s
13	90.	.004	4.0	.0755	.1925	.0905	.1652	.497	8.75	3016.	ignition
14	90.	.004	6.0	.0503	.1925	.0603	.1652	.497	7.18	3016.	ignition

* For $D=.005"$ and initial conditions of Figure 10

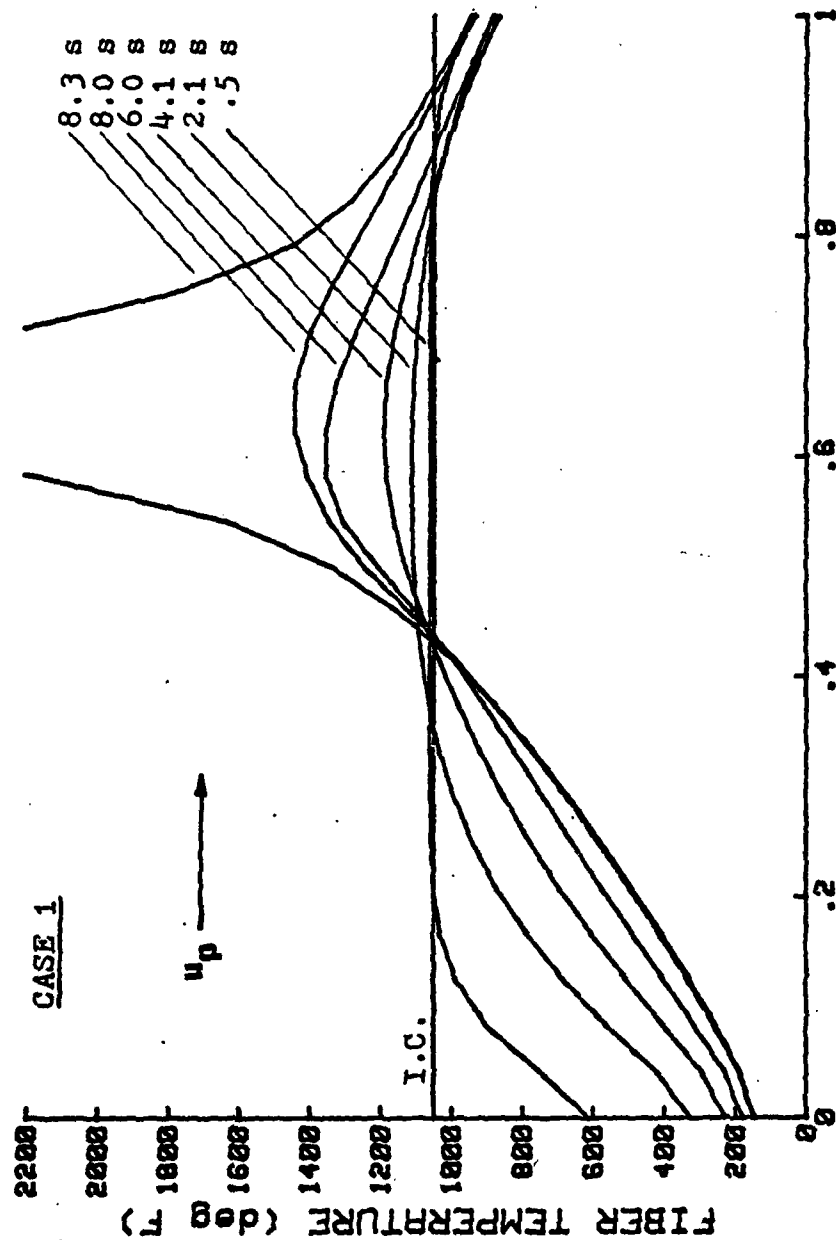


FIGURE 10 Fiber temperature response of Case 1 ($u_g=50$ kt.; $d=.004$;
 $L=.25$).

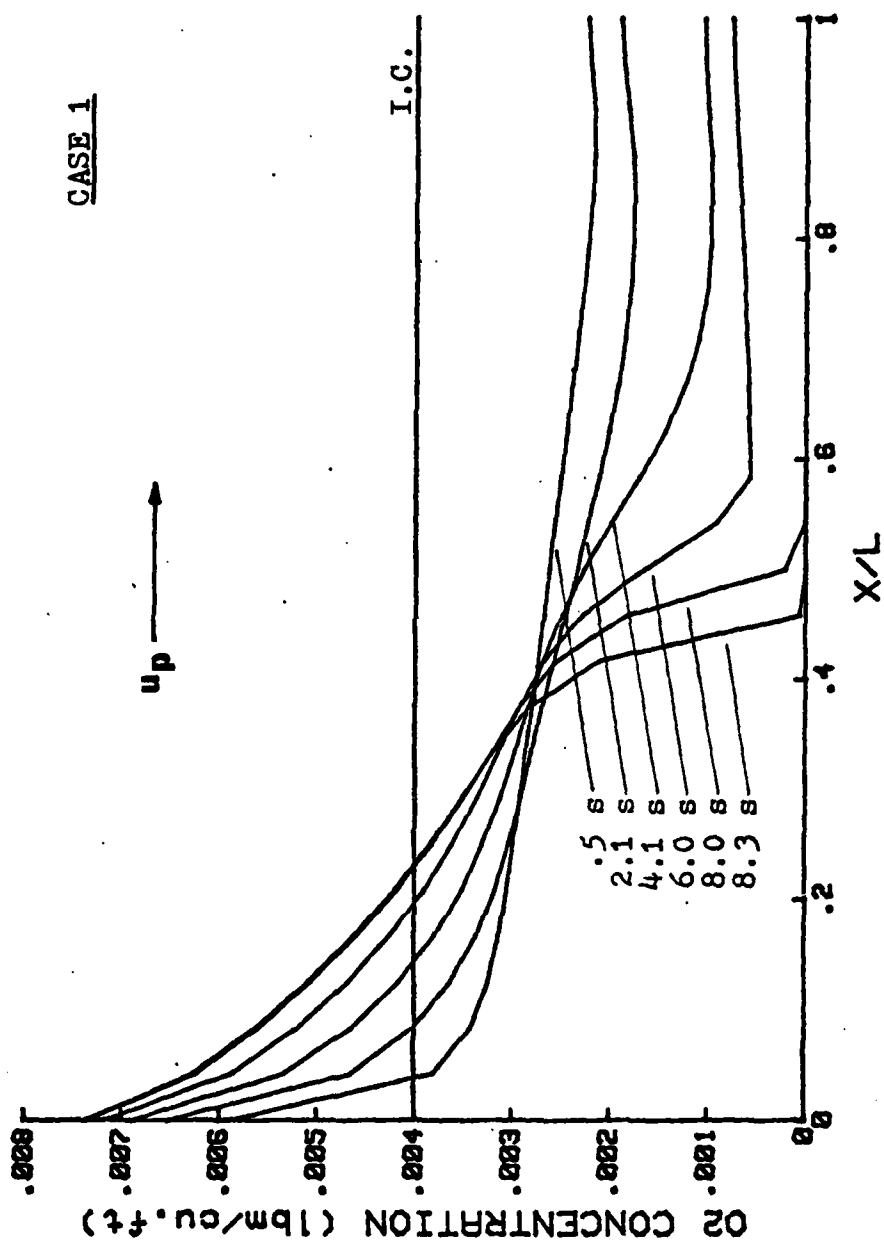


FIGURE 11 Oxygen concentration response of Case 1 ($U_\infty = 50 \text{ kt.}$; $d = .004''$; $L = .25''$).

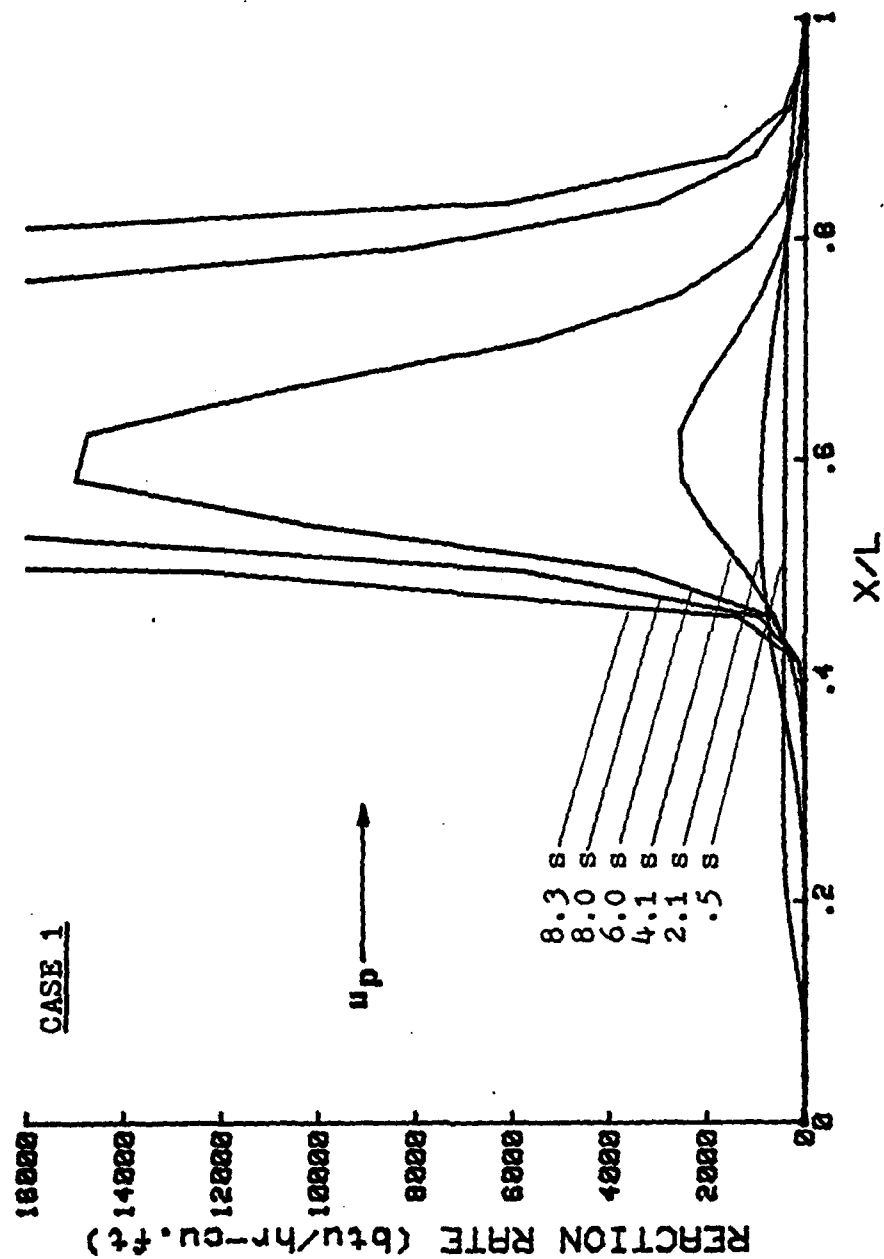


FIGURE 12 Observed reaction rate for Case 1.

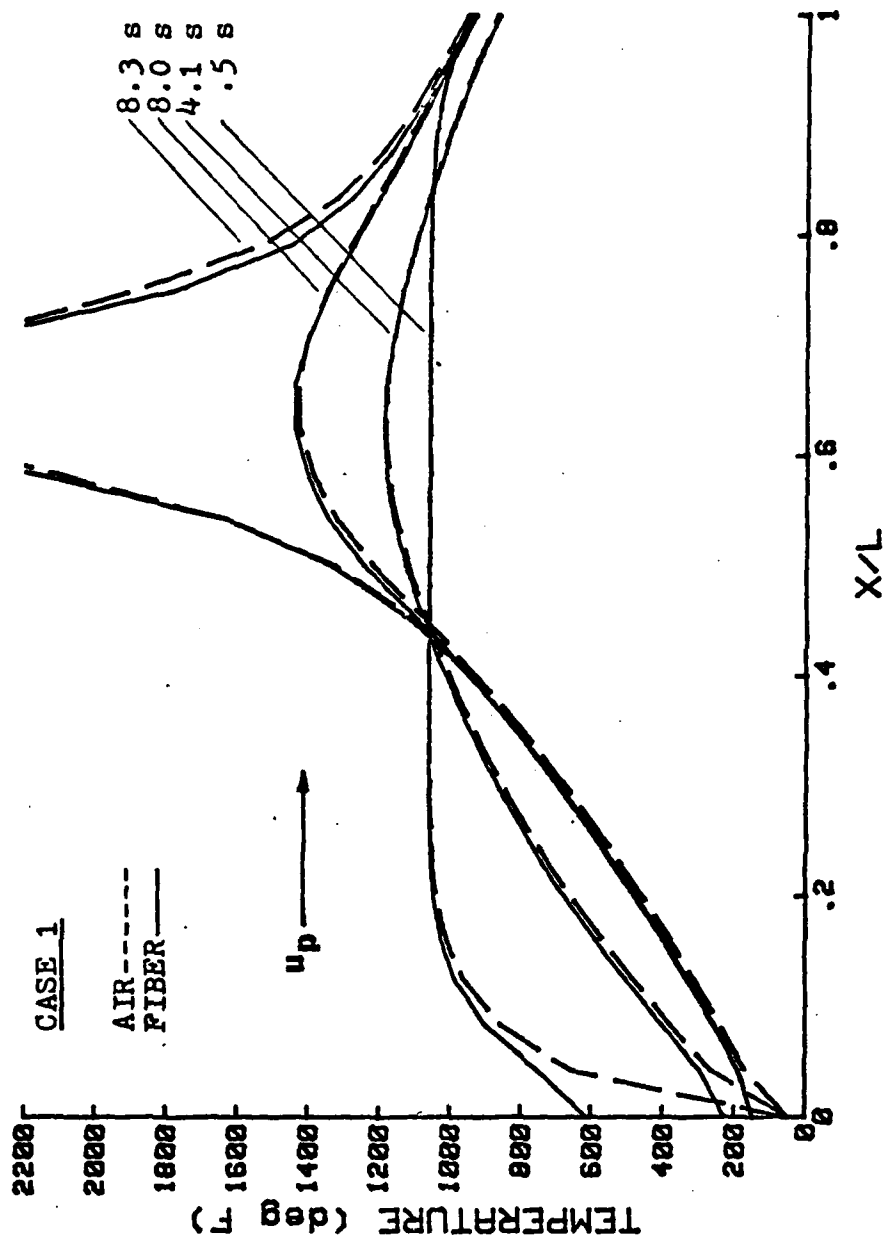


FIGURE 13 Flow temperature follows the fiber temperature.

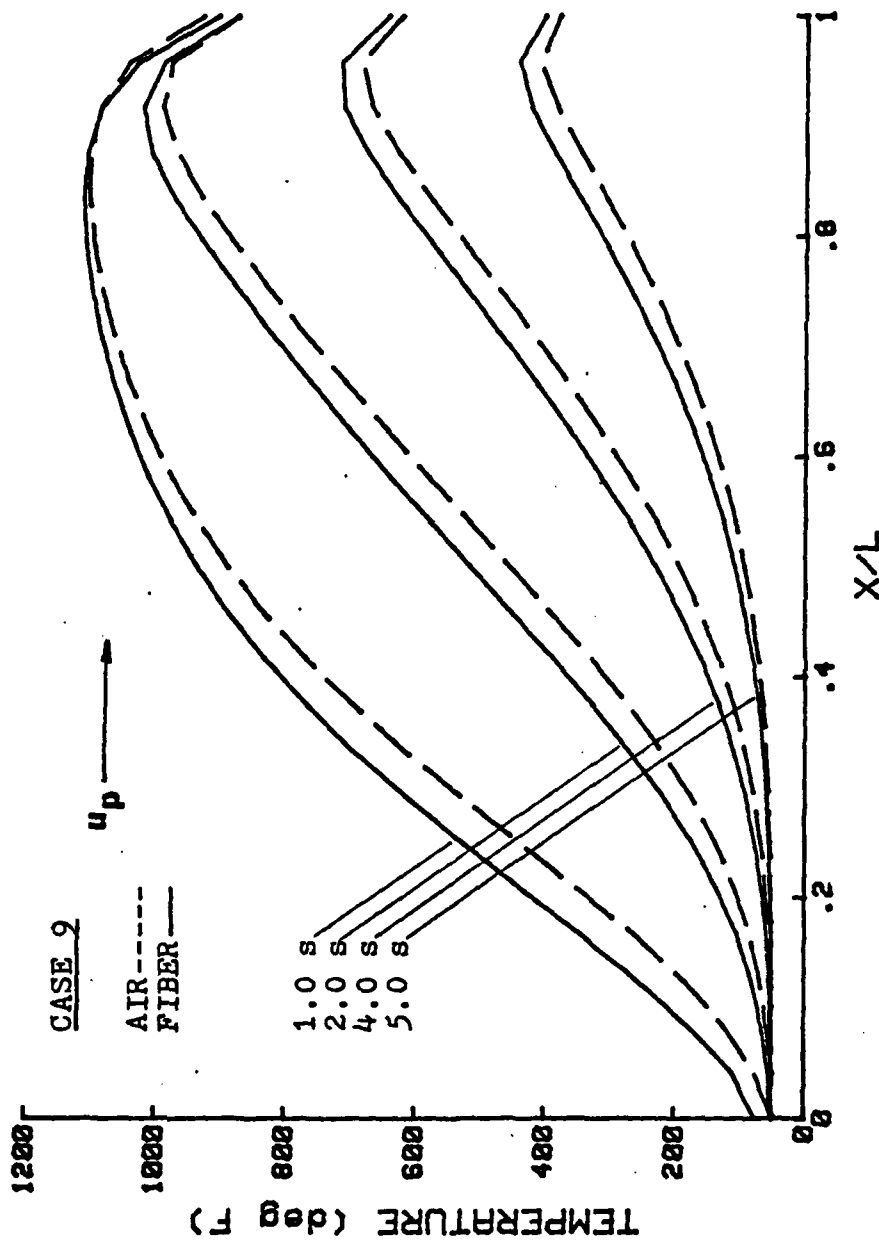


FIGURE 14 Flow and fiber temperature difference at high porosity and flow rate (for Case 9, $p=.87$, $U_0=90\text{kt.}$).

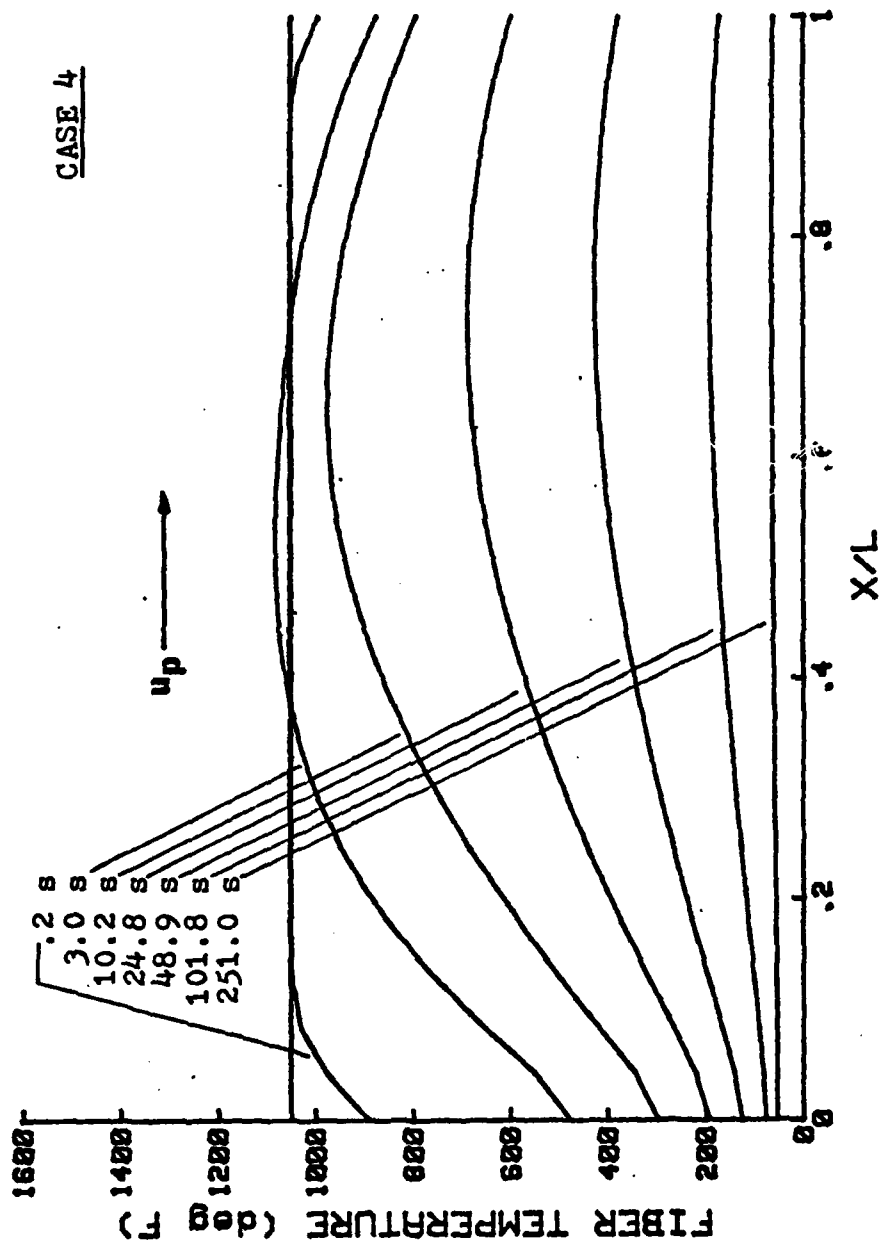


FIGURE 15 For Case 4, $U_\infty = 20 \text{ kt.}$, $d = .004$ ", $L = .25$ " (for effect of varying exterior velocity, U_∞ , compare Figures 15, 16 and 17).

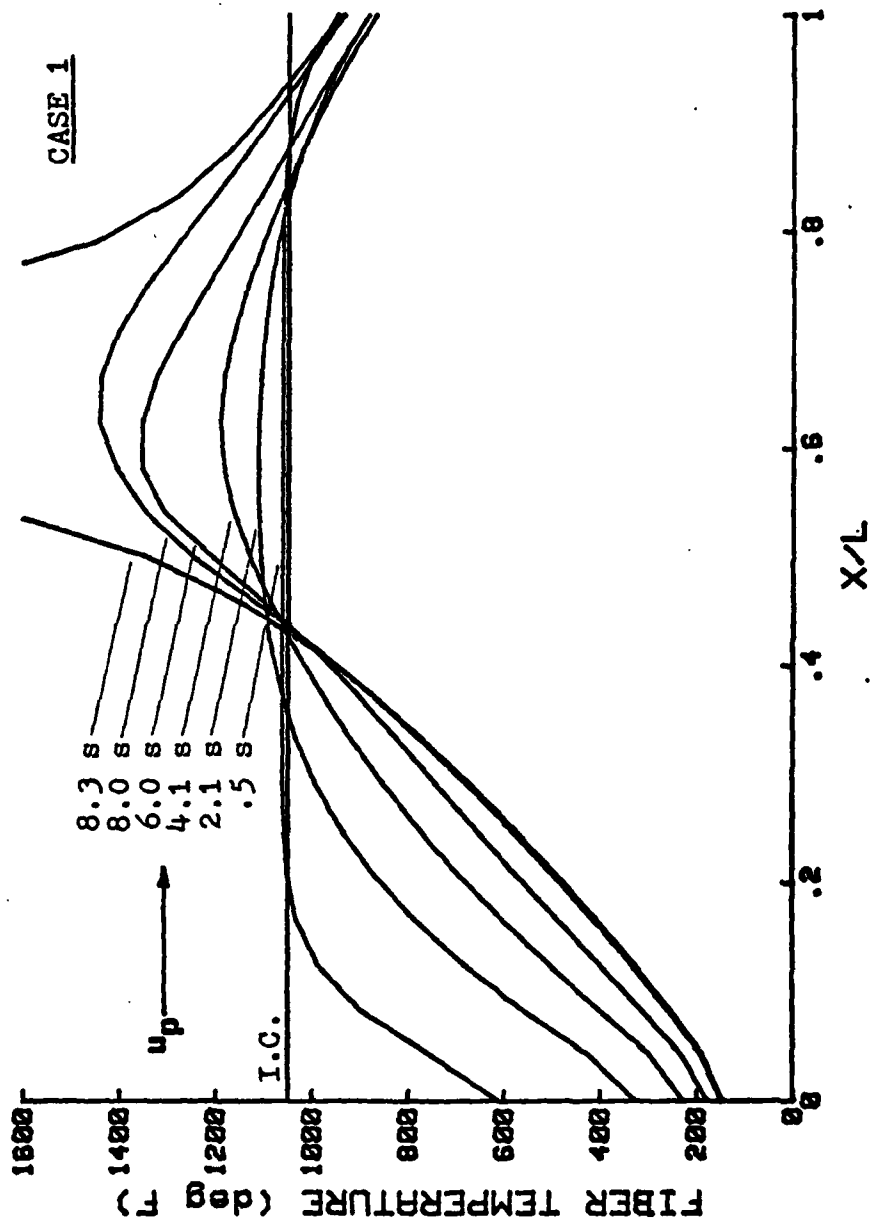


FIGURE 16 For Case 1, $u_{\infty} 50 \text{ kt.}$, $d = .004''$, $L = .25''$.

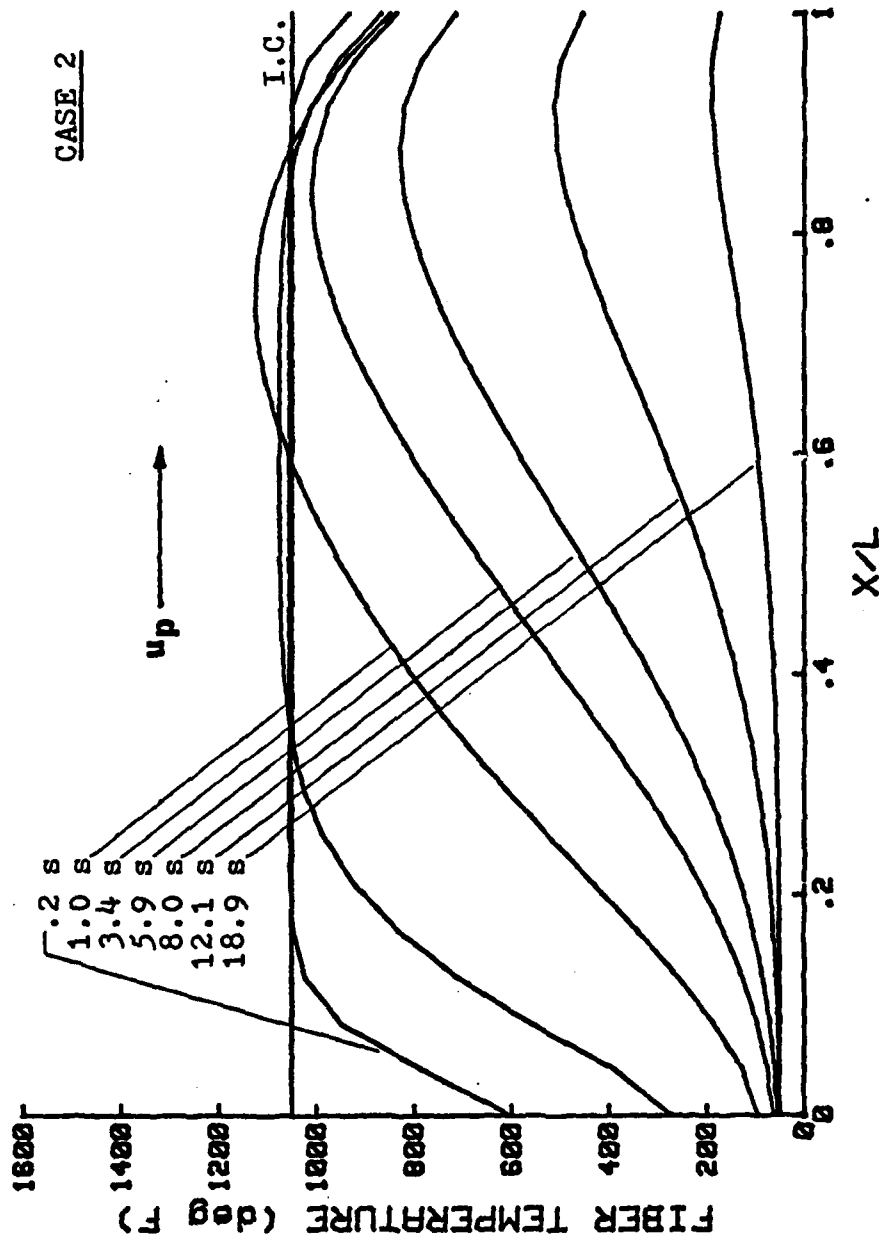


FIGURE 17 For Case 2, $U_2=90$ kt., $d=.004$ ", $L=.25$ ".

CASE 2

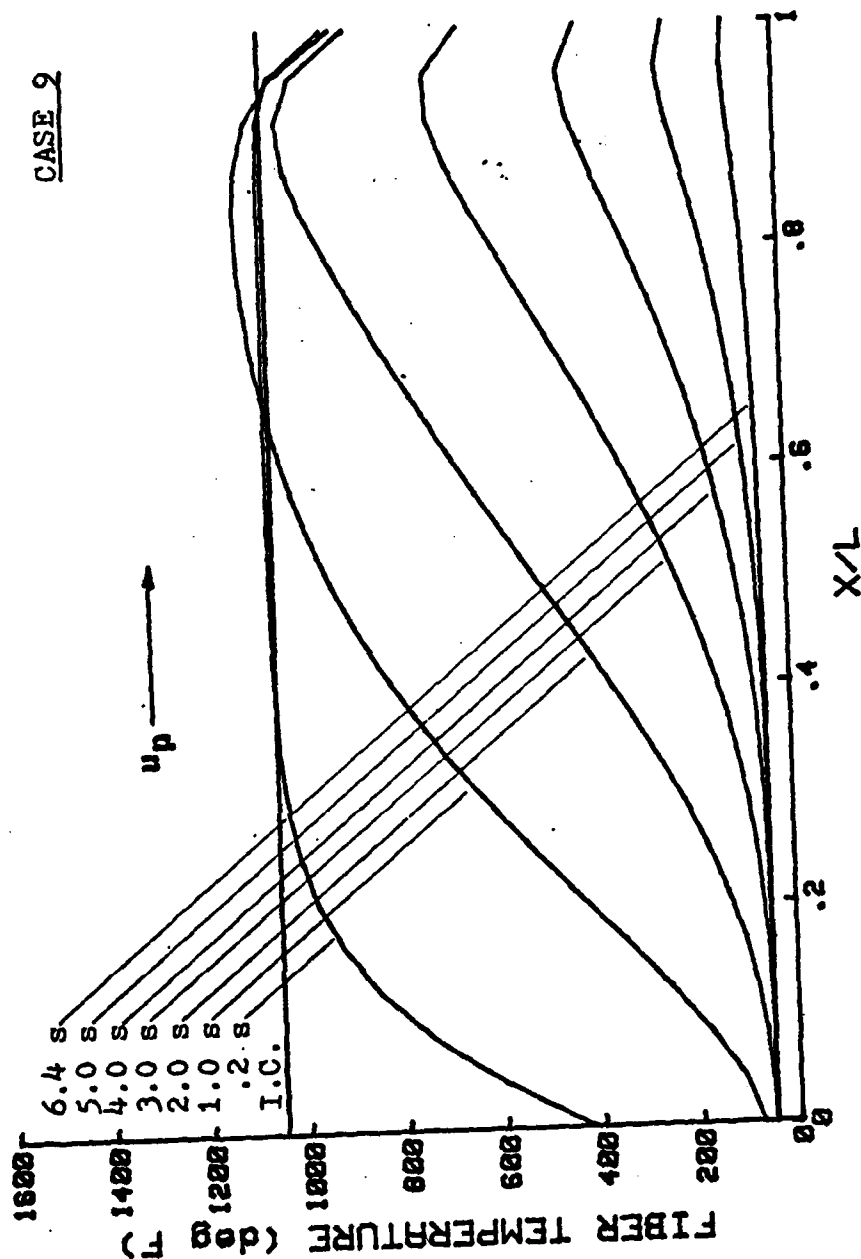


FIGURE 18 For Case 9, $U=50\text{kt.}$, $d=.002$ ", $L=.25$ " (for effect of varying fiber diameter, d, compare Figures 16, 18 and 19).

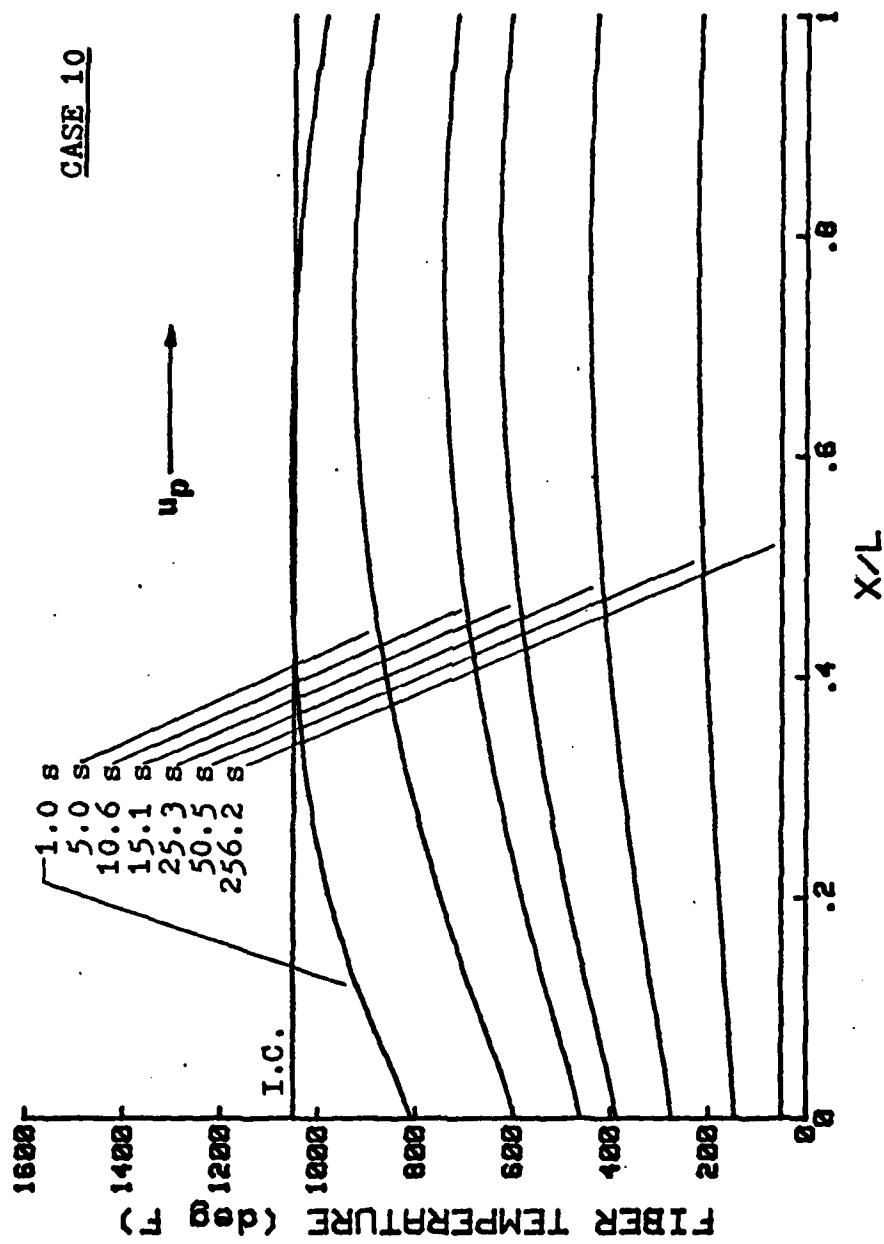


FIGURE 19 For Case 10, $U_{\infty} = 50 \text{ kt.}$, $d = .0048''$, $L = .25''$.

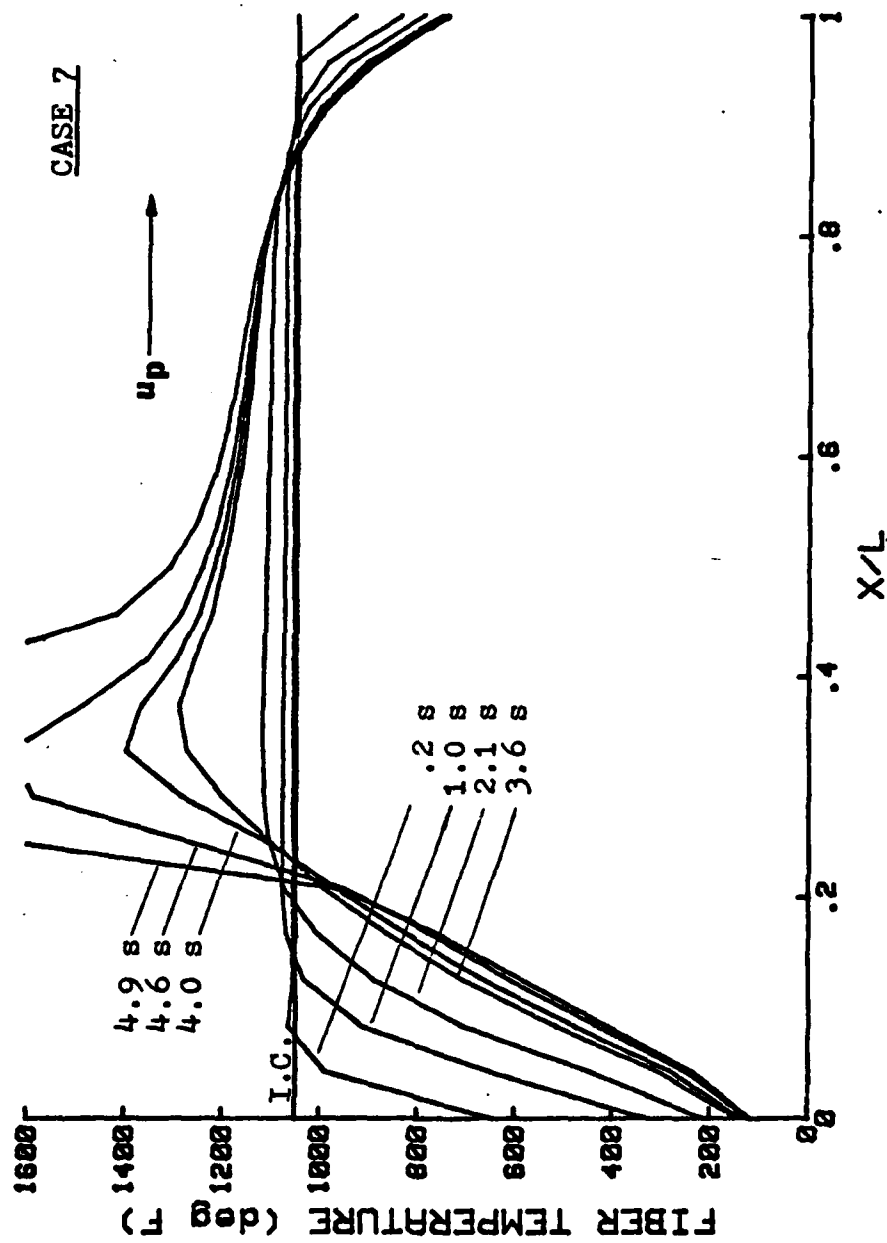


FIGURE 20 For Case 7, $U_\infty = 90 \text{ kt.}$, $d = .004$ ", $L = .5$ " (for effect of varying plate thickness, L , compare Figures 17, 20 and 21).

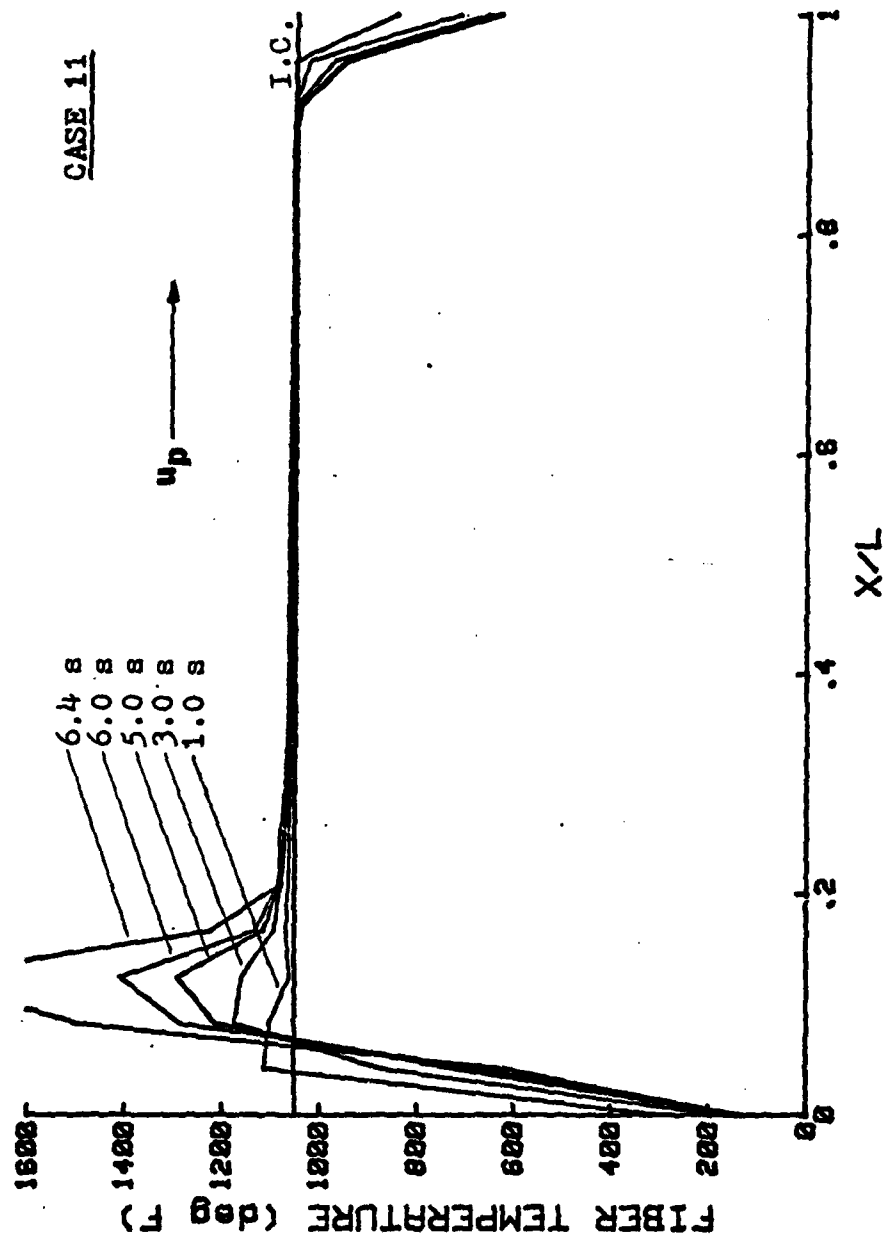


FIGURE 21 For Case 11, $U_{\infty} = 90 \text{ kt.}$, $d = .004$ ", $L = 1.5$ ".

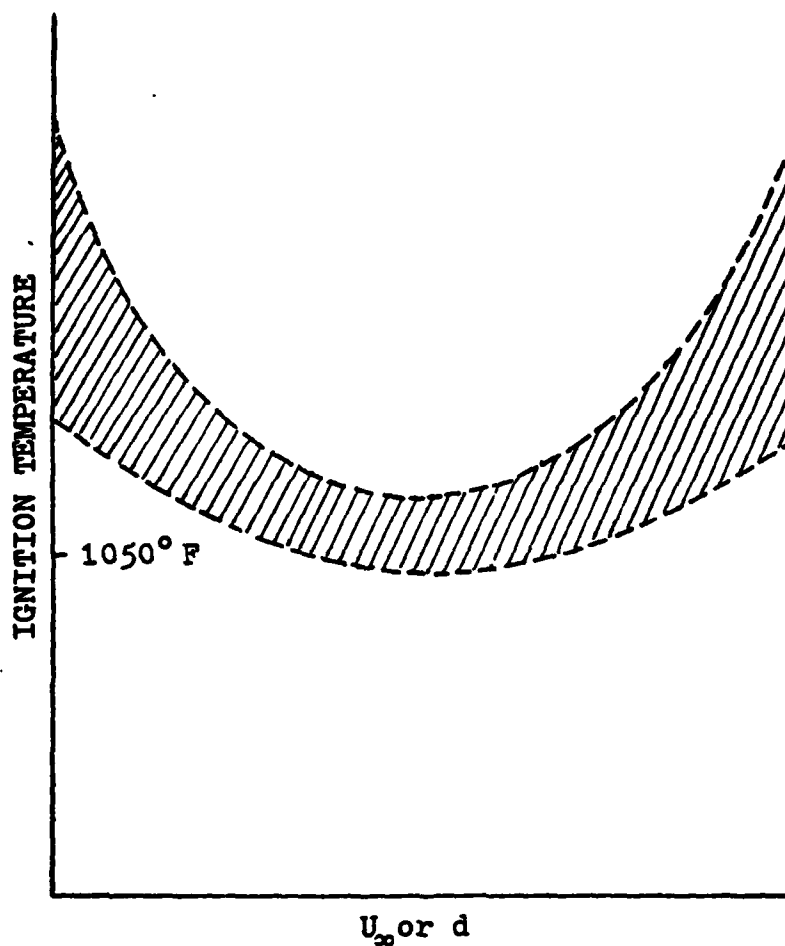


FIGURE 22 Shaded region represents shape of ignition temperature curve as a function of U_∞ or d.

[illegible]

CNE-DIM'L TRANSIENT HEAT TRANSFER IN P'ROUS GRAPHITE
WITH COMBUSTION

```

NNP=NUMBER OF NODAL FCINTS
TAMB=AMBIENT TEMP. (F)
TORT=TORQUE
SPACE1=FLY THICKNESS (IN.)

XLENT1=FLATE THICKNESS (IN.)

GCOND=CONDUCTIVITY OF BULK GRAPHITE (BTU PER FT**2*F)
SPHYS=SPEC. HEAT OF GRAPHITE (BTU PER LBM*F)
HSURF=APPROX. CONV. HEAT TRANS. COEFF. AT X=C (BTU PER FT**2*F)
T=TIME OF STEEP AT WHICH PRINT OUT OF VARIABLES DESIRED (SEC.)
TSTART=START TIME FOR PROBLEM (SEC); USED FOR BOOKKEEPING
IF AS A RESTART FROM PREVIOUS PROBLEM (INPUT 0.0)
X(I)=NODAL DIMEN. NODAL POINT LOCATIONS (VALUES BETWEEN 0.0-1.0)
CHI(I,I)=ARRAY HOLDING INITIAL CONDITIONS (DEG-F; LBM PER FT**3); TEMP-G ENTERED INTC LOC. (1,1),(1,4)...(1,3*NNP-2); TEMP-A ENTERED INTC (1,2),(1,5)...(1,3*NNP-1); CONC-A ENTERED INTO (1,3),(1,6)...TEMP-A, FINALLY CONC-A.
IELEV=CCCE FOR N.P. DISTRIBUTION (0=ENTER NODAL POINT, X/L; 1=AUTOMATICALLY DIVIDES XLENT1 INTO NNP NODAL POINTS)

CFR INPUT OF DATA LOCK AT SAMPLE INPUT FILE IN TESIS.

```

```

PROGRAM CALCULATES FOLLOWING PROPERTIES FOR AMBIENT CONDITIONS
AT START OF PROGRAM:

DELPL=PRESSURE DIFFER ACROSS PLATE (PSI)
Z=SURF.AREA OF FIBER PER UNIT VOLUME (FT**2 PER FT**3)

```

0047
0048
0049
0050
0051
0052
0053
0054
0055
0056
0057
0058
0059
0060
0061
0062
0063
0064
0065
0066
0067
0068
0069
0070
0071
0072
0073
0074
0075
0076
0077
0078
0079
0080
0081
0082
0083
0084
0085
0086
0087
0088
0089
0090
0091
0092
0093
0094

```

PCRC=PERCCTY OF PLATE (SQ.FT.)
FEORE=FEORECTY OF PORES (FT. PER SEC)
ZU=ZU=AVG. VEG. (IN)
RCA=REACTY OF AIR (BTU PER FT**2*HR)
VCON=VCONCTY OF AIR (BTU PER FT**2*HR)
CCND=CCNDCTY OF PLATE (BTU PER FT**2*HR)
RACCON=ACTY OF PLATE (BTU PER FT**2*HR)
RE=REYNOLDS NUMBER
REIN=INTERNAL CONVECTION HEAT TRANSFER COEF. (BTU PER HR*FT**2*F)
CCNV=INTERNAL CONVECTION HEAT TRANSFER COEF. (BTU PER HR*FT**2*F)
HSURF=HEAT TRANSFER COEF. AT RIGHT SURFACE (BTU PER HR*FT**2*F)

PCRC=PERCCTY OF PLATE (SQ.FT.)
FEORE=FEORECTY OF PORES (FT. PER SEC)
ZU=ZU=AVG. VEG. (IN)
RCA=REACTY OF AIR (BTU PER FT**2*HR)
VCON=VCONCTY OF AIR (BTU PER FT**2*HR)
CCND=CCNDCTY OF PLATE (BTU PER FT**2*HR)
RACCON=ACTY OF PLATE (BTU PER FT**2*HR)
RE=REYNOLDS NUMBER
REIN=INTERNAL CONVECTION HEAT TRANSFER COEF. (BTU PER HR*FT**2*F)
CCNV=INTERNAL CONVECTION HEAT TRANSFER COEF. (BTU PER HR*FT**2*F)
HSURF=HEAT TRANSFER COEF. AT RIGHT SURFACE (BTU PER HR*FT**2*F)

FOLLOWING PROPERTIES ARE EVALUATED AT THE PREVIOUS TIME STEP IN
S.R. FOR EACH NCCAL PCNT:

1. VISCOSITY OF AIR (VISC2)
2. CONDUCTIVITY OF AIR (ACCD2(I))
3. DENSITY OF AIR (ROA2(I))
4. AVG. FCFE VELOCCTY (U2(I))
5. INTERNAL REYNOLDS NUMBER (REIN)
6. INTERNAL CONVECTION HEAT TRANS. COEF (CCNV2(I))
7. EQUVALENT CONDUCTYVITY CUE TO RAD. AND THERM. CCNC.
8. CONDUCTYVITY OF PLATE (CCND2(I))
9. DIFFUSIVTY IN TERM
10. HEAT GENERATION TERM (RA TEH)
11. OXYGEN CONSUMPTION TERM (RATE)

MAIN PROGRAM *****
INPUT DATA***

REAL*6 Z, ZDCT, GAMMA, GAM
EXTERNAL LIFFUN, JACMAT, LCCASUB, COPYZ, NUTSL, Derval
COMMON /K(75,75), ZCCT(75,75), XLENTH, CCNC, RACCON, CONV, Z, ROG,
XCELP, PCFCS, CHI(7,75), TAMB, CAMB, F(75),
XPARB, ACACC(25,4), BCCI(25,4), BSH(25,4), X(75), U, CD(25,4),
XRGAS, BCECC(25,4), CC(25,4), ADDT(25,4), BETA, CCND, D, SPHTG, ROA, SPHTA,

```

CC


```

XCGND2(25), TORT, CC2(25,4), SPHT, ZMASS(75), PERM, VISC,
XU2(25), ANP, NNPA, NKPE, ANPC, NEL, ICOR(75,2), IJK
DIMENS ICN C(75), W(7500), VL(1), X2(1), Y4(1), V1(25), Y2(25), Y3(25),
XX(25), FFACTK(75), FCF(75)
XREAD(5,1) IELEM
FORMAT(11)
WRITE(6:6), IELEM
FORMAT(1:6,41)

```

GEOMETRY OF DOMAIN (1-CIM'L)***

```

READ(5,10) NNP
FORMAT(1,11)
NEL=NNP-1
IE(1) IELEM=EG,11 GO TO 20
READ(5,11) X(1), I=1, NNP
FORMAT(1,11)
GO TO 30
X(1)=C,C
CO 30 I=2, NNP
J=I-1
X(I)=X(J)+1.0/FLOAT(NEL)
CONTINUE
WRITE(6:6), 'NODAL P1, X-POSITION'
FORMAT(6,4) (1,X(I), I=1, NNP)
WRITE(6:6), '4X, I2, 9X, F5.3/'
FORMAT(1:4, I2, 9X, F5.3)

```

PHYSICAL PROPERTIES***

```

READ(5,10) T, HMAX, X, I, START, UINFL, IAMB, PAMB, TERT, DI, SPACE1, HLENT,
XLENT, G12, S, CCOND, EPS, RCX, SPHT, G, SPHTA, HSURFL, CAMBI
FORMAT(1,11)
UINF=UINFL+1.688
PAPR=PAAB+SPACE1-144.0
CELL=CELL/12.0
C=C1/12.0
SPACE=SPACE1/12.0
XLENT=XLENT/12.0
TABS=TABS+459.7
BETA=C/SPACE
POROS=1.0-C-FCRCSI

```

```

0095
0096
0097
0098
0099
0100
0101
0102
0103
0104
0105
0106
0107
0108
0109
0110
0111
0112
0113
0114
0115
0116
0117
0118
0119
0120
0121
0122
0123
0124
0125
0126
0127
0128
0129
0130
0131
0132
0133
0134
0135
0136
0137
0138
0139
0140
0141
0142

```

WRTITLE(0.00) TURT
FORMAT(0.0). TORTUOSITY (LENGTH OF PATH PER LENGTH THICKNESS OF ME

0191
0192
0193
0194
0195
0196
0197
0198
0199
0200
0201
0202
0203
0204
0205
0206
0207
0208
0209
0210
0211
0212
0213
0214
0215
0216
0217
0218
0219
0220
0221
0222
0223
0224
0225
0226
0227
0228
0229
0230
0231
0232
0233
0234
0235
0236
0237
0238

```

70  FORMAT('C','FILAMENT DIAMETER=',E10.4,' INCHES')
71  WRITE(6,72) FLENT, LENGTH OF SQUARE POROUS PLATE=',E10.4,' FT.')
72  FORMAT('Q','SIDE LENGTH OF SQUARE POROUS PLATE=',E10.4,' FT.')
73  WRITE(6,74) ZPAC, THICKNESS OF SINGLE MATRIX-FILAMENT LAMINATE=',E10.4,'
74  INCHES')
75  WRITE(6,76) XLENT, THICKNESS OF POROUS PLATE=',E10.4,' INCHES')
76  WRITE(6,78) RGAS, GAS CONSTANT OF AIR=',E10.4,' LBF*FT. PER LBM*DEG-R')
77  WRITE(6,80) CAMBI, AMBIENT CONCENTRATION OF OXYGEN=',E10.4,' LBM PER CU.F
78  XT, )
79  WRITE(6,82) GCCND, CONDUCTIVITY OF FILAMENT MATERIAL=',E10.4,' BTU PER FT
80  X*HR*CEG-F')
81  WRITE(6,84) EMIS, EMISSIVITY OF FILAMENT MATERIAL=',E10.4')
82  WRITE(6,86) RCG, MASS DENSITY OF FILAMENT MATERIAL=',E10.4,' LBM PER CU
83  X*FT.)
84  WRITE(6,88) SFHTG, SPECIFIC HEAT OF FILAMENT MATERIAL=',E10.4,' BTU PER L
85  X*HR*CEG-F')
86  WRITE(6,90) SPHTA, SPECIFIC HEAT OF AIR=',E10.4,' BTU PER LBM*DEG-F')
87  WRITE(6,92) FSURF, SURFACE AREA PER UNIT VOLUME=',E10.4,' SQ.FT.PER CU.FT
88  X*BTU PER FT**2*HR*DEG-F')
89  WRITE(6,94) /, EX, 'THE FOLLOWING PROPERTIES ARE CALCULATED FOR AMBIE
90  NAT CALCULATION')
91  WRITE(6,96) DELP, PRESSURE DIFFERENTIAL ACROSS PLATE=',E10.4,' PSI.')
92  WRITE(6,98) Z, SURFACE AREA PER UNIT VOLUME=',E10.4,' SQ.FT.PER CU.FT
93  X*BTU PER FT**2*HR*DEG-F')
94  WRITE(6,100) FCROS, POROSITY (VOLUME OF VOID PER UNIT VOLUME=',E10.4')
95  WRITE(6,102) PERM, PERMEABILITY OF POROUS MEDIUM=',E10.4,' SQ.FT.')
96  WRITE(6,104) ZPORS, NUMBER OF PORES PER SQ.FT.=',E10.4')
97  WRITE(6,106) U2, PORE VELOCITY=',E10.4,' FT. PER SEC.')
98  WRITE(6,108) DELI, DELTA T=',E10.4,' INCHES')
99  WRITE(6,110) RGA, AVERAGE PORE DIAMETER=',E10.4,' INCHES')

```


[illegible]

[illegible]

124

```

004778 12Z00T(2,2)=1.0  

004779 ZK(3,3)=ZK(3,3)-U2(1)*XLENT+  

004780  

004781 ITEGRATE ZCCT***  

004782 CALL SCFSC(CHI,YL,TIME,TEND,NNPC,NL,NNPC,JSKF,MAYDER,O,I,HMIN,HMA  

004783 X),RMSEF(.6)  

004784 {O=310-2  

004785 JJ=JJ+1  

004786 KK=KK+1  

004787 C(I,J)=C(I,J)+TAME  

004788 C(J,J)=C(J,J)+TAMB  

004789 IF(C(I,J).LT.O.O) C(I,J,KK)=1.0E-12  

004790 C(KK,C(I,J))=CAPE  

004791 TAMES=TAMB+C(I,J)+455.7  

004792 FGR(KK)=(1.0-FGRQS)*14QBF  

004793 X(TABSS)=EXP(39EE=C/TABS)*{12.0**3}  

004794 CONTINUE  

004795  

004796 BCNCARY CCNCLION ADJUSTMENT AFTER INTEGRATION***  

004797  

004798 ZK(1,1)=ZK(1,1)-ZKACC1  

004799 ZK(NNPB,NNPA)=ZK(NNPA,NNFA)-ZKADD2  

004800 ZK(NNPB,NNPA)=ZK(NNPB,NNPA)-ZKADD2  

004801 ZK(3,3)=ZK(3,3)+U2(1)*XLENT+  

004802  

004803 PRINT NEW CT-I.5***  

004804 TIME2=TIME+TIME2  

004805 WRITE(6,315), AT TIME=' ,F8.4,' SEC.', /  

004806 FORMAT(315), /  

004807 WRITE(6,320), NP TEMP-G  

004808 FORMAT(320), NP TEMP-A  

004809 F.C.F.(BTU PER CU.IN*F.), /  

004810 FORMAT(330), 3X,I2,6X,FE.2,6X,F8.2,8X,F7.5,8X,F11.3)  

004811 NN=1  

004812 A=1,NAF  

004813 KKA=KK+2  

004814 WRITE(6,330) N,(C(I),I=NA,NNN),HGR(NNN)  

004815 NA=NA+1  

004816 CONTINUE  

004817  

004818 310  

004819  

004820 315  

004821  

004822 320  

004823  

004824 330  

004825  

004826 335

```


[illegible]

[illegible]

128

131

```

100 IB=3
200 JA=1
300 JB=6
400 CO=3
500 CY(I)=C
600 DO I=1,C
700 J=JA,JB
800 CY(I)=ZDOT(I,J)*HINV-ZK(I,J)*Y(1,J)
900 CY(I)=CY(I)-F(I)
1000 CONTINUE
1100 IA=IA+1
1200 IB=IB+1
1300 IF(K.EC.1) GO TO 5
1400 JA=JA+1
1500 JB=JB+1
1600 CONTINUE
1700 RETURN
1800 END
1900
2000
2100
2200
2300
2400
2500
2600
2700
2800
2900
3000
3100
3200
3300
3400
3500
3600
3700
3800
3900
4000
4100
4200
4300
4400
4500
4600
4700
4800
4900
5000
5100
5200
5300
5400
5500
5600
5700
5800
5900
6000
6100
6200
6300
6400
6500
6600
6700
6800
6900
7000
7100
7200
7300
7400
7500
7600
7700
7800
7900
8000
8100
8200
8300
8400
8500
8600
8700
8800
8900
9000
9100
9200
9300
9400
9500
9600
9700
9800
9900

```

```

100  FW(I,J)=A+ZCOT(I,J)-ZK(I,J)
200  CONTINUE
300  IA=IA+1
400  IB=IB+1
500  IF(K.EC.NEL) GC TC ECC
600  JA=JA+1
700  JB=JB+1
800  RETURN
900  END
1000  SUERCUTINE SDESCL (Y,YL,T,TEND,NY,NL,M,JSKF,MAXDER,IPRT,T,TMIN,
1100  1PMAX,RMSEPS,M)
1200  -----
1300  SUBROUTINE SCESCL IS A DRIVER ROUTINE FOR SUBROUTINE LDASUB.
1400  ITS PURPOSE IS TO SET UP THE NECESSARY REFERENCES TO A LARGE
1500  BLOCK OF AUXILIARY STORAGE, AND OBTAIN INITIAL VALUES OF
1600  DERIVATIVES.
1700  THE CALLING SEQUENCE FOR SDESCL IS
1800
1900  CALL SDESCL(Y,YL,T,TEND,NY,NL,M,JSKF,MAXDER,IPRT,M,HMIN,HMAX,RMSEPS,M)
2000  WHERE THE PARAMETERS ARE DEFINED AS FOLLOWS.
2100
2200  Y      - ARRAY DIMENSIONED (7,NY). THIS ARRAY CONTAINS THE
2300  DEPENDENT VARIABLES AND THEIR SCALED DERIVATIVES. THE
2400  Y(J+1,I) CONTAINS THE J-TH DERIVATIVE OF THE I-TH VAR
2500  IABLESIZ. H=J/J-FACTORY. WHERE H IS THE CURRENT
2600  INITIAL VALUE. CN FIRST ENTRY THE CALLER SUPPLIES THE
2700  STEPSIZ. VALUES OF EACH VARIABLE IN Y(I,I). ON SUB-
2800  SEQUENTIAL ENTRIES IT IS ASSUMED THE ARRAY HAS NOT
2900  BEEN CHANGED. IT IS ASSUMED THE NON-MESH POINTS
3000  THESE VALUES CAN BE USED AS FOLLOWS. IF H IS THE
3100  CURRENT STEPSIZ. CAN BE USED AS FOLLOWS. T+H ARE
3200  NEEDED, LET S = E/H AND THEN
3300
3400  I-TH VARIABLE AT T+H IS
3500  JSUM Y(J+1,I)*S**J
3600  J=0
3700
3800  THE VALUE OF JS IS OBTAINED IN THE CALLING PROGRAM
3900  BY JS=IAES(JSKF/10)

```


[illegible][illegible]

14C PRINT 1. JSKF
STOP

1 FORMAT ('CIT IS AN ERROR TO ENTER SDESL WITH JSKF = ',I10//
1. RUN HAS BEEN TERMINATED.')

END

SUBROUTINE LCASUB (Y,YL,T,TEND,N,NY,M,J,START,KFLAG,MAXOR,IPRT,H,
I,MIN,P,MAX,FMSEPS,SAVE,YLSV,YMAX,ER,ESV,FI,DY,PM)

WHICH IS CUE TO R. L. BROWN AND C. W. GEAR. DFASUB IS DOCUMENTED
IN THE REFERENCE.

BY R. L. BROWN AND C. W. GEAR
RECEIVED JULY 1973
UNIVERSITY OF ILLINOIS AT URBANA-CHAMPAIGN

THIS SUBROUTINE IS A LABEL FOR THE NATIONAL TECHNICAL INFORMATION
SERVICE OF THE U. S. DEPARTMENT OF COMMERCE UNDER ACCESSION NUMBER
CCC-1465-225.

THE PCLLICATION HERE IS DOCUMENTED IN THE REPORT
A PCLLIGRAM FOR THE NUMERICAL SOLUTION OF LARGE SPARSE SYSTEMS OF
ALGEBRAIC AND IMPLICITLY DEFINED STIFF DIFFERENTIAL EQUATIONS
BY RICHARD FRANKEL MAY 1976
REFRPT NES53FE76CE1, CHFCCL
NAVAL POSTGRADUATE CENTER,
MCNTREY, CALIFORNIA 93540

THE CALLING SEQUENCE FOR LCASUB IS

CALL LCASUB(Y,YL,T,TEND,N,NY,M,J,START,KFLAG,MAXOR,IPRT,H,MIN,
P,MAX,FMSEPS,SAVE,YLSV,YMAX,ER,ESV,FI,DY,PM)

WHERE THE PARAMETERS ARE DEFINED AS FOLLOWS:

Y - ARRAY CONTAINS THE
DEPENDENT VARIABLES AND THEIR DERIVATIVES.
Y(J+1,I) TIMES H**J/J-FACTORY THE CURRENT
ESTIMATE OF EACH VARIABLE OF THE DERIVATIVE
IN THE ARRAY Y(I,I) AND ANS
IN THE SUBSEQUENT CHANGES TO INTERPOLATE TO
NON-ARREST POINTS. THESE VALUES CAN BE USED AS FOLLOWS.

0559C
0560C
0561C
0562C
0563C
0564C
0565C
0566C
0567C
0568C
0569C
0570C
0571C
0572C
0573C
0574C
0575C
0576C
0577C
0578C
0579C
0580C
0581C
0582C
0583C
0584C
0585C
0586C
0587C
0588C
0589C
0590C
0591C
0592C
0593C
0594C
0595C
0596C
0597C
0598C
0599C
1000C
1001C
1002C
1003C
1004C
1005C
1006C

CC

CC

[illegible]

137

10557
10558
10559
10560
10561
10562
10563
10564
10565
10566
10567
10568
10569
10570
10571
10572
10573
10574
10575
10576
10577
10578
10579
10580
10581
10582
10583
10584
10585
10586
10587
10588
10589
10590
10591
10592
10593
10594
10595
10596
10597
10598
10599
10600
10601
10602

```

MAXCF - MAXIMUM CRD RETURN FROM SUBROUTINE NUTSL
        METHOD DERIVATIVE THAT SHOULD BE USED IN THE
        GREATER THAN SIX, THE MAXIMUM CRD USED WILL BE SIX.
        INTERNAL PRINT CONTROL INDICATOR
        = 0
        > 0
        - CURRENT STEP AN INITIAL VALUE MUST BE SUPPLIED
        BUT NOT NECESSARILY ONE WHICH WILL BE USED SINCE THE
        SUBROUTINE WILL CHOOSE A SMALLER ONE IF NECESSARY TO
        KEEP THE STEP SIZE SMALLER THAN THE SPECIFIED
        STEP SIZE. IT CAN BE CHANGED BY THE USER.
        NORMALLY STEP SIZE IS ALLOWED
        MAXIMUM STEP SIZE ERROR
        THE SINGLE STEP ERROR
        YMAX(1) = MAX(X(1), Y(1), I)
        VARIATION IN LENGTH AT LEAST 7*NY
        AN ARRAY OF LENGTH NY
        A VECTOR OF LENGTH NY
        BE VECTOR OF LENGTH NY
        A VECTOR OF LENGTH NY
        A VECTOR OF LENGTH NY
        AN ARRAY OF LENGTH NY
        IN SUBROUTINE NUTSL, THE J MATRIX WILL BE STORED IN THE
        UNIQUE SUBROUTINE NUTSL, BUT NOT IN THE NUTSL
        N*2 THE LINEAR EQUATION SOLVER.
        DIMENSION Y(7,1), YL(1), SAVE(7,1), VMAX(1), ER(1), YLSV(1), F(1)
        1, PERTURB(2), COF(2), ES(1), DY(1), PA(1), SAV(1), A(29)
        EQUIVALENCE(A(8),ENC), (A(9),ER), (A(10),F), (A(11),EDW), (A(12),EUP)
        1(A(13),ENC), (A(14),ENC), (A(15),EAS), (A(16),EUP)

```

CC


```

STEP IS REDUCED TO TRY AND GET CONVERGENCE.
-----
1 = 1
CALL I=1, 280, 300, 320
IF (I.E. FMIN+.00001) GC TO 310
RACUP = FACUM*.25
CONTINUE
CALL I=20
IF FLAG = -3
RESTORE Y AND YL AFTER CONVERGENCE FAILURE
-----
320 CALL CCPYZ (Y,SAVE,LCCPYI)
CALL CCFYZ (YL,YLSV,LCCPYI)
H = FCLL
NQ = NCLL
GO TO 170
-----
THE CORRECTOR CONVERGED, SO NOW THE ERROR TEST IS MADE.
-----
330 C = C.
-----
DO 340 I=1,N
YH = APAX(Y(I,I),YMAX(I))
C = C+EF(I)/YM)*2
-----
IWEVAL = C
GC TO 380
IF (C.GT.E) GC TO 380
-----
THE EFFECT OF TEST IS OKAY, SO THE STEP IS ACCEPTED, IF YOU SIZE
NOW EFFECT IS NEGATIVE, TEST IS MADE TO SEE IF THE STEP SIZE
CAN BE INCREASED AT THIS ORDER OR ONE HIGHER CR CASE LOWER AT
THE CHANGE IS MADE ONLY IF THE STEP CAN BE INCREASED BY AT
LEAST 10%. IDOUB IS SET TO PREVENT FURTHER TESTING
FOR A WHILE. IF NO CHANGE IS MADE, IDOUB IS SET TO 9.
-----
IF (K.L1.E) GO TO 360
GO 350 -3.K
-----
DO 350 I=1,NY
Y(J,I) = Y(J,I)+A(J)*ER(I)
-----
350 KFLAG = 1
IDCLB = 1
IF (IDCLB = 1) GO TO 370, 370, 370
CALL CCFYZ (ESV,ER,PI)
GO TO 370
-----
370

```

```

C-----
C THE ERFCR TEST FAILED. IF JSTART = 0, THE DERIVATIVES IN THE
C SAVE ARRAY ARE UPDATED. TESTS ARE THEN MADE TO FIX THE STEPSIZE
C AND PERTURBS. REDUCE THE CRCLER. AFTER RESTORING AND SCALING THE
C Y VARIABLES, THE STEP IS RETRIED.
C-----
38C IF (JSTART.GT.0) GC TC 400
C
C39C GO 390 I=1,NY
C39C SAVE(2,I) = Y(2,I)
C
C40C KFLAG = KFLAG-2 GO TC 550
C40C IF (KFLAG.LE.FMIN) GO TC 550
C40C IF (KFLAG.LE.-5) GC TC 530
C41C PR2 = (C/E)*ENQ2*1.2
C41C PR2 = 0
C41C IF (KFLAG.LE.-1) GC TC 420
C41C C = C
C
C42C CC 420 C=1,M1
C42C YM = APMX(AES(Y(1,J)),YMAX(J))
C42C C = C+(Y(K,J)/YM)**2
C
C43C FRI = (C/ECM)**ENCI*1.3
C43C IF (PR1.GE.PR2) GC TC 43C
C43C FRI = FF1
C43C IF (KFLAG.LT.0.OR.NC.GE.MAXDER) GO TO 450
C43C C = 0
C
C44C GO 440 J=1,M1
C44C YM = APMX(AES(Y(1,J)),YMAX(J))
C44C D = C+(CER(J)-ESV(J))/YM)**2
C
C45C FRI = (C/ECF)**ENC3*1.4
C45C IF (PR1.GE.PR2) GC TC 45C
C45C FRI = FF1
C45C L = 1
C45C R = 1/(AMA)*1/(PR2*1.E-5)
C45C IF (KFLAG.LT.0.CR.R.GE.1.1) GO TO 460
C45C IDCLP = 5
C45C GO TC 510
C46C NENC = NC+1
C46C IF (NENC.LE.NC) GO TC 480
C46C R1 = A(NENC)/FLCAT(NENC)
C

```


146

148850
 148851
 148852
 148853
 148854
 148855
 148856
 148857
 148858
 148859
 148860
 148861
 148862
 148863
 148864
 148865
 148866
 148867
 148868
 148869
 148870
 148871
 148872
 148873
 148874
 148875
 148876
 148877
 148878
 148879
 148880
 148881
 148882
 148883
 148884
 148885
 148886
 148887
 148888
 148889
 148890
 148891
 148892
 148893
 148894
 148895
 148896
 148897
 148898
 148899
 148900
 148901
 148902
 148903
 148904
 148905
 148906
 148907
 148908
 148909
 148910
 148911
 148912
 148913
 148914
 148915
 148916
 148917
 148918
 148919
 148920
 148921
 148922
 148923
 148924
 148925
 148926
 148927
 148928
 148929
 148930
 148931
 148932
 148933
 148934
 148935
 148936
 148937
 148938
 148939
 148940
 148941
 148942
 148943
 148944
 148945
 148946
 148947
 148948
 148949
 148950
 148951
 148952
 148953
 148954
 148955
 148956
 148957
 148958
 148959
 148960
 148961
 148962
 148963
 148964
 148965
 148966
 148967
 148968
 148969
 148970
 148971
 148972
 148973
 148974
 148975
 148976
 148977
 148978
 148979
 148980
 148981
 148982
 148983
 148984
 148985
 148986
 148987
 148988
 148989
 148990
 148991
 148992
 148993
 148994
 148995
 148996
 148997
 148998
 148999
 149000

```

C-----
ENTRY LCA$AV(SAV)
LCCPY$ = 25
CALL CCFY2 (SAV,A,LCCPY$)
CALL CCFY2 (SAVE,Y,LCCPY$)
CALL CCFY2 (VLSV,YL,LCCFYL)
RETURN

C-----
ENTRY LCA$EST(SAV)
LCCPY$R = 25
CALL CCFY2 (A,SAV,LCCPY$R)
RETURN

C-----
1 FORMAT (2I5.12,1P2E10.2,7E14.6/(32X,7E14.6))
2 FORMAT (32X,1P7E14.6)
3 FORMAT (11I13.0,13.0 RMSEPS =,1PES.2, TEND =,
  1 ES.2, P =,E5.2//)
4 FORMAT (10NS N4C H,8X,T ,8X,Y(1,*) AND YL(*)//)
END
SUBROUTINE CCFY2(S,Y,L)
DIMENSION S(1),Y(1)
C-----
THIS SUBROUTINE CCFIES THE ARRAY Y, OF LENGTH L, INTO THE ARRAY S
C-----
IF (L.LE.0) RETURN
DO 100 J=1,L
  S(J) = Y(J)
100 CONTINUE
RETURN
END
SUBROUTINE Derval (Y,YL,T,N,NY,W,KERET)
C-----
THIS SUBROUTINE CALCULATES THE INITIAL VALUES OF THE DERIVATIVES
IN THE GENERAL CASE. IT IS WRITTEN SO THAT IT SHOULD WORK IF THE
FIRST SEVERAL ICNS ARE ALL INVOLVED DERIVATIVES. IT ATTEMPTS TO SOLVE
THE EVALUATION OF THE CF/DV BY CALLING NEWTON'S METHOD. A WAY AS TO TRY THAT
DE/DT IS IN SIGNIFICANT, OTHER REASON THAT IT MAY FAIL FOR THAT
REASON. IT MAY FAIL FOR OTHER REASON, AVE LL OR MODIFY VALUES OF
THE LINEAR VARIABLES, HAVE BEEN SUPPLIED PREVIOUSLY. IF THE USER
MUST SUPPLY HIS OWN VERSION OF Derval.
C-----

```

UU

```

DIMENSION Y(7,1), YL(1), H(1)
-----

```

148

UU

[illegible]

KEY

```

CIMEASIC(A, Pk(1), CY(1), F1(1), YMAX(1)
NL = N - A
IF (A.EQ.0) GO TO 100
NEWPA = C + 1
NN = N + 2 + 1
NNA = A + N
CALL LLOCATF (PW, Pk, A, O, C1, D2, PW(NN), PW(NNA), F1, IER)
IF (IER.EC.0) GO TO 100
KRET = 1
KRETURN
CALL LLOCATF (PW, DY, Pk(NN), N, N, F1)
CALL KRET = KRETURN
KRETURN
ENC
100

```

SAMPLE INPLT FILE FOR CASE 1
(ZERO COLUMN LOCATION)

25 _____ IELEM= 0, must input N.P. locations; 1, automatically
divides domain into NNP-1 equilength elements.

20.0 _____ NNP= number of nodal points.

20.0 _____ T= time step of integration (sec.)

20.0 _____ HMAX= maximum allowable time step (sec.)
14.7 _____ TSTART= start time of problem, normally equal zero (sec.)
1.1 _____ UINF1= exterior surface velocity (kt.)

20.0 _____ TAMB= ambient temperature (deg F)

1.0 _____ PAMB= ambient pressure (p.s.i.)

20.0 _____ TORT= tortuosity

52.0 _____ D1= filament diameter (inches)

20.0 _____ SPACE1= ply thickness (inches)

70.0 _____ HLENT1= reference length (equal to 1 ft.)

2.0 _____ XLENT1= plate thickness (inches)

2.0 _____ RGAS= gas constant for air (lbf*ft.per lbm*deg-R)

2.0 _____ GCOND= bulk conductivity of graphite (btu per hr*ft*deg-F)

2.0 _____ EMIS= fiber emissivity

2.0 _____ ROG= bulk density of graphite (lbm per cu.ft.)

2.0 _____ SPHTG= specific heat of graphite (btu per lbm*deg-F)

2.0 _____ SPHTA= specific heat of air at constant pressure
(btu per lbm*deg-F)

2.0 _____ HSURFL= heat transfer coefficient at x=0 (btu per sq.
ft*hr*deg-F)

2.0 _____ CAMB1= ambient concentration of O2 (lbm per cu.ft.)

} Initial temperature of fibers (deg-F)

400.
:004

LIST OF REFERENCES

1. Fontenot, J.S., "Graphite-Epoxy Composite Material Response to Carrier Deck Fires," Naval Weapons Center, NWC Technical Memorandum 3351, November, 1979.
2. Franke, R., "A Program for the Numerical Solution of Large Sparse Systems of Algebraic and Implicitly Defined Stiff Differential Equations," Naval Postgraduate School Report NPS-53F376051, 1976.
3. Frank-Kamenetskii, D.A., Diffusion and Heat Transfer in Chemical Kinetics, Plenum Press, New York, 1969.
4. Vulis, L.A., Thermal Regimes of Combustion, McGraw-Hill Book Co., New York, 1961.
5. Green, D.W., and Perry, R.H., "Heat Transfer with a Flowing Fluid Through Porous Media," Chemical Eng. Prog. Symp., Series No. 32, 57, 1961, pp. 61-68.
6. Riaz, M., "Analytical Solutions for Single- and Two-Phase Models of Packed-Bed Thermal Storage Systems," Journal of Heat Transfer, 99, 1977, pp. 489-492.
7. Muskat, M., The Flow of Homogeneous Fluids Through Porous Media, McGraw-Hill Book Co., New York, 1946.
8. Scheidegger, A.E., The Physics of Flow Through Porous Media, University of Toronto Press, Toronto, 1974.
9. Carman, P.C., Flow of Gases Through Porous Media, Academic Press, London, 1956.
10. Schlichting, H., Boundary Layer Theory, McGraw-Hill Book Co., New York, 1956.
11. Denbigh, K.G., and Turner, J.C.R., Chemical Reactor Theory, Cambridge Press, London, 1971.
12. Colladay, R.S., and Stepka, F.S., "Examination of Boundary Conditions for Heat Transfer Through a Porous Wall," NASA TN-D-6405, 1971.
13. Rohsenow, W.M., and Hartnett, J.P., Handbook of Heat Transfer, McGraw-Hill Book Co., New York, 1973.

14. Yoshida, F., Ramaswami, D., and Hougen, D.A., "Temperature and Partial Pressures at the Surfaces of Catalyst Particles," A. I. Ch. E. Journal, 8, 1962.
15. Parker, A.S., and Hottel, H.C., "Combustion Rate of Carbon," Ind. Eng. Chem., 28, 1936, pp. 1334-1341.
16. Kanury, A.M., Introduction to Combustion Phenomena, Gordon and Breach Science Publishers, 1975.
17. Bennett, C.O., and Myers, J.E., Momentum, Heat, and Mass Transfer, McGraw-Hill Book Co., 1974.
18. Treybal, R.E., Mass Transfer Operations, McGraw-Hill Book Co., New York, 1968.
19. Gilliland, E.R., "Diffusion Coefficients in Gaseous Systems," Ind. Eng. Chem., 26, 1934, p. 681.
20. Holman, J.P., Heat Transfer, McGraw-Hill Book Co., New York, 1976.
21. Kays, W.M., Convective Heat and Mass Transfer, McGraw-Hill Book Co., 1966.
22. Dankwerts, P.V., "Distribution of Residence Time," Chem. Eng. Sci., 2, 1, 1953.
23. Bischoff, K., "A Note on Boundary Conditions for Flow Reactors," Chem. Eng. Sci., 16, 1 and 2, 1961, pp. 131-133.
24. Shampine, L.F., and Gordon, M.K., Computer Solution of Ordinary Differential Equations, W.H. Freeman and Company, 1975.
25. Gear, C.W., Numerical Initial Value Problems in Ordinary Differential Equations, Prentice-Hall, Inc., 1971.
26. Vatikiotis, C.S., and Salinas, D., "Heat Transfer in a Fibrous Composite with Combustion," to be presented at the National Heat Transfer Conference, July, 1980.

INITIAL DISTRIBUTION LIST

	No. Copies
1. Defense Technical Information Center Cameron Station Alexandria, Virginia 22314	2
2. Library, Code 0142 Naval Postgraduate School Monterey, California 93940	2
3. Department Chairman, Code 69Mx Department of Mechanical Engineering Naval Postgraduate School Monterey, California 93940	2
4. Associate Professor M. Kelleher, Code 69Kk Department of Mechanical Engineering Naval Postgraduate School Monterey, California 93940	1
5. Associate Professor D. Salinas, Code 69Zc Department of Mechanical Engineering Naval Postgraduate School Monterey, California 93940	10
6. Professor R. Newton, Code 69Ne Department of Mechanical Engineering Naval Postgraduate School Monterey, California 93940	1
7. Associate Professor R. Franke, Code 53Fe Department of Mathematics Naval Postgraduate School Monterey, California 93940	1
8. Associate Professor D. Netzer, Code 67Nt Department of Aeronautics Naval Postgraduate School Monterey, California 93940	1
9. LT Costa S. Vatikiotis, USN Naval Engineering Curricular Office, Code 34 Naval Postgraduate School Monterey, California 93940	5

- | | | |
|-----|--|---|
| 10. | Mr. John Fontenot, Code 3183
Survivability and Lethality Division
Systems Development Department
Naval Weapons Center
China Lake, California 93555 | 2 |
| 11. | Mr. Joseph Mansfield, Code 223-6
Chemical Research Project Office
NASA Aimes Research Center
Moffett Field, California 94035 | 2 |
| 12. | LCDR James Farlay, USN, AIR-03PA
Naval Air Systems Command
Washington, D.C. 20361 | 1 |